Discussion of currently used practices for: "Creation of Meteorological Data Sets for CSP/STE Performance Simulations

Kristian Pagh Nielsena, Philippe Blanc, Franck Vignola, Lourdes Ramirez, Manuel Blanco, Richard Meyer

Discussion of currently used practices for: "Creation of Meteorological Data Sets for CSP/STE Performance Simulations"

Kristian Pagh Nielsen[a], Philippe Blanc[b], Frank Vignola[c], Lourdes Ramírez[d], Manuel Blanco[e], Richard Meyer[f]

[a] Danish Meteorological Institute, DK-2100 Copenhagen, Denmark.

[b] ARMINES, F-75272 Paris Cedex 06, France.

[c] The Solar Radiation Monitoring Lab, University of Oregon, Eugene, OR 97403-1274, USA.

[d] CIEMAT, E-28040, Madrid, Spain.

[e] The Cyprus Institute, Athalassa Campus, 20 Konstantinou Kavafi Street 2121, Aglantzia, Nicosia, Cyprus.

[f] Suntrace GmbH, D-20457 Hamburg, Germany.

Introduction

A Concentrating Solar Power (CSP)/Solar Thermal Electric (STE) power plant is a substantial long-term investment. To evaluate the opportunities and risks associated with such a long-term investment requires careful technical and economic analysis. Usually, the results of such analysis are presented in what are known as feasibility studies.

Traditional CSP/STE feasibility studies start by defining an economic model to estimate the economic metrics that characterize the quality and attractiveness of the investment project associated with the building and exploitation of the CSP/STE power plant. Typical economic metrics are the Levelized Cost of Energy (LCOE), the Internal Rate of Return (IRR), the Net Present Value (NPV), and the Debt Coverage Ratio (DCR).

Once the model is defined, the main challenge is to accurately estimate the technical and economic variables and parameters that informs the model (see Figure 1), such as the project's Total Investment, the Annual O&M costs, the Annual Electricity Generation, the Discount Rates, the Equity-to-Debt ratio, etc.

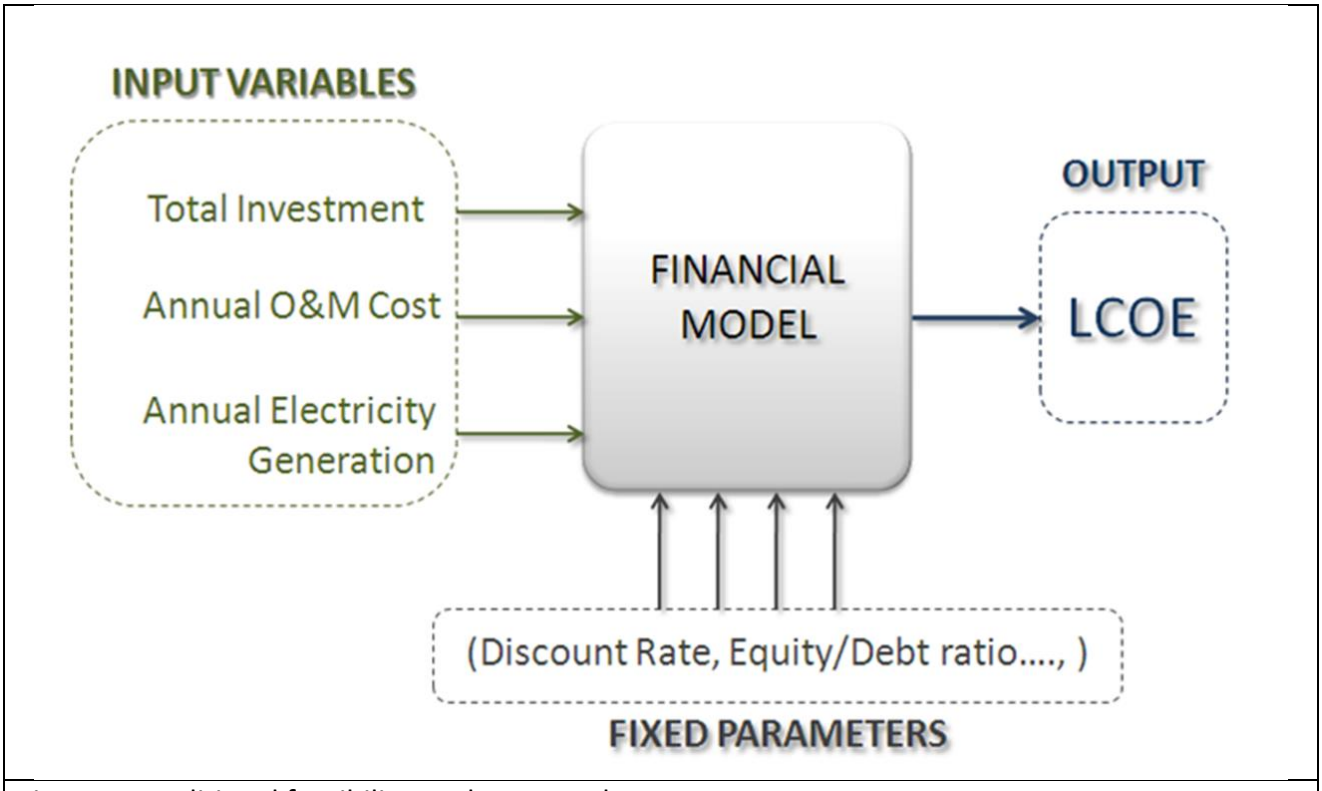

Figure 1. Traditional feasibility study approach.

Of all of these variables and parameters, the Annual Electricity Generation is the one that characterizes the quality of the solar resource at the CSP/STE plant site and the technical performance of

the CSP/STE technology selected to build the solar power plant. To estimate it, one should first develop or acquire a year of relevant solar radiation and other meteorological data that is representative of the long-term meteorology at the solar plant site, and use it, together with the technical parameters that define the plan technology, configuration and operation strategy, to feed a technical model of the plant and estimate the Annual Electricity Generation estimate.

Often, only one yearly data set is used that is representative of the average meteorological year to be expected at the site in the long-term. Sometimes this is supplemented by estimates of the production in a bad year that will be exceeded with a certain probability.

While the above approach, combined with a sensitivity analysis of the economic variables and parameters of the economic model is useful to banks and other potential investors in the decision making process related to the decision of carrying out the investment, there are other more sophisticated approaches that can be pursued.

The one we think is worth exploring is a full stochastic approach (see Figure 2), in which the following aspects are explicitly modeled and taking into account:

- The intrinsic variability of the solar resources and other meteorological variables.
- The intrinsic variability of the price of commodity-like plan components, such as molten salt.
- The uncertainty of the technical model used to determine the annual electricity yield.
- The uncertainty associated with all the different component costs and other costs that determine the aggregate values of the plan investment and the Annual O&M cost.

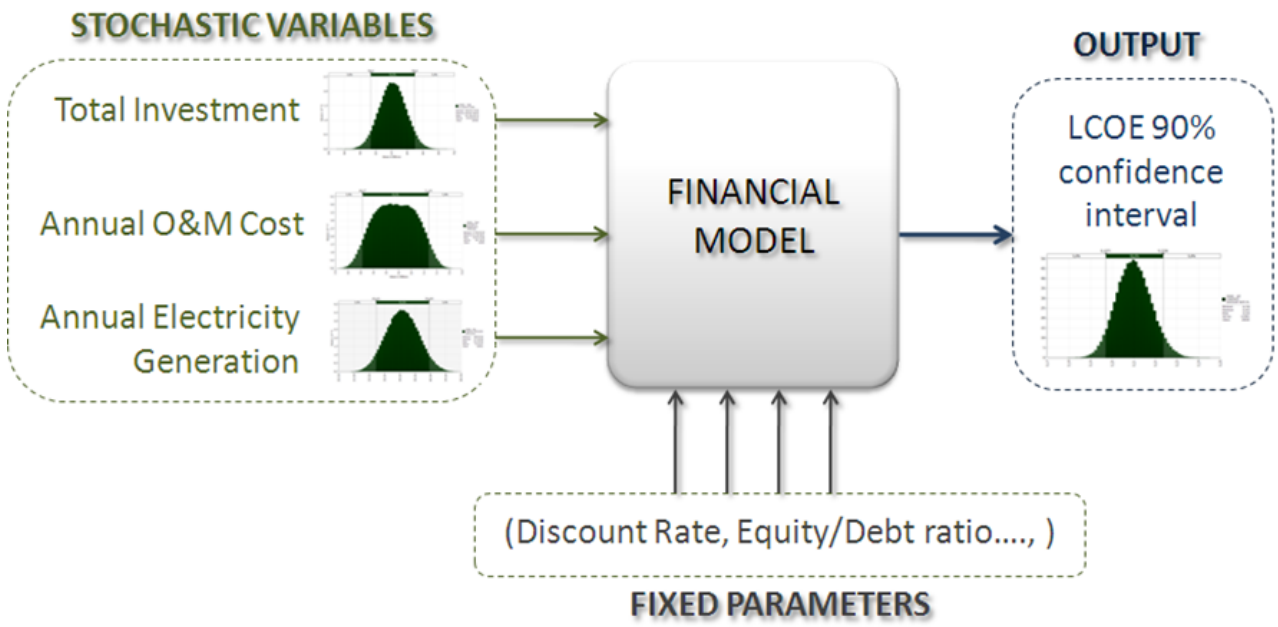

Figure 2. Stochastic feasibility study approach.

In such a model, all the input variables and parameters are considered probability distributions. The challenge is to determine these distributions. How to determine the probability distribution of the Annual Electricity yield of the CSP/STE plant is the overarching theme of this document. Obviously, it starts with how to model the probability distribution of the solar radiation and other relevant meteorological variables. In this report we discuss the factors affecting this distribution.

In Chapter 1 we review the current methods and standards. In Chapter 2 we describe and discuss methods for quantifying the uncertainties in irradiance data from various sources. Chapter 3 is about the other relevant meteorological variables. In Chapter 4 the sources of the natural variability of direct normal irradiances are discussed. In Chapter 5 methods for statistical characterization of solar resource long-term variability are described. In Chapter 6 current methods for assessing the quality of a yearly meteorological data set are detailed. Finally, in Chapter 7 we go through economic feasibility analysis and discuss the advent of stochastic approaches to perform such analysis.

Forecasting and nowcasting of the solar resource for CSP/STE plants is an important issue of the use of meteorological data, however, it is not one that we address in the present report.

Data formatting and metadata are important aspects of meteorological data sets for solar energy in general. If these are not addressed properly errors and misunderstood uses of the data become much more likely. These topics will be detailed as a part of the final report to IEA SHC Task 46, where the “IEA MET Data format” will be described. We recommend this format.

Economic support from the IEA Technology Collaboration Programme for Solar Power and Chemical Energy Systems (SolarPACES) for meeting and travel expenses connected to making this report is highly appreciated. Additional funding from the Energy Development and Demonstration Program (EUDP) of the Danish Energy Agency, The Energy Trust of Oregon, The National Renewable Energy Laboratory, Bonneville Power Administration, Suntrace GmbH, the Danish Meteorological Institute, and CIEMAT is also acknowledged.

1. Standards and methods for making typical meteorological data sets for CSP/STE

In this chapter, we summarize the historical development and current methods and practices used for making meteorological data sets for solar energy simulations. The chapter reviews the pros and cons of current data sets, and the reasoning for why meteorological data sets "beyond typical meteorological years (TMY)" are needed, when simulating ***concentrating solar power/solar thermal electric (CSP/STE)*** *power plants.*

1.1 Introduction

The classical methodology for characterizing meteorological conditions according to WMO (2011) is using 30 years of data to calculate the average ***climate normal*****.** These are averages of meteorological variables including temperature, wind and precipitation. The main 30-year periods used are 1901-1930, 1931-1960 and 1961-1990. The choice of 30-year periods comes from the fact that this was the time span of good quality measurements available when this standard process was defined. Some meteorological institutes also make 15-year or 10-year climate normals. The strict definition of the time spans used for climate normals enables them to be used as references to which current data can be compared. The climate normals can be subtracted from a set of meteorological measurements to obtain an anomaly data set.

In the case or ***renewable energy***, where the system's behavior is strongly dependent on meteorological conditions, appropriate knowledge of these is needed to assess the system's response. To estimate the ***project profitability*** (the financial gain to be expected) and the pay-back period (the time required to recover an investment) (Varela et al., 2004), detailed meteorological data are needed. The met data to be supplied for financing purposes should represent as good as possible the local conditions to be expected at the plant site at least over the tenure of the loan, which typically is in the order of 15 years. Some investors interested in the 'golden end' of a power project might also consider up to 20-25 years. Thus, in case of CSP/STE projects the long-term average of solar resources should well represent the average but also inter-annual variability of the DNI. As the short-term variability of DNI also plays a major role on yields of CSP/STE-plants (Chhatbar and Meyer, 2011) the met data sets to be provided also should include hourly data sequences and true interdependencies between the meteorological variables. For some variables sub-hourly or even

minute scale temporal resolution is preferable. In particular, when it comes to heat and energy storage management detailed meteorological data are needed.

The availability of this information is not common. In the 1970s it was even less so, and even when it was, computers were not fast enough to perform the simulations in the expected time. For these reasons, methodologies for collecting the hourly weather conditions in a reduced period of data were developed.

One of the first meteorological data sets for simulations was made by (Benseman and Cook, 1969) represent the starting point of the called ***typical meteorological years*** (TMY) methodology (Hall et al., 1978) or ***test reference years*** (TRY) in the case of the Danish methodology (Andersen et al., 1974). ASHRAE (American Society of Heating, Refrigerating, and Air-Conditioning Engineers) have made the Weather Year for Energy Calculations WYEC2 data sets in collaboration with NREL (Stoffel, 1998).

In this document, we review the main practices for the creation of meteorological data sets for solar thermal electricity (STE) performance simulations. STE technologies have been using basic and /or modified TMY / TRY methodologies, but the specific needs and special characteristics of this technology make relevant have into account new considerations not included in classical TMY. In recent years, several initiatives at national (Spain or Germany) as well as international (International Electrotechnical Committee) level are pushing for standardizing the new proposed methodologies for assessing relevant subject for solar energy project's profitability as uncertainty or probability.

1.2 Review of methodologies for creating reduced meteorological data sets

For engineering simulations, climate normals are not sufficient, as they do not contain hourly or daily variability and the interdependency of the meteorological variables on short time scales. In order to accommodate this shortcoming, specific data sets were developed for solar project profitability assessments and simulations.

It is generally accepted that a data set of meteorological measurements with true sequences and real interdependencies between the meteorological variables is needed. There were proposals based on the use of only one week at each month (Petrie and McClintock, 1978), but most of the proposals were focused on the use of one whole year, using real months selected from a long-term hourly database.

This is the case of (Benseman and Cook, 1969) using only solar radiation as the criterion for the selection of each month and the monthly distribution of daily totals. In their publication several methods are pioneered. Firstly, they introduce the method of selecting 12 standard months from a long-term data set. Secondly, they use the mean square differences of the cumulative distribution of the clearness index (the global horizontal irradiance at the surface relative to that at the top of the atmosphere) relative to the long-term average cumulative distribution. Thirdly, they use the number of cycles due to low-pressure system passages in a month to pick the best months.

(Andersen et al., 1974) include 20 meteorological variables for the selection of twelve individual months with hourly data for most variables with some exceptions – for instance, daily maximum and minimum temperatures. The twelve months chosen are selected based on how close their mean values and (Gaussian) standard deviations are to the average mean values and standard deviations of the full long-term meteorological data sets. Since it is impossible to find months with representative data for all meteorological variables, Lund (1974) made the selection only based on global radiation, temperature and daily maximum temperature. These references (Andersen et al., 1974; Lund, 1974) are the base of what is often referred to as the Danish method.

These models are the precursors of the so-called ***Typical Meteorological Year*** (TMY) in the USA and ***Test Reference Years*** (TRY) in Europe. In both cases, true frequencies, true sequences and true correlations between different variables are main requirements.

TRY evolves to ***Design Reference Year*** (DRY) when adding some new variables and new types of variables as 5-minute values for direct irradiance, and forecast information. Lund (1995) shows a detailed description of the DRY using ten years as the minimum period of input data. The selection criterion contains two parts: a climatological evaluation and a mathematical selection. In the climatological evaluation mean values and standard deviations for each month are checked. Each month is given a qualification label according to the weighted difference to the long term averages of fourteen meteorological variables. In the mathematical selection, means and variances for daily values of three variables (dry-bulb temperature, daily maximum temperature, and global irradiance) have been taken into account. This selection gives three candidates, and from these, the best qualified is chosen. (Festa and Ratto, 1993) study the use of different distance parameters for the month's selection, using means, standard deviations and Kolmogorov-Smirnoff (KS) statistics as well as taking into account the correlations of daily values. For more details on KS statistics see section 5.2.

To address the needs for simulating building energy performance, the Sandia National Laboratories developed a methodology for generating Typical Meteorological Year (TMY) data sets from long-term observational records (Hall, et al., 1978). This is often called the Sandia methodology. In this, data from twelve individual months are chosen from a period of 15-30 years of hourly mete-

orological data – just as for the TRYs – from 26 weather stations with measurements of solar irradiance. The main difference between the TRY and the TMY is that the TRY months are chosen based on the mean values and the (Gaussian) standard deviations of the 2-meter temperatures and global radiation. For the TMYs, the Finkelstein & Schafer method for arbitrary (non-Gaussian) cumulative distributions is used, and the selection is based on nine weighted meteorological variables. Twelve typical months are selected in a two-step process. The first step is the selection of five candidates, those with cumulative distribution functions (CDFs) closest to the average CDFs of the long-term meteorological variables. Finkelstein-Schafer (FS) parameter (Finkelstein and Schafer, 1971) is used for this purpose. The hourly global horizontal irradiance measurements were given one-half of the weighting for the meteorological parameters considered in order to make the TMYs broadly applicable for the energy simulations of buildings that account for both active and passive solar energy. In the second step, statistics and persistence structure associated with both mean and median daily dry-bulb temperature and daily total global solar radiation are taken into account for the final selection. This methodology was applied to 26 sites in the United States providing meteorological input data for simulating the performance of various technologies and systems. Nearly twenty years later, new TMYs were developed to meet the demands for data from more locations and improved estimates of direct normal irradiance. Typical Meteorological Year Version 2 (TMY2) data for 239 locations are representative of the period 1961-1990 (Marion and Urban, 1995). Further refinements to the process for including more locations with more recent data, the TMY3 files are representative of the hourly weather observations from 1991-2005 at 1,020 stations (Wilcox and Marion, 2008).

Through the years, few research projects have been related to this topic, but the method for making TMY/TRY data sets has not evolved much. During the eighties, only one relevant work can be pointed out (Pissimanis et al., 1988). They revised the Sandia methodology to create meteorological data sets for the City of Athens.

During the next twenty years, modifications of the Sandia or Danish methodologies are shown around the world. From the methodological point of view, the main differences are related to (1) the variables needed to build the final series; (2) the weight of each variable in the selection procedure; (3) the application of one, two or several steps in the selection procedure. In Egypt (Mosalam Shaltout and Tadros, 1994) uses only solar radiation data in a one-step FS based selection procedure; In Cyprus (Petrakis et al., 1998) uses also a one-step FS methodology, but using 15 different meteorological variables; In Greece the project of Argiriou et al. (1999) is worth highlighting. In this work, the original methodologies are compared. Additionally, modified weights are tested for each methodology. Their impact on performance simulations for solar systems (flat plane collector, photovoltaic, and large-scale solar heating) is assessed and the Festa and Ratto

(1993) modification to the Danish methodology, using the FS weighed sum for the selection criteria instead of the KS statistic, is the most suitable methodology (Argiriou et al. 1999).

In Figure 1.1 the most relevant TMY/TRY research publications and the distribution through the years can be shown. 49 works has been selected from the Institute for Scientific Information (ISI) and using the Web of Science, citations of this selected works are shown. It is interesting to see how the industry needs pushed for an increasing number of works during 2012 which were cited and revised mainly during 2014 and 2015.

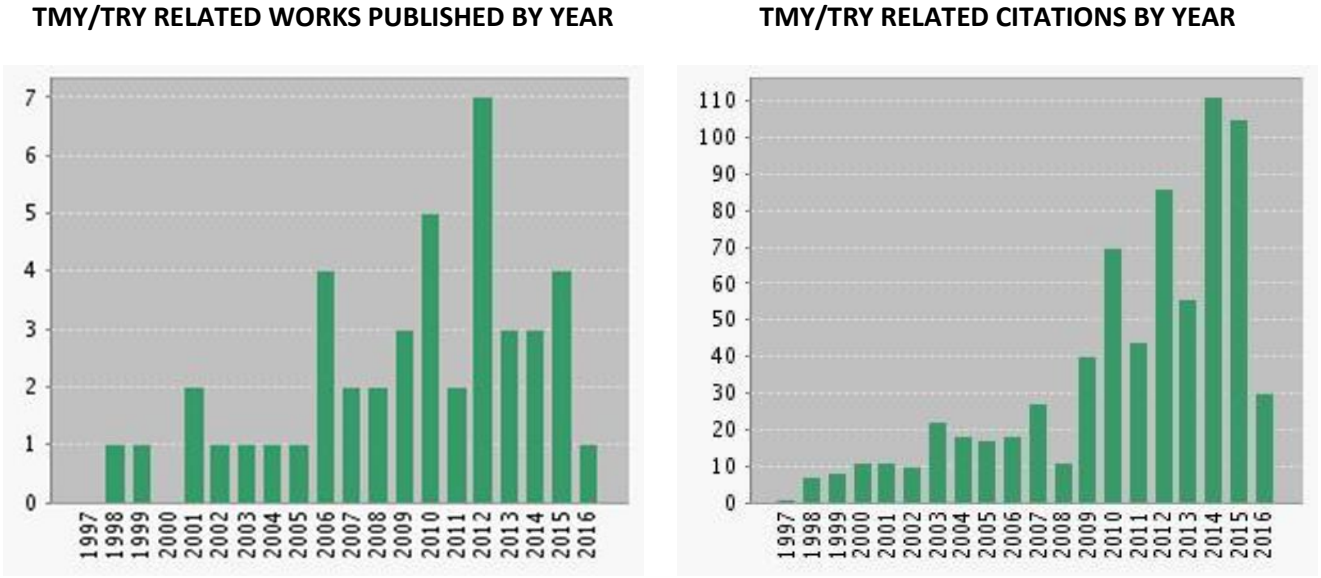

Figure 1.1. TMY/TRY related works and citation report since 1997.

For simulations of the thermal performance of buildings the ISO 15927-4 standard (ISO 15927-4, 2005) describes a standardized version of previous TRY methodologies: using dry-bulb temperature, solar radiation and humidity as main variables; not specifying the weight of each variable but using a global ranking combination; using a two steps procedure based on the FS as the first step, but adding wind speed in a second step selection criterion among the three preselected through the ranking. This method is applied and well described in (Lee et al., 2010) and (Kalamees et al., 2012). In general, it is important to mention that the use of FS statistic is a very robust selection methodology because it does not rely on any specific probability distribution function to capture the internal variability of monthly or annual values.

1.3 Recent works on the creation of reduced meteorological data sets

In recent years, the growing number of solar thermal electricity projects has pushed researchers to look for solutions to specific needs of this technology. Main topics to be discussed are related to: (1) the use of direct normal irradiance (DNI) as unique relevant input, or the need for additional related meteorological variables; (2) The use of measured and / or modeled data; (3) The need to provide probabilistic information for profitability assessments and annual payback.

There are works focused in ***typical solar radiation years*** (TSRY) (Mosalam Shaltout and Tadros, 1994; Zhou et al., 2006; Bulut, 2010; Zang et al., 2012) where relatively large weighting factors are given to the solar radiation variables compared to the TMY and TMY2 weighting factors. For solar thermal electricity (STE) applications, ***direct normal irradiance (DNI)*** is the single most important meteorological variable. Therefore, new methodologies where DNI is 100% weighted have been designed by Hoyer-Klick et al. (2009) or Habte et al. (2014). In addition to DNI a maximum wind threshold can be taken into account, as is shown in the ENDORSE TMY generation service (Espinar et al., 2012). In the case of the Spanish standard (AENOR, 2014), DNI can be weighted with 100% or with 50% sharing with global horizontal irradiance (GHI) the whole weight.

Threshold effective DNI as discussed by Rheinländer et al. (2008) and (Meyer et al., 2009), can replace DNI to take into account the DNI angle of incidence, the shut down and the dumping effects respectively for too low and too high effective DNI, and the effect of wind speed above a certain speed threshold for which the collectors is in an security position.

Due to the high cost of solar radiation measurements and the impossibility to have 20 years of measurements in all locations with potential solar installations, the use of ***gridded data sets*** (Hoyer-Klick et al., 2009; Habte et al., 2014) has become essential. Gridded data sets cover all land points with a specific spatial resolution, unlike local measurements that provide information only for a specific location. Gridded data sets can be derived from satellite observation data, from numerical weather prediction (NWP) model analysis, or interpolated between ground-based measurement stations. In Zelenka et al. (1992) and Zelenka et al. (1999) validation exercises of several satellite-derived solar radiation databases are shown. They also analyzed the impact of distance from the nearest measurement station on the gridded data representation. Each of these options (satellite-derived data sets vs. measurements) has different qualities and uncertainties, which are not always clear to the user. In order to minimize uncertainties in the satellite data sets, at least one year of hourly ground-based measurements should be used for site-adaptation of the satellite data (Ramírez et al., 2012; Polo et al., 2015). This should be used to ensure that the satellite-derived data do not have major biases in daily profiles, even when monthly and yearly values could be similar. Site-adaptation can also provide empirical corrections for the effects of small scale clouds that the satellite images cannot resolve. Meyer et al. (2009) summarize requirements

to satellite-derived irradiances, including the need for higher time resolution than one hour, site adaptation, and a minimum spatial resolution of 0.1°.

Although solar radiation is the main impact variable in STE power plants, in order to cover all the possible applications as well as to improve the system characterization, temperature, humidity and wind speed are also needed. For most meteorological variables the highest quality gridded data sets are obtained by re-analyzing all available and quality-controlled measurements with a numerical weather prediction (NWP) model (Daley, 1993). For solar irradiance data, this is, however, not the case. Boilley and Wald (Boilley and Wald, 2015) show that both the ERA-Interim (Dee et al., 2011) and MERRA reanalysis (Rienecker et al., 2011) data sets are of lower quality than the best satellite-derived data sets. This may well change in the future as the NWP models used for reanalysis improve. Currently, reanalysis data sets are not recommended as a solar radiation data source.

In order to enable reliable ***profitability and annual pay back assessments***, one annual series of meteorological data is not enough. Additional probabilistic information related to the energy output has to be available. Festa & Ratto started their work on statistical properties of solar radiation more than 20 years ago (Festa and Ratto, 1992); but this type of investigations where decoupled from the TMY assessments until 2013 (McMahan et al., 2013; Vignola et al., 2013), and in relationship with the fast growth of STE plants in Spain. A typical CSP project in Spain provides 50 MW nominal installed power. Such an installation could cost more than 300 M€ (Ruíz et al., 2011), and the investment of such size usually requires loans from banks. For risk analysis financial experts need to know the project's incomes even in very bad years. For detailed analysis of potential cash flows they need information related to the probability distribution of the generated income through the years. It should be noted that this is not necessarily proportional to the probability distribution of the solar radiation through the years!

1.4 Ongoing initiatives and future needs

TMY Standardization is one of the main related ongoing initiatives, pushed and requested by companies. Figure 1.2 shows timeline of TMY activities. When researchers are dealing with uncertainty, probability or variability topics, companies have needs related to harmonization of existing techniques In this context, the goal of this report is to focus on the future stakeholder needs for a standard approach to address the variability of solar and meteorological resources.

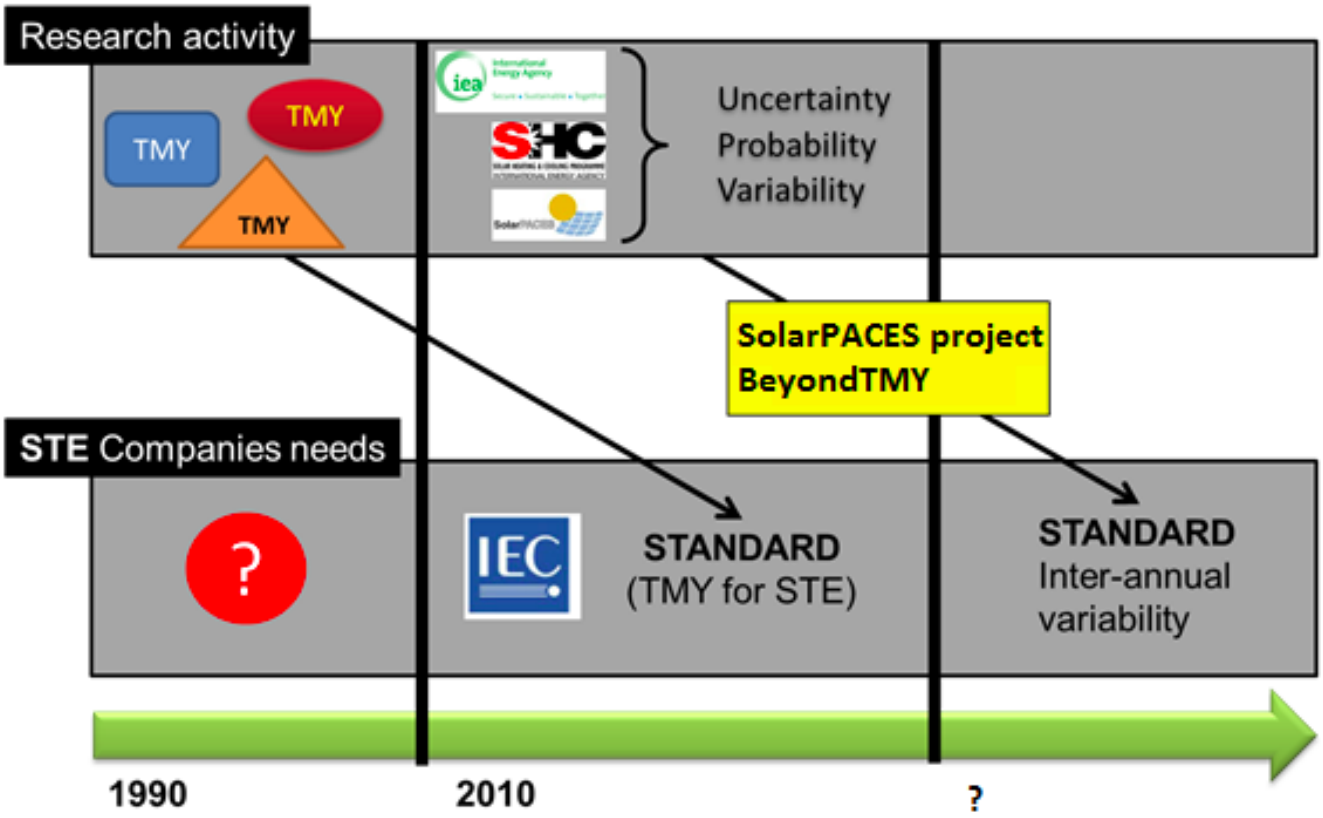

Figure 1.2. TMY/TRY activities timeline. The researchers' activities are a step ahead of the standardization activities. The latter are mainly made on the initiative of companies even when researchers are also involved.

At the international level the IEC Technical Committee (TC) 117 Technical Specification (TS) 62862-1-2 is addressing the needs for solar resource and meteorological time-series data as input for simulating solar thermal electric (STE) systems. The main intention of this specification is to provide a methodology for solar radiation yearly data set generation that provides high-quality local series for solar thermal electricity projects. Typically, the TMY to be defined in IEC TS 62862-1-2 will be used for prefeasibility studies. The TS 62862-1-2 will include procedures for quality control, gap filling, combination of data sets from different sources, and replacement of daily data to get the monthly mean values. For financing of CSP/STE plants TMY data sets generated according to TS 62862-1-2 might be used as a base case. For detailed feasibility studies and profitability assessments of CSP/STE projects additional characterization of variability and uncertainty of the provided TMY is needed.

The original draft is based on AENOR (2014), where one year of local surface measurements is required, and at least of 10 years of gridded data, based on estimates from satellite observations, are strongly recommended (Figure 1.3) as a minimum requirement for preparation of sound me-

teorological input data into performance simulation models. Two main options can be considered: the long-term gridded data adaptation to local measurements, the local measurements adaptation to the long-term gridded data. The first option is a simplification of the TMY or TRY, where local gridded data cover at least 10 years of DNI hourly values. These data have to be checked and corrected with the simultaneous hourly local measurements. In a second step, months are selected through calculation of FS based on DNI (and GHI if available). The long-term monthly value (LTMV) is derived from the selected month as the monthly sum. In addition to this option, the carefully revised local measurement can be used as the base for the TMY. Month by month, days of the local measurement are replaced by another near day trying to achieve the LTMV, calculated form the described methodology in the first option. As originally proposed by Hoyer-Klick et al. (2009) a maximum distance of 5 days between replaced days is allowed to prevent that sun angles and day length shows noticeable differences from the angles which should appear at the specific day, which is replaced. The now proposed IEC code further limits the maximum number of changes to 15 and the same day can only be used 4 times as an additional requirement to avoid to many identical days.

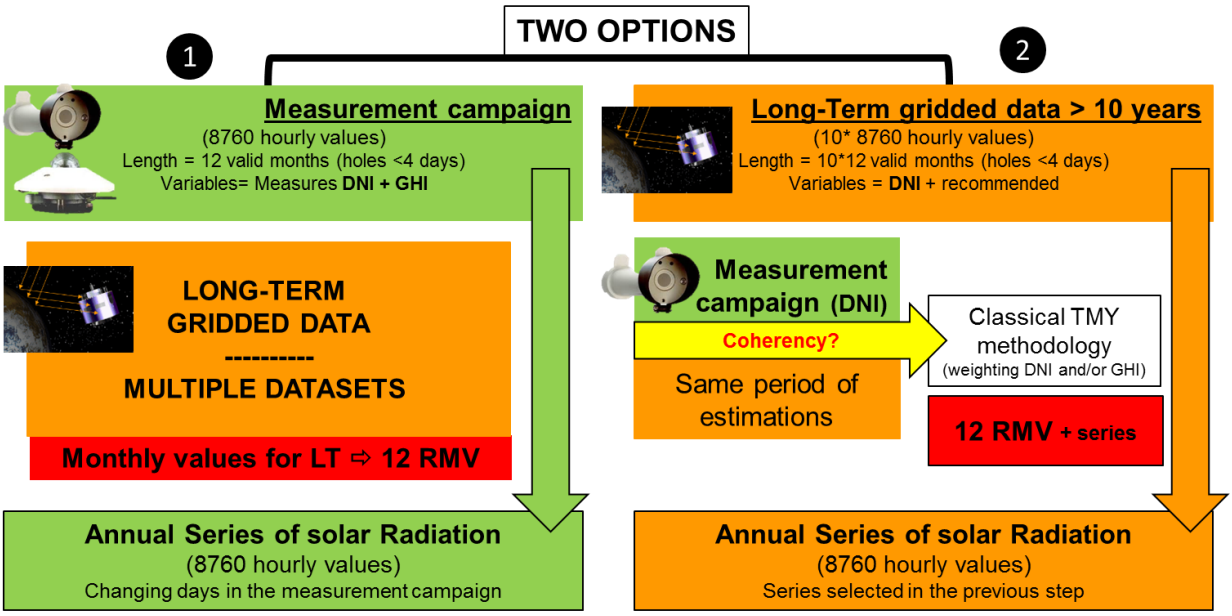

Figure 1.3. Summary of the IEC standard for TMY generation. Two main options can be considered:1. local measurements adaptation to the long-term gridded data; 2. long-term gridded data adaptation to local measurements. Where RMV refers to "Reference Monthly Value" and are the DNI or GHI monthly values in the final TMY, depending on the main variable for typical month selection considered in the approach. LT means "Long –Term".

TMY data sets in general aim to express the most likely average weather situation at a site, which for CSP/STE plants is best characterized by the P50 DNI value expressing the 50% level of exceed-

ance. In addition to the TMY standardization the financial community requests data sets for analysis of the DNI resource risk. Such meteorological data sets should either result in ***the electricity generation in a very bad year and simultaneously the consequences of a systematic overestimation of DNI or only the latter effect***. Typically, these data sets are designed in a way that the average DNI is representing a specific conservative case.

Various approaches for calculating such risk analysis data sets have been proposed in recent works (Cebecauer and Šúri, 2015; Roettinger et al., 2015). Proposals have a methodological path not so far from the TMY, using months as candidates among the worsts available months instead from the available *mean* months. Thus, the main differences are related to the way of selecting the bad months for building the low DNI year (Espinar et al., 2012; Fernández-Peruchena et al., 2015; Cebecauer and Šúri, 2015).

The most requested annual series is that related to the 10^{th} percentile of the DNI long-term average in terms of statistical terminology. That is a meteorological year, which should be exceeded with a probability of 90 percent. Thus, such a case in energy finance usually is indicated b P90 – although statistics literature rather refers to such as P10.

When banks should finance CSP/STE-plants some ask for a P90-data sets representing only the more dramatic case, when the average DNI is overestimated due to uncertainty of the long-term mean DNI. As this P90-level is referring to the uncertainty of the multi-year average this is called **multi-year-P90**. Other banks, which also want to see the effect of inter-annual variability in the same data set, ask for a so called **single-year-P90**. Such $P90_{single}$ in addition to uncertainty considers the effect of a year with unfavorable weather conditions for CSP-electricity production.

A debate related to adequate methodologies to generate this P90 series is still ongoing and will be discussed in future chapters. One discussion is related to the correlation between P90 meteorological series vs. P90 energy output. The objective is to provide a P90 annual energy output, but there is not a linear correlation between an annual DNI value and an annual energy output. Another open discussion is related to the possibility to build near infinite annual series with the same annual DNI value, and these series will derive into very different annual energy output values.

In order to avoid the shortcomings of using single years there is the need to apply multi-year data sets. Pernigotto et al. (2014) show the influence of TRY data sets on the energy needs of buildings in five Italian locations. E.g., the energy output from a TRY month could be out of the inter-quartile-range of all available monthly energy outputs for a specific month. Similar studies are now under evaluation for STE-projects and will have a importance in future years. The simplest multi-year data set is the use of gridded data sets locally corrected during the whole available period of years (typically more than 20), and use it to simulate the energy output (Fernández-Peruchena et al., 2015). The output data set gives sample years for possible annual electricity yields. From such

results the frequency distribution due to natural variability of DNI can be fitted, which allows derivation of all percentiles. However, the approach of using multi-year data sets is only representing the resource risk due to inter-annual variability. The effect of a general systematic overestimation of the DNI due to uncertainty could be much severe and is not represented in multi-annual time-series, which on average should represent the P50 DNI.

To consider in addition to natural variability the effect of uncertainty on CSP/STE-yields Roettinger et al. (2015) make a first approach by manipulating DNI-values towards increased or reduced individual DNI values by simply multiplication with a linear factor. From application of such a wide population of synthetic years a frequency distribution of STE-yields can be derived, which is representing both risk effects. Thus, from such a distribution function the single-year-P90 and other percentiles could be derived. This advanced statistical approach still needs to be verified and established in the energy and financial community.

1.5 Conclusions

For several decades yearly "Typical" and "Reference" meteorological data sets have been used for a broad range of solar technology simulations. Recently, specialized yearly data sets have been developed for specific solar technologies. Thus, users of yearly data sets need to use data sets designed for their purpose. A TMY that is weighted primarily with DNI is the current recommendation for a yearly data set for CSP/STE simulations.

Standardization of procedures for TMY generation for STE projects has much progressed in the context of IEC TC 117. The respective Technical Specification is expected to be finished in 2016. It aims to define the most suitable methodology for generating an annual series of meteorological data for the simulation of solar thermal electricity power plants, which should represent the P50 long-term average of DNI. Such high quality and accuracy TMY data sets today should be used for obtaining the financial base cases, when financing a CSP/STE plant.

It is planned that IEC TC 117 in addition to a standardized TMY generation is preparing a code for generation of P90 or similar meteorological years. This code should clarify the most suitable methodology to obtain a data set from which the energy output of a bad cases could be calculated. It should define how uncertainty of long-term DNI data should be calculated and how this leads to multi-year P90 levels. Further it should fix how the additional effect of natural variability has to be expressed in single-year P90 levels. With such a single-year P90 annual data set it can be evaluated how the debt-service is covered even if the very bad case of unfavorable CSP-weather occurs coincident with overestimation of DNI-averages. Very conservative risk assessments assume such in the first year of plant operation, when there are perhaps no reserve accounts filled.

The approach of using only few annual data sets, such as a P50 TMY, and a P90 and perhaps a meteorological year representing P75 DNI levels, has shortcomings: due to non-linear relation of DNI with power output of CSP/STE plants the resulting P90 level related to electricity production might significantly differ from the actual probability. Thus, methodologies that try to characterize the whole probability density function (PDF) of meteorological conditions through the power plant lifetime need to be investigated. Once the PDF of meteorological variables is clarified, an unlimited number of annual series can be synthesized.

1.6 References

AENOR, 2014. Centrales termosolares. Procedimiento de generación de Año Solar Representativo, UNE. UNE 206011.

Andersen, B., Eidorff, S., Lund, H., Pedersen, E., Rosenørn, S., Valbjørn, O., 1974. Referenceåret - Vejrdata for VVS beregninger, (The Reference Year - Weather data for HVAC-calculations), Report no. 89. Danish Building Research Institute.

Argiriou, A., Lykoudis, S., Kontoyiannidis, S., Balaras, C.A., Asimakopoulos, D., Petrakis, M., Kassomenos, P., 1999. Comparison of methodologies for tmy generation using 20 years data for Athens, Greece. Solar Energy 66, 33–45. doi:http://dx.doi.org/10.1016/S0038-092X(99)00012-2

Benseman, R.F., Cook, F.W., 1969. Solar radiation in New Zealand--The standard year. New Zealand journal of science 12, 698–708.

Boilley, A., Wald, L., 2015. Comparison between meteorological re-analyses from ERA-Interim and MERRA and measurements of daily solar irradiation at surface. Renewable Energy 75, 135–143. doi:10.1016/j.renene.2014.09.042

Bulut, H., 2010. Generation of representative solar radiation data for Aegean Region of Turkey. International Journal of the Physical Sciences 5, 1124–1131.

Cebecauer, T., Suri, M., 2015. Typical Meteorological Year Data: SolarGIS Approach. Energy Procedia 69, 1958–1969. doi:10.1016/j.egypro.2015.03.195

Daley, R., 1993. Atmospheric Data Analysis, Cambridge University Press. Cambridge University Press. Atmospheric and Space Science Series, New York, NY, USA.

Dee, D.P., Uppala, S.M., Simmons, A.J., Berrisford, P., Poli, P., Kobayashi, S., Andrae, U., Balmaseda, M.A., Balsamo, G., Bauer, P., Bechtold, P., Beljaars, A.C.M., van de Berg, L., Bidlot, J., Bormann, N., Delsol, C., Dragani, R., Fuentes, M., Geer, A.J., Haimberger, L., Healy, S.B., Hersbach, H., Hólm, E. V., Isaksen, L., Kållberg, P., Köhler, M., Matricardi, M., McNally, A.P., Monge-Sanz, B.M., Morcrette, J.-J., Park, B.-K., Peubey, C., de Rosnay, P., Tavolato, C., Thépaut, J.-N., Vitart, F., 2011. The ERA-Interim reanalysis: configuration and performance of

the data assimilation system. Quarterly Journal of the Royal Meteorological Society 137, 553–597. doi:10.1002/qj.828

Espinar, B., Blanc, P., Wald, L., 2012. Report on the production S4 “TMY FOR PRODUCTION,” in: Project ENDORSE. p. 12.

Fernández-Peruchena, C.M., Ramírez, L., Silva, M., Bermejo, D., Gastón, M., Moreno, S., Pulgar, J., Liria, J., Macías, S., Gonzalez, R., Bernardos, A., Castillo, N., Valenzuela, R.X., Zarzalejo, L., 2015. Estimation of the probability of exceedance of Direct Normal solar Irradiation series, in: Conference Proceedings SolarPACES. p. 5.

Festa, R., Ratto, C.F., 1993. Proposal of a numerical procedure to select Reference Years. Solar Energy 50, 9–17. doi:10.1016/0038-092X(93)90003-7

Festa, R., Ratto, C.F., 1992. Solar radiation statistical properties. Task 9, Solar Heating and Cooling. International Energy Agency.

Finkelstein, J.M., Schafer, R.E., 1971. Improved Goodness-Of-Fit Tests. Biometrika 58, 641. doi:10.2307/2334400

Habte, A., Lopez, A., Sengupta, M., Wilcox, S., 2014. Temporal and Spatial Comparison of Gridded TMY, TDY, and TGY Data sets, NREL/TP-5D00-60886. National Renewable Energy Laboratory.

Hall, I.J.R., Prairie, R.R., Anderson, H.E., Boes, E.C., 1978. Generation of Typical Meteorological Years for 26 SOLMET Stations, SAND78-1601. Sandia National Laboratories, Albuquerque, NM, USA.

Hoyer-Klick, C., Hustig, F., Schwandt, M., Meyer, R. (2009): Characteristic meteorological years from ground and satellite data. SolarPACES Symp., Berlin, Germany, Sep. 2009, 8 p.

ISO 15927-4, 2005. Hygrothermal performance of buildings -- Calculation and presentation of climatic data -- Part 4: Hourly data for assessing the annual energy use for heating and cooling. International Organization for Standardization, Geneva, Switzerland.

Kalamees, T., Jylhä, K., Tietäväinen, H., Jokisalo, J., Ilomets, S., Hyvönen, R., Saku, S., 2012. Development of weighting factors for climate variables for selecting the energy reference year according to the EN ISO 15927-4 standard. Energy and Buildings 47, 53–60. doi:10.1016/j.enbuild.2011.11.031

Lee, K., Yoo, H., Levermore, G.J., 2010. Generation of typical weather data using the ISO Test Reference Year (TRY) method for major cities of South Korea. Building and Environment 45, 956–963. doi:10.1016/j.buildenv.2009.10.002

Lund, H., 1995. Design Reference Years. Task 9, Solar Heating and Cooling. International Energy Agency.

Lund, H., 1974. The “Reference Year”, a set of climatic data for Environmental Engineering. Also

published as: Report no. 32, Thermal Insulation Laboratory, Technical University of Denmark, in: Second Symposium on the Use of Computers for Environmental Engineering Related to Building. Paris (France), p. 12.

Marion, W., Urban, K., 1995. User's Manual for TMY2s, NREL. National Renewable Energy Laboratory, Golden.

McMahan, A.C., Grover, C.N., Vignola, F.E., 2013. Evaluation of Resource Risk in Solar-Project Financing, in: Solar Energy Forecasting and Resource Assessment. Elsevier, pp. 81–95. doi:10.1016/B978-0-12-397177-7.00004-8

Meyer, R., Beyer, H.G., Fanslau, J., Geuder, N., Hammer, A., Hirsch, T., Hoyer-klick, C., Schmidt, N., Schwandt, M., 2009. Towards Standardization Of CSP Yield Assessments, in: Proceedings of the SolarPACES Conference. Berlin, p. 8.

Mosalam Shaltout, M.A., Tadros, M.T.Y., 1994. Typical solar radiation year for Egypt. Renewable Energy 4, 387–393. doi:10.1016/0960-1481(94)90045-0

Pernigotto, G., Prada, A., Cóstola, D., Gasparella, A., Hensen, J.L.M., 2014. Multi-year and reference year weather data for building energy labelling in north Italy climates. Energy and Buildings 72, 62–72. doi:10.1016/j.enbuild.2013.12.012

Petrakis, M., Kambezidis, H.D., Lykoudis, S., Adamopoulos, A.D., Kassomenos, P., Michaelides, I.M., Kalogirou, S.A., Roditis, G., Chrysis, I., Hadjigianni, A., 1998. Generation of a "typical meteorological year" for Nicosia, Cyprus. Renewable Energy 13, 381–388. doi:10.1016/S0960-1481(98)00014-7

Petrie, W.R., McClintock, M., 1978. Determining typical weather for use in solar energy simulations. Solar Energy 21, 55–59. doi:10.1016/0038-092X(78)90116-0

Pissimanis, D., Karras, G., Notaridou, V., Gavra, K., 1988. The generation of a "typical meteorological year" for the city of Athens. Solar Energy 40, 405–411. doi:10.1016/0038-092X(88)90095-3.

Polo, J., S. Wilbert, J. A. Ruiz-Arias, R. Meyer, C. Gueymard, M. Šúri, L. Martín, T. Mieslinger, P. Blanc, I. Grant, J. Boland, P. Ineichen, J. Remund, R. Escobar, A. Troccoli, M. Sengupta, K. P. Nielsen, D. Renne, N. Geuder, 2015. Integration of ground measurements to model-derived data. IEA Report from SHC Task 46: Solar Resource Assessment and Forecasting.

Ramírez, L., Barnechea, B., Bernardos, A., Bolinaga, B., Cony, M., Moreno, S., Orive, R., Polo, J., Redondo, C., Salbidegoitia, I.B., Serrano, L., Tovar, J., Zarzalejo, L.F., 2012. Towards the standardization of procedures for solar radiation data series generation, in: Proceedings of the SolarPACES Conference. p. 5.

Rheinländer, J., Bergmann, S., Erbes, M. R., 2008. Technical and economic performance of parabolic trough solar power plants—A computational tool for plant feasibility studies. *In* 14th SolarPACES International Symposium on Concentrated Solar Power and Chemical Energy Tech-

nologies, Las Vegas, NV, USA.

Rienecker, M.M., Suarez, M.J., Gelaro, R., Todling, R., Bacmeister, J., Liu, E., Bosilovich, M.G., Schubert, S.D., Takacs, L., Kim, G.-K., Bloom, S., Chen, J., Collins, D., Conaty, A., da Silva, A., Gu, W., Joiner, J., Koster, R.D., Lucchesi, R., Molod, A., Owens, T., Pawson, S., Pegion, P., Redder, C.R., Reichle, R., Robertson, F.R., Ruddick, A.G., Sienkiewicz, M., Woollen, J., 2011. MERRA: NASA's Modern-Era Retrospective Analysis for Research and Applications. Journal of Climate 24, 3624–3648. doi:10.1175/JCLI-D-11-00015.1

Ruíz, V., Blanco, M., Maraver, A., Silva, M., Ramírez, L., Cárdenas, B., Lillo, I., Sánchez, M., Regidor, A., Moreno, S., García-Barberena, J., Muñóz, J., Domínguez, J., Gracía, P., Pallardo, I., Pascal, E., Luna, S., 2011. Evaluación del potencial de energía solar termoeléctrica: Estudio tecnico PER 2011 - 2020, IDAE. IDAE.

Röttinger, N., Remann, F., Meyer, R., Telsnig, T., 2015. Calculation of CSP yields with probabilistic meteorological data sets: a case study in Brazil. Energy Procedia, 69, 2009-2018.

Stoffel, T., 1998. Production of the Weather Year for Energy Calculations Version 2 (WYEC2). NREL TP-463-20819. National Renewable Energy Laboratory, Golden, CO, USA.

Varela, M., Ramírez, L., Mora, L., Sidrach de Cardona, M., 2004. Economic analysis of small photovoltaic facilities and their regional differences. International Journal of Energy Research 28, 245–255. doi:10.1002/er.963

Vignola, F.E., McMahan, A.C., Grover, C.N., 2013. Bankable Solar-Radiation Data sets, in: Solar Energy Forecasting and Resource Assessment. Elsevier, pp. 97–131. doi:10.1016/B978-0-12-397177-7.00005-X

Wilcox, S., Marion, W., 2008. User's Manual for TMY3 Data sets, NREL/TP-581-43156. National Renewable Energy Laboratory.

WMO, 2011. Guide to climatological practices, WMO. World Meteorological Organization, Geneva.

Zang, H., Xu, Q., Bian, H., 2012. Generation of typical solar radiation data for different climates of China. Energy 38, 236–248. doi:10.1016/j.energy.2011.12.008

Zelenka, A., Czeplak, G., D'Agostino, V., Josefsson, W., Maxwell, E., Perez, R., 1992. Techniques for supplementing solar radiation network data. Volume 1. Task 9, Solar Heating and Cooling. International Energy Agency.

Zelenka, A., Perez, R., Seals, R., Renné, D., 1999. Effective Accuracy of Satellite-Derived Hourly Irradiances. Theoretical and Applied Climatology 62, 199–207. doi:10.1007/s007040050084

Zhou, J., Wu, Y., Yan, G., 2006. Generation of typical solar radiation year for China. Renewable Energy 31, 1972–1985. doi:10.1016/j.renene.2005.09.013

2. Uncertainty of DNI values

All data, whether measured or modeled, is uncertain. The uncertainty is important to quantify and account for in simulations and statistical analyses. Uncertainty should not be confused with the actual variability of the data. Here the uncertainties in various sources of DNI data are described and discussed.

The performance of a solar thermal electric (STE) facility is linearly dependent upon the Direct Normal Irradiance (DNI), the solar flux coming directly from the disk of the sun and the area immediately adjacent to the solar disk. Any uncertainty in the DNI leads to equivalent uncertainty in the estimated STE facility performance. There are two main sources of DNI resource information. One is measured with ground-based instruments and the other derived from models that utilize information from satellites. There are a wide variety of methods that utilize information from satellites and other sources to estimate the DNI resource. These methods range from models that use reanalysis data in which satellite and other measurements are combined with atmospheric models to estimate DNI (Daley, 1993) to more empirical models that rely on correlations of cloud cover data from satellite images and measured irradiance.

As with all measurements, the solar irradiance measurements are not exact and there are uncertainties associated with obtaining the DNI values. Before going into an analysis of the uncertainties associated with obtaining DNI values from ground-based measurements or from modeling satellite data, the characteristics and nature of uncertainties are discussed. The discussion on uncertainties will be followed by a detailed description of the uncertainties associated with ground-based and satellite-derived DNI values. The use of ground-based measurements to validate and/or adjust satellite-derived values is then examined. Characterization of differences between ground-based measurements and satellite-derived values can be used to reduce uncertainties and better quantify biases in satellite-derived DNI values.

2.1 Uncertainty in Measurements

All measurements have an ***uncertainty*** associated with the measurement. These uncertainties are dependent on the instruments used, the way the measurements are made, and the manner in which the measurements are recorded. For example, when one measures the length of a table a number of times, the results will likely vary slightly. If the same measurement is made by another person, the results will vary from the first observations because the tape measure may be read slightly differently or the perceived edge of the table may differ. If one uses a different tape measure, one could get a slightly different set of measurements because the tape measures may not match exactly. Other factors such as temperature may affect the measurement because the expansion rate of the tape measure will likely differ from that of the table.

In general, length can be measured with great accuracy, especially if lasers are used because the wavelength of light is used to define the standard meter and the wavelength of laser light can be measured to a very high degree of accuracy. Even these reference measurements have some associated degree of uncertainty as required by the fundamental Heisenberg uncertainty principle. The act of repeated measurements of any object will generate a set of values and in most cases, these values are randomly distributed and the set of data will form a Gaussian distribution around some average value. Conditions for data following the Gaussian distribution are given by the central limit theorem. The average or mean value is the sum of the measurement values divided by the number of measurements. The half-width of the Gaussian distribution is defined as one standard deviation and about 68% of the data points will be less than one standard deviation from the average value. Standard deviation is a measure of the spread of measurement values. It is the square root of the average of the squared differences from the mean. Approximately 95% of the measured values will fall within two standard deviations of the mean. Therefore one can characterize the probability that a measurement is within a given percentage of the mean value by examining the distribution of the measurements about the mean. This type of uncertainty is referred to as random uncertainty and helps define the likelihood that the measurement will be within a given uncertainty of the exact value.

Another type of uncertainty is exhibited by two different measuring devices. Consider the tape measure example. One tape measure might have a slightly different length scale than the other tape measure. The two different tape measures will then exhibit a bias compared to the other tape measure depending on the amount of the difference in the scale or markings on the two tape measures. The length from one tape measure will produce a longer or shorter mean distance as compared with the other tape measure. Part of this uncertainty is related to the precision on the distance markers on the tape measure and the other relates accuracy to which the tape measure can be read. These uncertainties are usually assigned to the tape measure and are not measured against a standard. Therefore the manufacturer will say that the uncertainty of the tape measure is ±2 mm and that information can be used when combining all the uncertainties.

To standardize the discussion of uncertainties and to set standards that provide guidelines for determining uncertainty and characterizing uncertainties, ***the Guide to Expressing Uncertainties in Measurements (GUM)*** was created (ISO, 2008). This document explains in detail the GUM terminology and explains how to perform uncertainty analysis using the GUM procedures. Several papers are now available evaluating irradiance measurements using the GUM methodology and the uncertainties discussed in this document are based on the GUM terminology (JCGM/WG 1, 2008).

The GUM model starts by defining the “measurand”, the quality that is being measured. The resulting measurement is an approximation or estimate of the measurand and a full description of the measurement includes the uncertainty of the measurement. In addition, other environment quantities that affect the measurement should be included. For example, the WRR calibrations are measurements of DNI made when DNI values >700 W/m2 under clear sky, stable weather conditions. Measurements are not exact and there are uncertainties in the measurements. Traditionally, errors are viewed as having two components, a random and a systematic component.

Random errors arrive from unpredicatable or stochastic temporal and spatial variations of quantities that influence the measurements. These variations are called random effects and result in the variations of repeated measurements of the measurand. Random errors can usually be reduced by increasing the number of measurements. The experimental standard deviation is a measure of the uncertainty of the mean resulting from random effects.

Systematic errors arise from a recognized effect that influences the measurements. The effect can be quantified and if it is significant in size, a correction factor can be devised and applied to compensate for the effect. The uncertainty in the correction factor is a measure of incomplete knowledge of the value required for the correction. The terms error and uncertainty should be used precisely and care should be taken to distinguish them.

The following is a sampling of possible sources of uncertainty in measurements from the GUM document.

a) Incomplete definition of the measurand;
b) Imperfect realization of the definition of the measurand;
c) Nonrepresentative sampling — the sample measured may not represent the defined measurand;
d) Inadequate knowledge of the effects of environmental conditions on the measurement or imperfect;
e) Measurement of environmental conditions;
f) Personal bias in reading analogue instruments;
g) Finite instrument resolution or discrimination threshold;
h) Inexact values of measurement standards and reference materials;
i) Inexact values of constants and other parameters obtained from external sources and used in the data-reduction algorithm;
j) Approximations and assumptions incorporated in the measurement method and procedure;
k) Variations in repeated observations of the measurand under apparently identical conditions.

The sources of uncertainty are not necessarily independent. In addition, unrecognized systematic effects can contribute to the error in the measurement.

The GUM methodology breaks the uncertainties into two Types, A and B. Both types are quantified by variances and/or standard deviations.

The Type A evaluation is calculated from series of repeated observations and is the familiar statistically estimated variance. The estimated standard deviation for Type A evaluations is sometimes called Type A standard uncertainty.

For the Type B evaluations, the variance is evaluated using available knowledge, for example the characteristics of the measuring device. This estimated standard deviation is sometimes called a

Type B standard deviation. For example, if the specifications for the pyrheliometer state that it has a temperature dependence of ±0.5%, then Type B standard deviation is ±0.5%.

The GUM methodology then adds the uncertainties by quadrature (this approach has to be modified if the uncertainties are covariant). Adding in quadrature is summing the square the numbers and taking the square root of the sum. An expanded uncertainty is then generated by a coverage factor to give the level of confidence that the measurement accurately represents the measurand. For example for a 95% confidence level, the coverage factor is approximate 2 (1.96). Given an expanded uncertainty with a 95% confidence level is equivalent to saying that 95% of the measurements will be within the expanded uncertainty of the measurand.

Before going into a more detailed description of measurement uncertainties, the effects of time scales on uncertainties should be mentioned. All irradiance data are for a given time period whether it is instantaneous or hourly, daily, or monthly average values. As the time scale increases, the uncertainty decreases because random uncertainties tend to average out and some bias uncertainties may be offset by other bias uncertainties with opposite effects. For example, many pyrheliometers that measure DNI have a responsivity (i.e. microvolts per W/m^2) that varies in a systematic manner over the day. The calibration used for the pyrheliometer to change the voltage reading into irradiance is commonly determined when the solar zenith angle is 45°. (The calibration value for a pyrheliometer is 1 divided by the responsivity.) When the sun is higher in the sky the responsivity might be slightly higher than when the sun in lower in the sky. Therefore, the uncertainty in the measurement will vary slightly over the day. If one takes the daily average, the daily uncertainty will be less because the overestimate may be when the sun is higher in the sky is offset by the underestimate when the sun is lower in the sky. This means that when one is talking about hourly uncertainties, the uncertainty will likely be greater than when one is talking about daily or monthly average uncertainties. Therefore, it is important to specify the time scale when giving an uncertainty of the measurements.

2.2 Ground-based DNI value uncertainties

Ground-based DNI measurements can be recorded virtually instantaneous or averaged over time periods from one-minute to daily. The most accurate DNI measurements are made with electrically self-calibrating absolute cavity radiometers (ACR) that compare the thermal heating of the DNI against a known electrical power used to heat the detector to the same temperature as the DNI. The ACR DNI measurements are used as reference values because electrical current can be measured to a much higher degree of accuracy than measurements of thermal energy. The internationally recognized standard for DNI is the World Radiometric Reference (WRR) developed and maintained by the World Radiation Center (WMO 2011). The WRR is a detector-based measurement reference defined by six radiometers comprising the World Standard Group (WSG). The WRR is known to ± 0.3% at the 99% level of confidence for DNI greater than 700 W/m^2 (WMO, 2011, Frohlich, 1978). This accuracy is achieved under stable clear-sky conditions. Periodically,

other ACRs are calibrated against this standard and they achieve accuracies, at the 95% level of confidence, in the range of ±0.36% to 0.40% (Reda, 2014). These calibrated ACRs and then used to calibrate other DNI measuring instruments. All certifiable calibrations of DNI measuring instruments can trace their calibrations to the WRR.

ACR's are very expensive and are not intended for field operation. Many ACRs do not provide a continuous time series and are not designed to work under unstable weather conditions. Few long-term data sets using ACRs are available. ACRs with the lowest uncertainties have an aperture open to the atmosphere. This allows moisture, dust, and insects to enter the device. Some ACRs come equipped with windows that allow the use of the instrument under all weather conditions. Alternatively one can build a shelter that closes at night or under conditions, such as rain, that would damage the instrument (Vuilleumier, 2014). ACRs with windows are said to have an uncertainty of ±0.5% (McArthur, 2005). These uncertainties are for instantaneous measurements and not averaged over time. All uncertainties mentioned in this section have are at the 95% level of confidence unless otherwise noted.

Besides the ACR instruments, there are four ways to obtain DNI values from ground-based measurements:

1. Field Pyrheliometers
2. Rotating Shadowband Irradiometers
3. Pyranometers with a shadow masks
4. Calculations using Global Horizontal Irradiance (GHI) and Diffuse Horizontal Irradiance (D_fHI)

In most cases there are many varieties of each type of DNI instrument. This chapter is a general overview and only specific information will be given for a limited number of instruments.

2.2.1 Pyrheliometers

Most field pyrheliometers consist of thermopiles-based detectors at the end of a collimation tube that has a window covering the aperture. Voltage generated by the thermopile inside the pyrheliometer is proportional to the incident solar irradiance. The aperture and the collimation tube provide an opening with a full angle of view between 5.0° and 5.7°. The size of the opening angle was determined help ensure that solar tracker pointing inaccuracies did not significantly affect the measurements (CIMO, 2008). Newer models of pyrheliometers have 5.0° field of view that matches the geometry of ACRs. Along with the light coming directly from the sun, some circumsolar irradiance is added to the DNI irradiance value. Many concentrating technologies cannot utilize the circumsolar irradiance and this has to be considered when employing measured DNI values for STE performance estimates (Blanc et al., 2014). The preferred calibration of a pyrheliometer is against an ACR that has calibration traceability to the World Radiometric Reference (WRR). In the

field a pyrheliometer can also be calibrated against another pyrheliometer that has its calibration traceable to the WRR. This method will result in a slightly larger estimated measurement uncertainty.

Thermopile-based instruments have a time constant associated with the time it takes for the instrument to reach thermal equilibrium. This time constant can vary from a few seconds to tens of seconds, depending on the thermal characteristics of the pyrheliometer. Clouds moving in front of the sun can drop the DNI very quickly. The pyrheliometer's response time can affect average DNI measurements for time spans of less than a minute or when comparing DNI values with DNI values obtain from photodiode based devices that have response times on the order of μseconds. Calibrations of thermopile pyrheliometers are best performed with stable sky conditions (conditions that do not change rapidly).

The sources and types of uncertainty for DNI measured by pyrheliometers are given in Table 2.1. Good record keeping enables one to keep track of the maintenance and calibration history of the

Source	Orgin of Uncertainty	Type of Uncertainty	Corrections Exist
Light source	Uncertainty in reference measurements	Type B	No
Instrument	Calibration	Type A and B	No
	Non-linearity of response	Type A and B	No
	Time of day	Type A	No
	Detector stability	Type A	Yes
	Temperature effects	Type A or B	Exists for some instruments
Maintenance	Soiling	Type B	No
	Moisture on window	Type B	No
Tracker	Alignment	Type B	No
Source	Orgin of Uncertainty	Type of Uncertainty	Corrections Exist
Light source	Uncertainty in reference measurements	Type B	No
Instrument	Calibration	Type A and B	No
	Non-linearity of response	Type A and B	No
	Time of day	Type A	No
	Detector stability	Type A	Yes
	Temperature effects	Type A or B	Exists for some instruments
Maintenance	Soiling	Type B	No
	Moisture on window	Type B	No
Tracker	Alignment	Type B	No
Measurement	Data logger	Type B	No

Table 2.1: Source of Uncertainty for Pyrheliometers. The A and B type of uncertainties are described in section 2.1.

instrument and any problems that occur while data is being gathered. Records should also include a site diagram to identify and characterize any obstruction affects the recorded DNI. Good locations have obstructions that are no more than 5° above the horizon.

For instantaneous measurements, the uncertainties for DNI measurements can be as low as 0.75% to 1.5%, but the uncertainty of even well maintained stations is estimated to be ±2.5% (Stoffel et al., 2010) as a result of many minor potential sources of uncertainty. Of course when instruments are not maintained or records of calibrations are absent, the uncertainty in the data can be much larger.

2.2.2 Rotating Shadowband Irradiometers

Rotating Shadowband Irradiometers (RSI) are instruments with one pyranometer measuring global horizontal irradiance (GHI) and diffuse horizontal irradiance (D_fHI) as a band (shadowband) that rotates in above the pyranometer to block the direct sunlight. Rotation periods are typically one-minute or shorter. When the sun is blocked, the D_fHI is measured. The direct horizontal irradiance (D_rHI) is then obtained by subtracting the D_fHI from the GHI (Eq. 2.1). The DNI value is then calculated by dividing the D_rHI by the cosine of the incident solar zenith angle (Eq. 2.2).

$$D_rHI = (GHI - D_fHI) \quad (2.1)$$

$$DNI = D_rHI/\cos(SZA) \quad (2.2)$$

where SZA is the solar zenith angle. When instantaneous measurements are used, this formula is exact. When the measurements of GHI and D_fHI (or equivalently D_rHI) are integrated over time, then the equation becomes an approximation because the SZA has to be averaged over the same time period and the average value of cos(SZA) is weighted by the changing D_rHI (Vignola and McDaniels, 1986).

There are two types of RSI. One type uses fast photodiode based pyranometers to measure the GHI and the shadowband swipes across the sensor in a continuous motion. Extensive evaluations have been made on this type of RSI (Stoffel et al., 2010; Wilbert et al., 2015a; Sengupta et al., 2016; Vuilleumier et al., 2014; Vignola, 2006). Another type, the Total Solar Radiometer (TST), has the shadowband that stops its rotation in three places during the sweep. The first is just before it shades the pyranometer, the second is when it is shading the pyranometer, and the third is when it has just finished shading the pyranometer. During the stops it is possible to calculate the portion of the D_fHI shaded of the shadowband. For RSI instruments with continuous rotations, the extra shading of the band is estimated during rotation. The slow speed and stopping of the shadowband allows a thermopile-based pyranometer with a quick response time to be used for measuring the irradiance. Because the shadowband stops while shading the pyranometer, a thermopile based pyranometer can be used. A recent study of radiometers (Habte et al., 2016) at NREL contains an example of a TST instrument.

The most common RSI being deployed are the instruments using photodiode-based pyranometers. The problem with photodiode-based pyranometers is that their output is dependent on the spectral distribution of the incident solar radiation. Of even more concern is that the responsivity of the pyranometer to the DNI spectral irradiance is different than the responsivity of the pyranometer to D_fHI spectral irradiance on clear and partially clear days. There have been several studies to characterize this spectral dependence and algorithms (Vignola, 2006; King et al., 1997; Wilbert et al., 2015a; Vignola et al., 2015) have been developed to account for the differences in the DNI and D_fHI spectral irradiances. Models have also been developed to account for the uncertainty effects of temperature and deviations from true cosine response.

Photodiode-based pyranometers do not fit specifications of the WMO for first-class instrument performance because of the dependence on the spectral distribution of the incident irradiance. They are widely used because they are relatively inexpensive and can produce results that are equivalent to second class pyranometer producing GHI values with uncertainties within ±5%. Photodiode-based pyranometers are used in RSI instruments because they have a quick response time on the order of μseconds. Algorithms have been developed to account for much of the spectral dependence and other shortcomings of the photodiode-based pyranometer.

Because of the similarity between the photodiode and the solar cell, some postulate that these pyranometers produce results that more directly mimic photovoltaic module output than thermopile-based pyranometers. This assertion has not been satisfactorily validated by peer reviewed articles. That said, algorithms have been developed that mimic the spectral and cosine response of the photodiode pyranometer and account for the thermal dependence of the instrument.

Often RSI instruments have been installed in remote locations or locations where the instruments are not maintained on a daily basis because acrylic diffusers can be more dust tolerant that optical glass domes or windows used by thermopile-based pyranometers to protect the detector. In the report of Maxwell et al. (1999) a list of papers that have studied this can be found. While the pyrheliometers on both manually adjusted and automatic solar trackers potentially have less uncertainty in the reported results when they are well maintained, they are more sensitive to the buildup of dust on the window resulting in scattering and absorption of DNI as it enters the pyrheliometer. Lack of maintenance allows the buildup of dust on the window that increases the uncertainty of the measurements and this can significantly reduce the measured DNI if the dust is not removed on a regular basis.

In RSI instruments, algorithms also account for the spectral differences between the DNI and D_fHI responsivities. Using these algorithms, DNI values produced using RSIs have been shown to have uncertainties of less than ±3.5% (Vignola, 2012). A list of factors involved in the uncertainties associated with RSI is shown in Table 2.2. The main concern about the adjustment algorithms is whether they apply as well in areas with atmospheric conditions that deviate significantly from the atmospheric conditions at the site(s) used to derive the adjustment algorithms. Specifically, this is the spectral or air mass adjustment. It has been shown that the spectral distribution on incident irradiance changes over the day in a systematic manner and that this affects the responsivity (and the output) of the photodiode based pyranometer. The change can be modeled as a function of air mass and this air mass adjustment is incorporated into the RSI adjustments (Vignola, 2006; King et al., 1997; Wilbert et al. 2015b; Vignola et al., 2015). Research is continuing to evaluate, validate, and possibly improve the algorithms used to adjust the RSI's GHI, DNI, and D_fHI values.

Source	Orgin of Uncertainty	Type of Uncertainty	Corrections Exist
Light source	Uncertainty in refrence measurements	Type B	No
Instrument	Spectral sensitivity	Type A and B	Yes
	Calibration	Type A and B	No
	Deviation from true cosine response	Type A	Yes
	Temperature effects	Type A or B	Yes
	Detector stability	Type A	Yes
	Non-linearity in response	Type B	No
Maintenance	Soiling	Type B	No
	Moisture on diffuser	Type B	No
	Leveling	Type B	No
Measurement	Data loggers	Type B	No

Table 2.2: Sources of Uncertainty for Rotating Shadowband Irradiometers

2.2.3 Pyranometers with Shadow Mask

Pyanometers with a shadow mask is a multi-sensor pyranometer that measures GHI and D_fHI and calculates D_rHI and hence DNI from the difference between the GHI and D_fHI measurements (see Eq. 2.1 and Eq. 2.2). The instrument that is currently available has seven small thermopiles distributed on the base of the instrument under a specially designed shield that shades half the sky and always permits at least one of the sensors to be totally unshaded and one sensor to be totally shaded. Since the shield obscures half the sky dome, the value obtained from the pyranometer that is totally shaded is doubled to estimate the D_fHI value.

There is one pyranometer with a shadow mask that has been subject to thorough testing, the SPN1. The SPN1 has no moving parts and the original documentation says that only needs to be mounted level. Comparisons with reference instruments show the DNI values have an uncertainty of about ± 8%. This uncertainty is dependent on the solar zenith angle and the cloudiness (Vuilleumier et al., 2014). The measurement of the D_fHI value is also off as the current use of the instrument assumes that the shield shades exactly 0.5 of the D_fHI. This is seldom true, especially under cloudless skies as the circumsolar D_fHI is significantly larger than that of the other parts of the sky.

Source	Orgin of Uncertainty	Type of Uncertainty	Corrections Exist
Light source	Uncertainty in reference measurements	Type B	No
Instrument	Spectral sensitivity	Type B	No
	Calibration	Type A and B	No
	Deviation from true cosine response	Type A	No
	Temperature effects	Type B	No
	Inter-thermopile variability	Type B	No
	Detector stability	Type B	Yes
	Non-linearity in response	Type B	No
Maintenance	Soiling	Type B	No
	Moisture on dome	Type B	No
	Leveling	Type B	No
Measurement	Data loggers	Type B	No

Table 2.3: Sources of uncertainty for pyranometers with shadow mask

Uncertainties associated with an SPN1 instrument are listed in Table 2.3. It has been suggested that the SPN1 does not fulfill the requirements for pyranometers from the WMO because of the spectral transmittances of the diffusors and glass dome (pers. comm. Wilbert 2016). A problem seen with this instrument is that the thermopiles responsivities vary from one thermopile to another. Because there is a limit to which a thermopile can be calibrated, reading will vary when the thermopile used in the measurement is changed from one thermopile to another. Calibration of the instrument can be another problem because there are several sensors. It would be very difficult to calibrate each sensor without removing the dome and shade. In addition, the responsivity of thermopile sensors degrades over time of depending on the amount of incident irradiance over time. It is not clear if each sensor's performance would deteriorate at the same rate as certain sensors may receive more irradiance than others.

Another issue may happen if the cloud formation is not uniform and the shield blocks a different portion of the sky when the sensors are switched. This can be a particular problem when there are clouds near the sun that reflect additional sunlight onto the sensors.

As more in learned about SPN1 performance, the development of measurement adjustment algorithms continues. This would require that the SPN1 be sited in a specific azimuthal direction so that a uniform set of adjustment algorithms can be derived. The idea of having an instrument with no moving parts that can measure DNI, GHI, and D_fHI certainly has a lot of appeal. Three recent studies (Vuilleumier et al., 2014; Habte et al., 2016; Badosa et al., 2014) present detailed analysis of uncertainties associated with SPN1 instruments.

Instrument Model	Sky Condition	SZA Range	17° to 20°	20° to 30°	30° to 40°	40° to 50°	50° to 60°	60° to 70°	70° to 80°	80° to 85°
TSR-590LH	Clear		0.52	0.51	0.24	0.73	0.67	0.23	-1.90	-8.32
	Mostly cloudy		-9.65	-5.04	-4.50	-0.37	-0.96	-0.27	-0.15	-4.13
SPN1	Clear		-0.77	-2.30	-1.83	-1.49	0.44	2.22	8.43	13.84
	Mostly cloudy		32.59	30.01	27.13	27.48	35.48	39.37	40.73	35.67
RSR2	Clear		0.05	0.05	-0.52	-0.36	0.37	0.53	0.85	2.92
	Mostly cloudy		-23.68	-36.21	-37.09	-33.69	-39.54	-41.04	-49.59	-50.76
NIP	Clear		0.05	0.18	0.52	0.04	0.24	0.99	0.80	1.92
	Mostly cloudy		6.82	11.59	12.85	10.73	10.28	18.88	11.10	11.81

Table 2.4. Hourly Average MBE in Percent under Various Solar Zenith Angle Ranges for DNI Data from Habte et al., 2016

A comparison of instruments at the National Renewable Energy Laboratory Solar Radiation Research Laboratory (NREL SRRL) has a comparison of a variety of instruments used to measure DNI (Habte et al., 2016) (see Table 2.4). Table 2.4 is a selection of instrument typed used to measure DNI from the study (Habte et al., 2016) compared against a Kipp & Zonen CHP1 pyrheliometer that has a 95% uncertainty of 0.7%. These instruments are run on a regular basis at SRRL and provide a good comparison of instruments that are well maintained. The hourly averaged Mean Bias Error (MBE) given in percent separated into SZA ranges and under clear and cloudy conditions. Note this is not the standard error but the MBE. Under clear skies, the MBE is small and increases with larger SZA. Under mostly cloudy conditions, the MBE is large, mainly because the DNI is relatively small and any uncertainty in the DNI measurements is large in comparison. Passing clouds, location of instruments, how the measurements are obtained, and the response time of the sensor all contribute to this difference. In addition, the measurements with differences greater than 100% from the reference instrument were eliminated from this analysis. The weather characteristics during the month will determine the monthly MBE. The more clear periods, the smaller the MBE.

2.2.4 Uncertainty in DNI values obtained from GHI and D_fHI data

As shown in Eq. 2.1 and Eq. 2.2, DNI can be calculated from GHI and D_fHI data, either from ground-based measurements or modeled from satellite data.

On an instantaneous basis, this is an exact equation. If longer time interval data is used, then a weighted average of the cosine is required and the equation becomes an approximation. During the middle of the day, when the SZA is not changing rapidly, this is a good approximation, but in the morning or evening hours, the uncertainty increases. If the GHI and D_fHI measurements have the same magnitude and the same uncertainty, adding them in quadrature yields a combined uncertainty that is about 40% greater than either the GHI or D_fHI values. In addition, the uncertainty generated by the use of Eq. 2.1 and Eq. 2.2 can add a percent or two, depending on the time interval and time of day. However, under clear skies, the GHI value is usually much greater than the D_fHI value and the uncertainty of the D_rHI value is only slightly greater than the uncertainty of the GHI value. Of course the D_rHI value is divided by the cosine of the solar zenith angle to get the DNI value, and small uncertainties can be magnified when the solar zenith angle is large (this means the cosine of (SZA) is small).

Uncertainties are quoted here as percentages, but the measurement also has uncertainties that don't scale. For example, a thermopile pyranometer can have a thermal offset, that is, the hot junctions radiate to the cold sky. Several second class thermopile-based pyranometers that are often recommended for use in D_fHI measurements have alternating black and white surfaces and do not have this thermal offset problem. If the GHI instrument has a thermal offset and the DfHI instrument does not, then the effect of the thermal offset can be significant when the difference is used to calculate DNI values. When the GHI and D_fHI values are close, any uncertainty in the values can have make significant differences in the calculated DNI values. This is particularly true in the morning or evening hours where the cosine is small and even a small difference can result in large uncertainties in the DNI value.

The uncertainties in the DNI values calculated from GHI and D_fHI are dependent on the difference in the GHI and D_fHI values, the time of day when the measurements are made, and the uncertainties in the GHI and D_fHI measurements themselves. Therefore, giving a percentage uncertainty for short-term measurements (1 minute to 1 hour) can vary significantly depending on the circumstances. However, when one is concerned with daily or monthly averages the uncertainties can be significantly reduced because instrument calibrations and design are typically designed to give good average results and uncertainties under one circumstance is often balanced out by an opposite uncertainty in another instance.

The comments so far in this section can also be applied to RSI and SPN1 instruments because the DNI obtained from those instruments are calculated from the GHI and D_fHI measurements.

Older D_fHI measurements are often made using a fixed shadowring the blocks the sun as the earth rotates and the sun appears to across the sky over the day. The adjustments made to account for the shading of the sky blocked by this shadowring are large (5 to 20%) and the uncertainty in the D_fHI values obtained from the data after the adjustments can also be a comparable in size to this adjustment, especially under clear and partially cloudy skies. Therefore the DNI values calculated using D_fHI measurements using shadowring have large uncertainties and diffuse measurements obtained from using a fixed shadowring are not reliable for DNI estimates.

2.3 Uncertainties in satellite derived values

There are a variety of ways to obtain estimates of surface solar irradiance values from satellites observations and other meteorological measurements. The basis for any modeling of solar irradiance data is the ability to accurately estimate the irradiance during cloudless periods. The uncertainty in the modeled GHI values is not as sensitive to the aerosol scattering as the DNI values because the scatter by aerosols tend to be in the forward direction and this increases the D_fHI in a somewhat circular pattern around the solar disk. The D_fHI around the sun adds to the GHI values and this compensates for the loss caused by aerosols on DNI. The circumsolar D_fHI component transform to the horizontal contribution to GHI much as the DNI does by multiplying by the cosine of the incident zenith angle. Therefore, much of the uncertainty caused by errors in the aerosol estimates on DNI estimates are partially offset by the opposite effect on the circumsolar D_fHI component. For DNI estimates it is important to accurately know the optical properties of aerosols and other atmospheric constituents that scatter the irradiance coming directly from the solar disk. The inherent optical properties are: The optical thickness, the single scattering albedo and the normalized volume scattering function. All these values depend on wavelength. They are best estimated from AERONET ground based stations (Holben et al., 1998).

There are three basic ways to estimate surface irradiance from satellite images. The first is to use radiative transfer models and cloud cover information that is part of the reanalysis methodology used for climate studies. These are called physical models and this method has been used for the NASA/SSE irradiance database (Sengupta et al., 2015). The empirical approach is based on statistical and correlation methods to model the irradiance from satellite images using ground-based measurements to determine the parameters and validate the model. Currently the best models use a combination of both approaches to take advantage of the physical information being gathered from satellites (Polo et al., 2015, 2016).

One has to remember that satellite images cover a specified area ranging from a few to hundreds of square kilometers and are not a point source measurement like ground base measurements. The resolution of satellite images are more accurately expresses in degrees of longitude and latitude, for example a grid of 0.1 degrees. In addition, the satellite images are taken periodically, at fifteen to sixty minute intervals. Therefore, when one compares the satellite-derived to ground-based measurements it is not a direct one to one comparison. There will be differences in the

values because are made from different perspectives with respect to the solar collector. If ground-based measurements and satellite models used to estimate DNI were exact, there would still be differences in the results due to the observational disparity of the measurements (i.e. looking up from a point-source collector location vs. viewing a surface area from space). The uncertainty associated with this disparity will decrease with the increase in the comparison period. For example, hourly comparisons will have much larger uncertainties as compared to monthly average differences. Therefore, the period of the data should be specified when the uncertainty is described, especially for satellite derived data.

Sources of uncertainty for satellite derived data:

I. The space borne instruments cannot be calibrated in the way that ground-based instruments are. Drift in the different spectral channels occurs. See [Doelling, 2004] the report on the calibration procedure and results for the MSG SEVIRI instrument. Contamination occurs due to moisture from the satellite. Decontamination is typically performed by heating the optical cold parts in the winter season. During the decontamination the backup MSG satellite at 9.5 degrees East is used. This can cause offsets in the images;
II. At low solar zenith angles high clouds cast shadows upon lower clouds that can be misinterpreted as cloud free areas;
III. At low viewing angles a parallax effect occurs, where the apparent cloud position is different from the actual cloud position;
IV. Sub-grid scale clouds, for instance cumulus humilis, are not resolved in the current geostationary satellite images;
V. Fresh snow on the ground beneath clouds cannot be recognized in the satellite data before clear sky conditions occur. This leads to temporary overestimations of cloud optical thicknesses or cloud indices.

The uncertainty in the satellite derived data used for the National Solar Radiation Data Base (NRSDB) created by NREL is approximately 8% for monthly average GHI values and 10% for monthly average DNI values. Commercial entities claim that they can reduce this uncertainty even further. In reality, the uncertainty varies by local climate and ground conditions and the cloud sky index during the month. This is a problem with expressing uncertainties in percentage. The uncertainty during the sunniest months may be exactly the same as the uncertainty during the cloudiest month but the percentage uncertainty would be significantly different (Sengupta et al., 2015; Ineichen et al., 2014).

As discussed earlier much of the difference and hence uncertainty in the satellite derived DNI data results from the difference in the type of measurements. During some hours and some days, the difference may be 100%. However, models using satellite data often incorporate statistical factors so that the statistics of satellite data sets match statistics of ground-based measurements. For

example, satellite data that is measured at 15 minutes after the hour is adjusted to represent irradiance values on the hour so that the irradiance and other meteorological data have the same time stamp. When doing these adjustments one has to keep in mind that the variability of the resource on an hourly time scale is not smoothed by the averaging and shifting process.

Studies reporting overall bias can be misleading. For example, one study reports that the bias of a certain model is -2% in the DNI value while the random error is 25% for the DNI. This was a comparison with data from 18 stations. More indicative of the accuracy of the model would be the standard error or the biases for all stations at the 50 or 95% level. A better measure would be the standard error for the bias for each month. This way one could determine that the bias was less than x for a 95% of the time. This would build confidence that the long-term DNI irradiance was at a given level.

As a simple example, half-hourly values of DNI measured at four stations in the Pacific Northwest during 2006 (2012 for Seattle) were compared to satellite-derived values modeled by NREL. The results are shown in Table 2.5. The statistics are for periods when the GHI is above zero. This doesn't have much of an effect on the % bias but could increase the % standard deviation because the average DNI is reduced if the nighttime values are taken into account. It is suspected that the data from the Seattle station had problems because the comparison between the ground-based Seattle DNI and the satellite derived DNI show two distinct patterns during clear periods. The Seattle DNI is not included in the discussion of bias, but was left in to illustrate the fact that **satellite-derived data can spot problems with ground-based measurements.**

Averaging the bias for the three other sites gives the appearance that the model has a bias on average of 2.6%. However, the range of bias is from -0.8 to 9.5%, depending on the station. The three sites are used as an illustration that one needs to look at the range of biases of the individual sites and not the average of the ensemble. The average standard deviation is 46%, but ranges from around 40% to 54%.

Further care must be taken when comparing ground-based data and satellite-derived estimates because there are obstacles on the horizon that can block DNI and hence result in substantial difference in the morning or evening hours when the obstacles are more likely to block the direct sunlight. In the comparison, no effort was made to eliminate periods when the obstacles effected the measurements.

Location	DNI Bias	DNI St. Dev.	DNI Bias	DNI St. Dev
	(W/m^2)	(W/m^2)	%	%
Seattle, 2012	39.8	143.9	17.3	62.4
Twin Falls, 2006	-3.7	179.5	-0.8	39.7
Eugene, 2006	31.5	148.1	9.5	45.0
Dillon, 2006	-3.2	217.9	-0.8	54.0

Table 2.5: A sample comparison of DNI mean bias and standard deviation for four locations.

One word of caution should be given when using DNI estimates from satellite observations. DNI data has a statistical characteristic besides an annual or monthly average. Figure 2.1 shows a comparison between DNI from a ground-based measurement against the DNI from a satellite-model for one year. The fit seems fairly reasonable given the uncertainties in the data and the different viewing perspectives of the two sources of DNI values. However, if one plots k_b (DNI divided by the equivalent extraterrestrial DNI) against k_t (GHI divided by the equivalent extraterrestrial GHI) the range and distribution does not match what is seen when this is done with ground-based measurements (see Figure 2.2). This discrepancy can affect the operational design of the facility and therefore illustrates the value of good ground-based data.

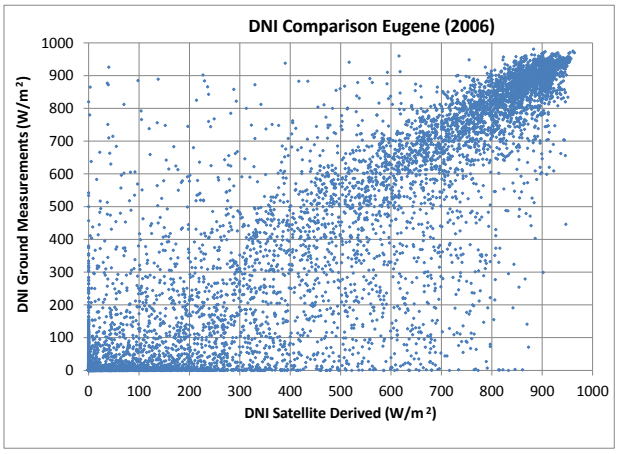

Figure 2.1. DNI comparison between ground-based measurements and satellite-derived values for half hourly data from Eugene, Oregon in 2006.

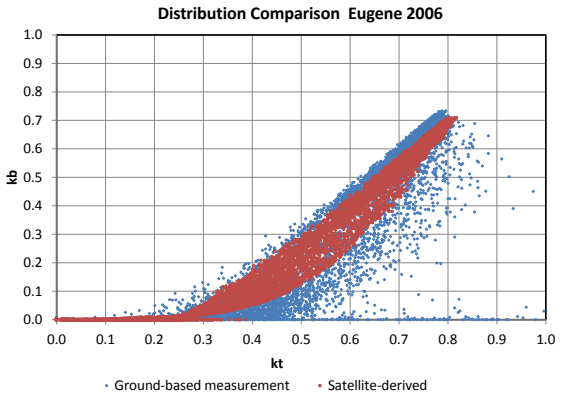

Figure 2.2: Plot of k_b verse k_t for ground-based measurements and satellite-derived values. Ground-based data near zero for $k_t > 0.6$ is probably associated with obstacles on the horizon.

2.3.1 Combining data from different satellites

In order to get long periods of solar irradiance it is necessary to model the irradiance from two or more satellites. Meteorological satellites have a finite lifetime and new satellites replace the older satellites as they fail or are taken out of service. Newer satellites often have new and improved equipment and the quality and frequency of the images and associated measurements are enhanced. Unless the two satellites are run side by side, it is often difficult to smoothly transition to the new data set with its own performance characteristics. Continuity is essential and considerable effort goes in to minimizing any bias between the two sets of data. However, this transition always engenders some uncertainty especially with sensors whose performance changes with time.

The uncertainty of DNI data derived by satellite is often quoted at ±15% [Perez, 2002], but can vary considerably from site to site and model to model. This number can be reduced to about ±8% is ground-based DNI data are available to validate and train the models. This percentage is some-

what misleading in that during the sunniest months the percent uncertainty is usually much less than during the months with the most clouds.

2.3.2 Biases and uncertainty associated with adjusting satellite-derived DNI based on ground measurements

Estimating the performance of satellite-derived DNI can be challenging for locations different from those used to develop and validate the model. These values are obtained from comparison of satellite-derived modeled estimates and ground-based measurement made at a variety of locations. Specific sites may have more or less issues than the general situation. Only by comparison with near-by ground-based measurements can one obtain a better idea of the quality of the satellite-derived values.

With properly installed and well maintained equipment to provide ground-based DNI measurements, most systematic problems with satellite-derived DNI values can be quantified and characterized. This information can be used to adjust the satellite-derived DNI data to improve the statistical characteristics of the data and reduce the uncertainty and bias in the values.

Ground-based histograms of short interval DNI values (hourly or shorter time interval) for monthly or seasonal values show a two peak distribution. One peak is during clear sky periods and the other peak is when the sky is totally cloud covered. An example is shown in Figure 2.3. The value of the clear sky peak is dependent on the atmospheric constituents and comparison between ground-based and satellite-derived DNI distribution can provide verification that the atmospheric constituents used in the model are appropriate. It is important that any problem data be removed from the ground-based measurements because they are to be used a reference data and any problems with the reference data will then propagate through the adjustment procedures. Problems seen with ground-based measurements are misalignment, dirt or moisture on the optics, and potential calibration issues. In addition to similar maintenance-related issues, the DNI data from an RSI **must be properly corrected for pyranometer response characteristics consistent with the measurement location**.

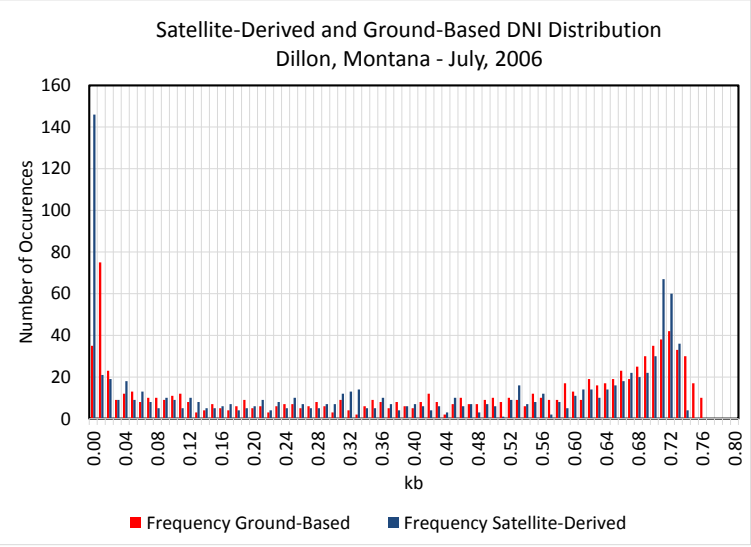

Figure 2.3. Histogram of half hourly satellite-derived and ground-based DNI for Dillon, Montana – July 2006.

The satellite-derived DNI values can sometimes identify and tracking problems with the ground-based DNI data. This is especially true if there is an alignment problem that gets worse with time or dirt buildup on the instrument. However, satellite-derived values are not as useful for spotting short term problems because of the inherent difference between the field of view of the satellite images and the instruments on the ground.

The monthly average and the distribution of data shown in Figure 2.3 are close enough to validate the satellite-derived data for the location in July. Other months should also be examined. The distribution differences at the low end don't affect the CSP/STE production because so little DNI is available for use. The distribution under clear sky conditions may not affect the average DNI, but the difference can be important for the facility operation. The ground-based measurements suggest that there is a wider range of values under clear skies and that the maximum irradiance values are 3% higher than the maximum indicated by the satellite-derived values.

Note that the clear sky distribution is often difficult to duplicate with models using satellite information because the available model input data lack the temporal and spatial resolution needed to estimate the short term variability of the atmosphere. It is these small differences in atmospheric conditions that give the broader range of the ground measured data.

The discussion on adjusting satellite-derived DNI values assumes that the ground-based DNI measurements have had any systematic problems removed. If the comparison between satellite-derived and ground-based values is off by more than a few percent, adjustments can be made to the satellite-derived data. It would be simple to just multiply the estimated by a few percent to make the two data set agree. However, other factors must be first considered. These factors include the height and width of the clear sky distribution peak and the DNI distribution peak near zero W/m^2. If these values are significantly different, then the simple percentage shift is likely lead to misleading results. For example, snow cover can sometimes be mistaken for clouds and vice versa. It is possible that the number of mistaken cloudy and clear periods under snowy conditions are the same and the overall average DNI is correct, however, it can be the case that the number of mistakenly identified cloudy periods and clear periods are significantly different and a bias in the DNI value will result. Comparison with ground-based measurements can determine the bias or frequency of such occurrences and adjustments can be made based on this information. In addition, snow cover limits the dynamic range of the image that interprets the amount of cloud cover. This can either narrow or widen the widths of the peaks in the histograms.

What is learned by these comparisons can lead to adjustments that can then be applied to the satellite-derived DNI values. These adjustments can improve the satellite-derived estimates and reduce the uncertainty of the resulting DNI values. More important, it can significantly reduce any bias in the satellite-derived data.

Often the ground-based data comes from a station that is not at the location chosen for the solar electric facility. The adjustments to the satellite-derived DNI values at the site with the ground-

based irradiance data can then be applied to the satellite-derived DNI values at the location for the potential facility. Again this reduces some of the bias and uncertainty in the satellite-derived DNI values at the site of interest. More research is needed to develop, evaluate, and standardize methodologies that adjust satellite-derived irradiance values to statistically match ground-based measurements.

2.4 Summary

Measurements are an estimate of the quantities being measured and a complete description of the measurement includes the uncertainty of the measurements and a listing of conditions under which the measurements were done. The GUM methodology was used in evaluation of the DNI uncertainties.

DNI measurements using thermopile-based pyrheliometers

- Produces the smallest uncertainties assuming instruments well maintained and soiling and alignment are not a problem
- If one uses an automatic tracker on which GHI and D_fHI measurements are also made, a three component test can be used to validate the DNI measurements

DNI measurements using a RSI instrument using photodiode pyranometers

- Correction algorithms must accurately account for the effects of the different spectral irradiance distributions of the DNI and D_fHI.
- Correction algorithms likely differ depending on the water vapor and aerosol loads in the atmosphere. Research is needed to determine the magnitude of this effect.
- Longer times between cleaning may be possible because soiling on the lens appears to be less of a problem than on thermopile-based pyrheliometers.

DNI measurements using pyranometers with shadow masks

- No correction methods have been developed to remove systematic errors.
- Larger uncertainties than RSI instruments.
- No moving parts.

DNI derived from models based on satellite and/or meteorological measurements

- Different perspective than ground-based measurements
- Validated against ground-based measurements
- Lack short interval DNI measurements (one to five minute)
- Provides near worldwide coverage
- Provides long-term DNI estimates created in a fairly consistent manner
- Can be used to identify inconsistencies in ground-based DNI measurements
- As satellite capabilities improve and enhanced models are developed, uncertainties in satellite-derived DNI values are expected to decrease

Satellite-derived and ground-based measurements can be combined to reduce the uncertainty in long-term DNI resource assessments.

2.5 References

Badosa, J., J. Wood, P. Blanc, C. N. Long, L. Vuilleumier, D. Demengel, M. Haeffelin, 2014. Solar irradiances measured using SPN1 radiometers: uncertainties and clues for development, Atmospheric Measurement Techniques, 7(12), 4267–4283, doi:10.5194/amt-7-4267-2014.

Blanc, P., B. Espinar, N. Geuder, C. Gueymard, R. Meyer, R. Pitz-Paal, B. Reinhardt, D. Renné, M. Sengupta, L. Wald, S. Wilbert, 2014. Direct normal irradiance related definitions and applications: The circumsolar issue, Solar Energy, 110, 561–577.

Daley, R., 1993. Atmospheric Data Analysis, Cambridge University Press. Cambridge University Press. Atmospheric and Space Science Series, New York, NY, USA.

Doelling, David R., Patrick Minnis, Louis Nguyen, 2004. Calibration Comparisons Between SEVIRI, MODIS and GOES Data, MSG-RAO Workshop, Salzburg, Austria 2004.

Fröhlich, C., 1978: World Radiometric Reference, Annex to Recommendation 3 (CIMO-VII). Abridged Final Report of the Seventh Session of the Commission for Instruments and Methods of Observation, Hamburg, 1-12 August 1977, World Meteorological Organization, WMO-No. 490, 7bis Avenue de la Paix, Geneva, Switzerland, 97–100.

Habte, A., Manajit Sengupta, Afshin Andreas, S. Wilcox, T. Stoffel, 2016. Intercomparison of 51 radiometers for determining global horizontal irradiance and direct normal irradiance measurements, Solar Energy, Volume 133, August 2016 pgs. 372-393.

Holben, B. N., T. F. Eck, I. Slutsker, D. Tanré, J. P. Buis, A. Setzer, E. Vermote, J. A. Reagan, Y. J. Kaufman, T. Nakajima, F. Lavenu, I. Jankowiak, A. Smirnov, 1998. AERONET—A Federated Instrument Network and Data Archive for Aerosol Characterization. Remote Sens. Environ. 66, 1–16.

Ineichen, P., 2014. Long term satellite global, beam and diffuse irradiance validation, Energy Procedia, 48(0), 1586 – 1596, doi:http://dx.doi.org/10.1016/j.egypro.2014.02.179.ISO. (2008). Guide 100-2008: Evaluation of Measurement Data—Guide to the Expression of Uncertainty in Measurement. Comité International des Poids et Mesures. www.bipm.org/utils/common/documents/jcgm/JCGM_100_2008_E.pdf.

ISO/IEC (2008), ISO/IEC Guide 98-3: Uncertainty of measurement - Part 3: Guide to the expression of uncertainty in measurement (GUM:1995),

JCGM/WG 1: Working Group 1 of the Joint Committee for Guides in Metrology, 2008. Evaluation of measurement data – Guide to the expression of uncertainty in measurement, http://www.bipm.org/en/publications/guides/gum.html

King, D., J. A. Dratochvil, W. E. Boyson, 1997. Measuring Solar Spectral and Angle–of–Incidence Effects of Photovoltaic Modules and Solar Irradiance Sensors. *In* 26th IEEE Photovoltaic Specialists Conference, Sept. 29-Oct. 3, 1997, Anaheim, California.

Maxwell, E.L, Wilcox, S.M., Cornwall, C., Marion, B., Alawaji, S.H., Mahfoodh, M., AL-Amoudi, A., 1999. Progress Report for Annex II – Assessment of Solar Radiation Resources in Saudi Arabia 1993-1997. NREL/TP-560-25374. Golden, CO: National Renewable Energy Laboratory.

McArthur L. J. B., 2005: Baseline Surface Radiation Network (BSRN). Operations Manual. Version 2.1. WCRP-121, WMO/TD-No. 1274, http://hdl.handle.net/10013/epic.39582.d001.

Perez, R. , Pierre Ineichen, Kathy Moore, Marek Kmiecik, Cyril Chain, Ray George, Frank Vignola, 2002, A new operational model for satellite-derived irradiances: description and validation, Solar Energy, Vol. 73, 5, pgs. 307-317.

Polo, J., S. Wilbert, J. A. Ruiz-Arias, R. Meyer, C. Gueymard, M. Šúri, L. Martín, T. Mieslinger, P. Blanc, I. Grant, J. Boland, P. Ineichen, J. Remund, R. Escobar, A. Troccoli, M. Sengupta, K. P. Nielsen, D. Renne, N. Geuder, 2015. Integration of ground measurements to model-derived data. IEA Report from SHC Task 46: Solar Resource Assessment and Forecasting.

Polo, J., S. Wilbert, J. A. Ruiz-Arias, R. Meyer, C. Gueymard, M. Šúri, L. Martín, T. Mieslinger, P. Blanc, I. Grant, J. Boland, P. Ineichen, J. Remund, R. Escobar, A. Troccoli, M. Sengupta, K. P. Nielsen, D. Renne, N. Geuder, T. Cebecauer, 2016. Preliminary survey on site-adaptation techniques for satellite-derived and reanalysis solar radiation data sets, Solar Energy, 132, 2016, pgs. 25-37.

Reda, I., M. Dooraghi, and A. Habte, 2014. NREL Pyrheliometer Comparisons: September 22–26, 2014 (NPC-2014) NREL/TP-3B10-63050 *in* Sengupta, M., A. Habte, S. Kurtz, A. Dobos, S. Wilbert, E. Lorenz, T. Stoffel, D. Renné, C. Gueymard, D. Myers, S. Wilcox, P. Blanc, R. Perez, 2015. Best Practices Handbook for the Collection and Use of Solar Resource Data for Solar Energy Applications Technical Report NREL/TP-5D00-63112.

Sengupta, M., A. Habte, S. Kurtz, A. Dobos, S. Wilbert, E. Lorenz, T. Stoffel, D. Renné, C. Guymard, D. Myers, S. Wilcox, P. Blanc, R. Perez, 2015. Best Practices Handbook for the Collection and Use of Solar Resource Data for Solar Energy Applications, NREL/TP-5D00-63112, National Renewable Energy Laboratory, Golden, CO, USA.

Schmidt, T., B. Kraas, R. Affolter, Prof. Dr. N. Geuder, Rotating Shadowband Irradiometer (RSI): Accurate Measurement of Direct Normal, Global and Diffuse Irradiance with a Single Device Sensor head with silicon photodiodes Rotating shadowband Motor drive

Stoffel, T., D. Renné, D. Myers, S. Wilcox, M. Sengupta, R. George, C. Turchi, 2010. CONCENTRATING SOLAR POWER Best Practices Handbook for the Collection and Use of Solar Resource Data NREL/TP-550-47465.

Vignola, F., D. K. McDaniels, 1986. Beam-Global Correlations in the Pacific Northwest, Solar Energy

36, 409.

Vignola, F., 2006. Removing Systematic Errors from Rotating Shadowband Pyranometer Data, Proc. of the 35th ASES Annual Conference, Denver, CO, USA.

Vignola, F., J. Michalsky, T. Stoffel, 2012. Solar and Infrared Radiation Measurements, CRC Press, Boca Raton, Florida, USA

Vignola, F., Z. Derocher, J. Peterson, L. Vuilleumier, C. Félix, J. Gröbner, N. Kouremeti, 2015. Effects of changing spectral radiation distribution on the performance of photodiode pyranometers. Submitted to Journal of Solar Energy.

Vuilleumier, L., M. Hauser, C. Felix, F. Vignola P. Blanc, A. Kazantzidis, B. Calpini, 2014. Accuracy of Ground Surface Broadband Shortwave Radiation Monitoring, JGR: Atmosphere, DOI: 10.1002/2014JD022335.

Wilbert, S., N. Geuder, M. Schwandt, B. Kraas, W. Jessen, R. Meyer, B. Nouri, 2015a. Best Practices for Solar Irradiance Measurements with Rotating Shadowband Irradiometers, IEA Solar Heating & Cooling Programme (SHC) Task 46 Solar Resource Assessment and Forecasting. http://task46.iea-shc.org/data/sites/1/publications/INSRSI_IEA-Task46B1_BestPractices-RSI_150819.pdf

Wilbert, S., S. Kleindiek, B. Nouri, N. Geuder, A. Habte, M. Schwandt, F. Vignola, 2015b. Uncertainty of Rotating Shadowband Irradiometers and Si-Pyranometers Including the Spectral Irradiance Error. In SolarPaces 2015 proceedings, Cape Town, South Africa.

WMO - World Meteorological Organization, 2011. International Pyrheliometer Comparisons XI, 27. Sep - 15. Oct 2010, Davos, Switzerland. WMO IOM Report No. 108

3. Auxiliary meteorological data needed for CSP/STE performance simulations

Direct normal irradiance is the primary variable with respect to CSP/STE performance simulations. Other meteorological CSP/STEvariables are also importance. Here these are described with a focus on the user needs.

3.1 Synoptic meteorological observations

Since the end of the 19th century meteorological observations have been shared between the countries of the World. This was done first in the framework of the International Meteorological Organization following the suggestions of Buijs-Ballot (1872), and since 1950 in the framework of ***the World Meteorological Organization (WMO)***. Today meteorological observations from land-based stations, radiosondes, ships, buoys, aircrafts and satellites are shared continuously in real time between the national meteorological services (WMO, 2005). WMO maintains and updates guidelines for meteorological instruments and observations (WMO, 2010). WMO is recognized as an international standardization body by the International Standardization Organization (WMO & ISO, 2008).

Figure 3.1. A synoptic weather station (WMO 06090). Instruments for measuring wind speed and direction are located on the 10-meter boom. Instruments for measuring temperature, humidity and global horizontal irradiance (GHI) are located on the 2-meter boom. At other stations GHI is measured on a separate post.

In Figure 3.1 a typical synoptic weather station can be seen. On the two booms at specific heights the following measurements are performed:

- Wind speed [m/s] (10 meters above the ground)
- Wind direction [degrees clockwise from true north] (10 meters above the ground)
- Temperature [K] (2 meters above the ground)
- Relative humidity [%] (2 meters above ground).

Due to the vertical gradients of these meteorological variables the heights of these measurements are important. Not all temperatures are measured at 2 meters height, and not all winds are measured at 10 meters height. In particularly regarding wind data, it is important to check the actual height of the measurements. For the temperature the dry adiabatic lapse rate is 0.0097-0.0098 K/m. The lapse rate is the negative of the derivative of the temperature with respect to height. For moisture saturated air the adiabatic lapse rate is approximately half of the dry adiabatic lapse rate. How to estimate winds at different heights than the measurement height, e.g. at the height of heliostats, parabolic troughs or central towers, will be explained in section 3.3.

Other measurements and observations at a typical weather station include (WMO 2010):

- Cloud amount [oktas]
- Cloud type
- Cloud base height [m]
- Visibility [m]
- Atmospheric pressure [hPa]
- Precipitation [mm]
- Snow cover [kg/m^2]
- Global horizontal irradiance [W/m^2] or radiant exposure [J/m^2]
- Soil temperature [K]
- Evaporation [mm]

Of these the cloud type and snow depths are always determined from manual observations, and cloud amount, cloud base height and visibility are sometimes determined from manual observations, but mostly from measurements. Surface observations of cloud amount and cloud type can be used to improve satellite-derived irradiances (see section 2.3), since the geostationary satellite images have to coarse resolution to resolve these variables.

3.2 Lower atmospheric aerosol extinction

For central receiver CSP/STE plants, the aerosol extinction between the heliostats and the central tower is important for the performance simulations. This can be estimated from visibility measurements.

Visibility is mostly measured with forward scattering visibility meters as the one shown in Figure 3.2 at WMO stations. These are originally designed to detect fog situations that can cause problems in road, sea and air traffic. These instruments are designed for water particles that, unlike most aerosols, have strong forward scattering phase functions and virtually no absorption. Thus, the visibility measurements cannot be directly used for aerosol extinction. Recently, a correction method has been developed for the scatterometers by Hanreider et al. (2015; 2016). They also study transmissometer data for this purpose, which needs less correction than the scatterometer data, since transmissometers measure the transmittance directly.

Figure 3.2. A forward scattering visibility meter (WMO station 06041).

A subset of the synoptic meteorological measurements is shared between the national weather

services. Typically, this subset includes measurements with hourly or 3-hourly resolution that are distributed at the main synoptic times 0 UTC, 6 UTC, 12 UTC and 18 UTC. The national weather services themselves will often store the measured data at 10 minute resolution. The availability of the measurements to companies and the general public varies from country to country. In some countries it is mandatory that the data are made freely available once it has been quality checked. The primary example of this practice is the United States. In other countries, it has been politically decided that the data should only be freely available for research purposes, but should be sold for commercial purposes. This is the case in many European countries, although some countries in recent years have switched to having a free data policy as in the United States.

3.3 Diagnosed and analyzed winds

As described in section 3.2 threshold wind speeds are important for the operation of sun-tracking systems such as parabolic troughs and heliostats. These threshold wind speeds are based on the 10-meter winds and not the winds at the actual heights of the sun-tracking components. Given the 10-meter winds, the winds at other heights can be estimated from basic expressions or analyzed with numerical weather prediction models. Estimating the wind speeds at different heights is important for central receiver systems with towers that can be more than 150 meters (500 feet) high. The change in wind speed with height impacts the thermal efficiency due to variations in the convective heat losses (Delgado et al., 2015). Winds are also important for soiling of components.

Delgado et al. (2015) diagnose the higher winds from the assumption that the wind profile follows a power law

$$u(z) = u_{10m}\left(\frac{z}{10}\right)^{\alpha}. \quad (3.1)$$

Here *u(z)* is the wind speed as a function of the height *z*, *u10m* is the measured wind speed at 10 meters height, and α is an empirically determined exponent. In the lower 100 meters of the atmosphere the logarithmic wind profile is a better assumption

$$u(z) = u_{10m}\left(\frac{\ln(z-d)-\ln(z_0)+\psi(z,z_0,L)}{\ln(10-d)-\ln(z_0)+\psi(10,z_0,L)}\right). \quad (3.2)$$

Here z_0 is the surface roughness length, *d* is the zero level displacement height, ψ is a stability term that depends on the Monin-Obukhov stability parameter *L* (Monin and Obukhov, 1954). The displacement height *d* can be assumed to be 0 meters outside forests or urban areas where no major obstacles are present. For neutral atmospheric conditions the stability parameter ψ is also 0.

With numerical weather prediction models the wind profile can be analyzed better than with the empirical and semi-empirical expressions described above. These models include advanced turbulence schemes such as (Mauritsen et al., 2007) that account for general atmospheric conditions that are not just adiabatic or neutrally stable profiles.

Individual wind gusts can cause CSP/STE plant shutdown and are therefore critical for plant operation. Wind gusts are defined by WMO to be the average wind speed over 3 s. The highest wind gusts during an hour can be very different from the hourly wind. Wichers Schreur and Geertsema (2008) describe a parameterization of wind gusts from hourly wind speeds based on turbulent kinetic energy from a numerical weather prediction model.

3.4 Sunshape measurements

The sunshape is the irradiance profile across the sun disk and beyond this. As discussed in section 4.5 this is particularly important because irradiance from a region around the sun disk can be utilized in CSP/STE plants. The sunshape is affected by clouds and the aerosols present. It is sensitive to the particular volume scattering function of the local aerosols. This is not a standard meteorological measurement, and has only been measured in a limited number of studies (e.g. Noring et al. 1991; Neumann et al. 2002; Wilbert et al. 2011; Kalapatapu et al. 2012). More measurements of the sunshape and better models of this are needed.

3.5 References

Buijs-Ballot, C. H. D., 1872. Suggestions on a Uniform System of Meteorological Observations. The Royal Dutch Meteorological Institute, The Netherlands.

Cuevas, E., C. Camino, A, Benedetti, et al., 2015. The MACC-II 2007–2008 reanalysis: atmospheric dust evaluation and characterization over northern Africa and the Middle East. Atmos. Chem. Phys, 15, 3991-4024.

Delgado, A., C. Gertig, E. Bleas, A. Loza, C. Hidalgo, R. Ron, 2015. Evaluation of the variability of wind speed at different heights and its impact on the receiver efficiency of central receiver systems. Poster presentation at the SolarPACES 2015 conference, Cape Town, South Africa.

Hanrieder, N., Wilbert, S., Pitz-Paal, R., Emde, C., Gasteiger, J., Mayer, B., Polo, J., 2015. Atmospheric extinction in solar tower plants: absorption and broadband correction for MOR measurements, Atmos. Meas. Tech., 8, 3467-3480, doi:10.5194/amt-8-3467-2015.

Hanrieder, N., Sengupta, M., Xie, Y., Wilbert, S., Pitz-Paal, R., 2016. Modeling beam attenuation in solar tower plants using common DNI measurements, Solar Energy, 129, 244–255.

Inness, A., F. Baier, A. Benedetti, et al., 2013. The MACC reanalysis: an 8 yr data set of atmospheric composition. Atmospheric Chemistry and Physics, 13(8), 4073-4109.

Kalapatapu, R., Chiesa, M., Armstrong, P., Wilbert, S., 2012. Measurement of DNI angular distribution with a sunshape profiling irradiometer, Proc. SolarPACES 2012 Conference, Marrakech, Morocco.

Mauritsen, T., G. Svensson, S. S. Zilitinkevich, I. Esau, L. Enger, B. Grisogono, 2007. A total turbu-

lent energy closure model for neutral and stably stratified atmospheric boundary layers. J. Atmos. Sci., 64 (11), 4113-4126.

Monin, A. S., Obukhov, A.M., 1954. Osnovnye zakonomernosti turbulentnogo peremeshivanija v prizemnom sloe atmosfery (Basic Laws of Turbulent Mixing in the Atmosphere Near the Ground). Trudy Geofiz. Inst. AN SSSR, 24(151): 163–187.

Neumann, A., Witzke, A., Jones, S. A., Schmitt, G., 2002. Representative terrestrial solar brightness profiles. J. Sol. Energy Eng. ASME 124 (2), 198-204.

Nielsen, K. P., E. Gleeson, L. Rontu, 2015. Radiation sensitivity tests of the HARMONIE 37h1 NWP model. Geosci. Model Dev., 7, 1433-1449.

Noring, J., Grether, D., Hunt, A., 1991. Circumsolar radiation data: The Lawrence Berkeley Laboratory reduced data base, NREL Rep. TP-262-4429.

WMO, 2005. World Weather Watch, Twenty-Second Status Report on Implementation. WMO-No. 986, Secretariat of the World Meteorological Institute, Geneva, Switzerland.

WMO & ISO, 2008. Agreement on working arrangements between the World Meteorological Organization and the International Organization for Standardization. Secretariat of the World Meteorological Institute, Geneva, Switzerland.

WMO, 2010. Guide to Meteorological Instruments and Methods of Observation. WMO-No. 8, Secretariat of the World Meteorological Institute, Geneva, Switzerland.

Wichers and Schreur, 2008. Theory for a TKE based parameterization of wind gusts, HIRLAM Newsletter 54, 177-188.

Wilbert, S., Reinhardt, B., DeVore, J., Röger, M., Pitz-Paal, R., Gueymard, C., 2011. Measurement of solar radiance profiles with the Sun and Aureole Measurement system (SAM), Proc. SolarPACES 2011 Conference, Granada, Spain.

4. Variability of direct normal irradiances

To be able to correctly describe the variability of direct normal irradiances it is important to understand the root causes of this. Here a review of the natural and anthropogenic sources of variability is presented.

4.1 Sources of solar irradiance variability – the Sun

Recent decades of satellite-based measurements of the solar irradiance outside the earth's atmosphere show the sun to be remarkably constant over time. The solar irradiances are quasi-periodical with a period of approximately 11-years. From maximum to minimum, in the recent cycles, the relative difference is about 0.1%, while the average solar irradiance at 1 astronomical unit is estimated to be 1361±0.5 W/m^2 (Kopp and Lean 2011). The variability is highest in the x-ray and extreme UV part of the solar spectrum. Solar irradiances at x-ray wavelengths do not reach the surface of the Earth and the UV irradiances that do penetrate the atmosphere are mostly scattered by Rayleigh scattering (Brasseur and Solomon 1986). Therefore, it is reasonable to assume that changes in the irradiance output of the sun do not noticably affect the variability in the direct normal solar irradiances (DNI) at the surface of the earth.

The solar variability also indirectly affects the atmosphere. In particular, the ozone layer is significantly affected by the UV irradiance variability over the solar cycle (Haigh et al. 2010). This again affects the height of the troposphere, which can affect the clouds in the troposphere. It has also been hypothesized that the solar plasma wind and its effect on the cosmic ray flux could indirectly affect clouds. A review of these indirect solar effects has been made by Gray et al. (2010). Many of them are still poorly understood. The 10.7 cm wavelength solar flux is often used as a proxy for the solar variability.

4.2 Sources of solar irradiance variability – the Earth orbit and rotation

The elliptical orbit of the Earth around the Sun causes variations in the top of the atmosphere solar irradiance of 6.68% from the perihelion in early January to the aphelion in early July (Michalsky 1988). The rotation of the Earth gives rise to the daily variability. The tilt of the rotation axis relative to the position of the Sun gives rise to the seasonal variability. Blanco-Muriel et al. (2001), Grena (2008) and Reda and Andreas (2004, 2007) have written algorithms for calculating the solar vector for a given time and place. Which of these algorithms to use depends on the level of accuracy required. Be aware that the fastest algorithms may be optimized for a limited period of time – for instance one or a few decades. An overview of solar position algorithms can be found in (Vignola et al. 2012).

4.3 Sources of solar irradiance variability – clouds

The variability of solar irradiances is mostly affected by the variability of clouds. Clouds consist of airborne water droplets and solids that are not precipitating or only precipitating slowly. Airborne liquid droplets and solids that are not made of water are referred to as aerosols.

Clouds cause variations at a time scale of minutes or seconds. Extratropical cyclones cause cloud variations at time scales from hours to days. In the tropics, the intertropical convergence zone (ITCZ) gives rise to a band of convective clouds around the globe. This band moves northward of the Equator during the northern hemisphere summer, and vice versa, affecting the seasonal cycle of the monsoon in many parts of the world. The ITCZ has quasi-cyclical variations in the convective patterns over tropical longitudes. These are called the Madden-Julian oscillation (MJO) and have time scales of 30-60 days (Madden and Julian 1971, 1972; Zhang 2005). The MJO influences and is influenced by the El-Niño Southern Oscillation (ENSO). The ENSO is a chaotic variation that affects the cloud conditions in and around the Pacific Ocean, and in lower latitude regions around the world (Walker 1923, 1924; Bjerkness 1969; Wagner et al. 2005). It is mostly quantified with the Multivariate ENSO index (MEI; NOAA 2015a) or the ENSO 3.4 index that is based on Pacific sea surface temperatures and is available from the National Oceanic and Atmospheric Administration (NOAA, 2015b). The clouds in the North Atlantic region are not affected much by the ENSO. Here the North Atlantic Oscillation (NAO) index is related to large scale variability in the tracks of extra-tropical cyclones over time scales of weeks and months (Walker 1923, 1924). The NAO index depends on the pressure difference between Iceland and the Atlantic region off the Iberian Peninsula. When the NAO index is positive, the cyclone tracks will tend to go across Northern Europe and come from South-Eastern North America. When the NAO index is negative the cyclone tracks will tend to go across Southern Europe and come from North Eastern North America (Stephenson et al. 2003). The specific influence of the NAO on solar irradiances in Europe has been investigated by Pozo-Vázquez et al. (2004) and Chiacchio and Wild (2010).

A general feature of the variations of clouds across multiple time scales is that they are not stochastic variations. Imagine a sky that is covered with 50% cumulus clouds and a site that is shaded by one of these clouds during one minute. The stochastic probability that the site is shaded during the next minute could be estimated as 50%, but the actual probability of this is much higher than 50% due to the cumulus clouds structure. Likewise, if a site is shaded by the warm front of an extratropical cyclone during one hour, the probability that it will be shaded during the next hour is also much higher than the climatological probability. If the ENSO is strongly positive during one month (El-Niño), it is much more likely to be positive also in the following month than to become strongly negative (La Niña).

The main driver of cloud variations is the speed of the clouds (Perez et al. 2012; Hoff and Perez 2012; Lave and Kleissl 2013), but not all clouds move. Fog mostly develops and dissolves over time without shifting position. Convective clouds can build up in windless conditions. Mountains can give rise to standing lenticularis clouds. The clouds also vary in vertical extent depending on the vertical air velocity, the net radiative heating balance, latent heating, precipitation and turbulence.

4.4 Sources of solar irradiance variability – volcanic aerosols

In addition to the local effect of volcanic debris, volcanic eruptions can have major impact on solar irradiances on a global scale. This requires two conditions. Firstly, the volcanic effluents need to contain SO_2. Secondly, significant (several Tg) amounts of SO_2 need to reach the stably stratified stratosphere. SO_2 is converted to sub-micrometer H_2SO_4/H_2O droplets in the atmosphere that scatter irradiance at solar wavelengths very efficiently (McCormick 1992; Sheridan et al. 1992; Valero and Pilewskie 1992). These droplets can stay in stratospheric suspension for several years and spread around the globe and thereby affect the solar irradiances globally (Stowe et al. 1992; Hansen et al. 1992). Since the sulfuric aerosols have high scattering efficiencies and low absorption efficiencies (Koepke et al. 1997) they affect the DNI much stronger than the global irradiances. This can be seen both in the measured irradiances (Michalsky et al. 1994; Molineaux and Ineichen 1996) and from radiative transfer simulations (Lohmann et al. 2006; Meyer et al. 2006). Strong temporal increases in stratospheric volcanic aerosols follow Plinian eruptions, with volcanic explosivity index (VEI; Newhall and Self 1982) 5 and larger eruptions; smaller eruptions are not observed as significant events but nevertheless affect the magnitude of the so-called background stratospheric aerosol load (Solomon et al. 2011).

Most of the references above are to studies of the 1991 Pinatubo eruption, which is the most recent and most investigated Plinian eruption. The effect of volcanic eruptions on solar irradiances has been known throughout historical time and is described in several historical and ancient texts. Sigl et al. (2015) give an overview of these texts. As an example Roman Pliny the Elder described a prolonged eclipse of the Sun with almost a year's continuous gloom, and in the Chinese Han-Shu a pale blue sun casting no shadows is described. Both refer to the effect of an Ultra-Plinian eruption (VEI 7) that occurred in 44 BC. Pliny the Elder was born almost 70 years after the eruption, so his account could be exaggerated; however, Sigl et al. (2015) document that this specific eruption corresponds to some of the largest deposits of sulfates in Arctic and Antarctic ice cores, and some of the coldest years on a global scale estimated from tree ring growth anomalies during the last 2,500 years.

Since the Pinatubo eruption occurred more than 20 years ago, many satellite-derived data are based only on years that are un-affected by major volcanic eruptions. The United States National Solar Radiation Data Base (NSRDB; Wilcox, 2007) covers periods in the early 1980s (El Chichón) and early 1990s (Pinatubo) that were affected by major volcanic eruptions. These can be used to estimate the solar resource under such circumstances (Vignola et al. 2013). In lack of a local data set, they can also be used to estimate the relative effect on DNI outside the USA. This is reasonable, if the assumption that the volcanic aerosols are spread around the globe is valid. That is the case as a function of longitude, but for different latitudes the ITCZ causes divergent flows in stratosphere that predominately keep volcanic aerosols in the hemisphere of their origin. For the Mexican El Chichón eruption, the aerosol optical depths were 2-3 times larger at northern latitudes than at southern latitudes in the years following the eruption (Sato et al. 1993). The stratospheric flow has also been observed to contain the bulk of the aerosols within certain latitudinal bands for

several months, but with the changes in this flow over the seasons, the aerosols eventually are spread to latitudes far from their origin (McCormick and Veiga 1992).

In a statistical sense the rarity of Plinian volcanic eruptions cause a challenge. As discussed above even with 35 years of irradiance data only two such eruptions occurred. With n = 2 no conclusions can be drawn about the variability of the eruptions, neither regarding the probability of occurrence, nor the distribution of magnitudes. Sato et al. (1993) made a reanalysis data set that includes the stratospheric aerosol optical depth back to 1850. This data set has been continuously updated and improved, and is available from NASA GISS (2015). For Plinian eruptions the e-folding-time is typically assumed to be about 1 year, i.e. the time it takes for the volcanic aerosol optical depths to be reduced to a fraction of 1/e as compared with their maximum values (Crowley and Unterman 2012). Sato et al. (1993) also assume that the effective radii of the H_2SO_4/H_2O droplets decrease exponentially over time from a maximum value that depends on the magnitude of a given eruption to a minimum value of 0.2 µm. This decrease in effective droplet size affects the normalized volume scattering function of the aerosols so that this becomes less forward scattering. This is important for the observed DNI, since this includes scattered irradiance within the numerical aperture of interest (typically a half-angle of 2.5°), as discussed by Blanc et al. (2014).

Based on historical estimates of volcanic aerosol optical depth data, as those mentioned above, it ought to be possible to assess both the likelihood and the distribution of volcanic eruption magnitudes. For instance De la Cruz-Reyna (1991) showed that the occurrence of higher VEI eruptions follow the Poisson distribution. To our knowledge, however, solar resource studies have not been made that account for the variability of stratospheric volcanic aerosols. Often periods affected by Plinian eruptions are simply omitted from irradiance and meteorological data sets (Vignola et al. 2013). This is only acceptable if the risk of volcanic eruptions is included elsewhere in the financing scheme of the plant yield analysis. When simulating future climate change, volcanoes are also important. In this regard a study has been made by Jackson et al. (2015). They used the nine largest eruptions from the Sato et al. (1993) data set to simulate volcanic eruptions in the coming century. A Monte Carlo algorithm was used to determine whether an eruption would occur in a given year of simulations, and another Monte Carlo algorithm was used to pick one of the nine eruptions from the previous 150 years. Each of the nine eruptions were represented by their temporal development of the aerosol optical depth within four latitudinal bands (0°S – 45°S, 45°S – Eq., Eq. – 45°N & 45°N – 90°N).

4.5 Sources of solar irradiance variability – other aerosols

Aerosols are mostly emitted or lifted from the surface. Such aerosols are referred to as primary aerosols. But aerosols can also arise from gaseous species in the atmosphere. Such aerosols and aerosols that are transformed while being airborne are referred to as secondary aerosols. Types of primary aerosols include: Mineral dust, sea salt, black carbon and primary biological aerosol particles (e.g. pollen). Types of secondary aerosols include: Sulphates, carbonates, nitrates and ammonium. How to group aerosols and name these groups vary. The definitions above are from the IPCC

AR5 chapter on clouds and aerosols by Boucher et al. (2013). An important aerosol group not included in these is biomass burning carbonic aerosols. Holzer-Popp et al. (2008) distinguish these from diesel carbonic aerosols as these two aerosol types have significantly different optical properties.

The aerosol optical properties determine the transmittance of the aerosols. For DNI the aerosol transmittance T_{DNI} at a given solar wavelength λ is

$$T_{DNI}(\lambda) = e^{-k(\lambda)\tau(\lambda)/\cos\theta}. \quad (4.1)$$

Here τ is the spectral aerosol optical thickness as a function of the wavelength λ, θ is the solar zenith angle, and k is a scaling factor that depends on the spectral aerosol single scattering albedo and the spectral normalized volume scattering function. The scaling factor also depends on the field of view (or numerical aperture) of interest (Reinhardt 2013; Blanc et al. 2014; Eissa et al. 2014). For aerosols that only absorb solar irradiance, k will be equal to 1. For aerosols that scatter solar irradiance, k will be less than 1. The magnitude of this reduction depends on the fraction of scattered irradiances that are scattered at angles small enough to remain within the DNI numerical aperture of interest.

Aerosols can also mix while airborne. Soluble aerosols can mix homogeneously. Insoluble aerosols mix heterogeneously. For instance mineral dust can be coated with secondary aerosols, which changes the optical properties from those of the primary dust aerosols (Kandler et al. 2011).

All aerosols that are not stratospheric volcanic aerosols affect irradiances regionally around the sources of the aerosols. Sea salt aerosols affect mainly coastal regions. Mineral dust predominately affects regions proximal to deserts. Anthropogenic aerosols affect regions near densely populated areas. In some cases, aerosols can be transported thousands of kilometers, but mostly aerosols of similar type have specific regional characteristics. The optical properties of biomass burning aerosols from various parts of the world differ significantly (Dubovik et al. 2002). The composition of anthropogenic aerosols is affected by national pollution regulations. The optical properties of mineral dust depend on the regional geology.

The best available aerosol optical properties are based on measurements. Since 1993 the global AERONET network has provided spectral measurements of the bulk aerosol optical properties as observed from ground-based stations (Holben et al. 1998). These data are available from NASA GSFC (2015). Other existing aerosol data sets are SKYNET (Takamura and Nakajima 2004) and the LIDAR data set Earlinet (Bösenberg et al. 2003). In order to achieve global data coverage, the AERONET data can be combined with satellite retrieved aerosol optical depths – for instance from the multispectral Moderate-Resolution Imaging Spectroradiometer (MODIS) instruments (Levy et al. 2007). Furthermore, the observed aerosol data can be re-analyzed with atmospheric models. A good example of this is the Monitoring Atmospheric Composition and Climate (MACC) reanalysis, which is being continuously improved (Morcrette et al. 2009; Benedetti et al. 2009; Belloiun et al. 2013). Unfortunately, AERONET data and multispectral satellite data are only available a few dec-

ades back in time. This leaves major questions regarding the long-term variability potentially caused by aerosols unanswered: How much has the atmospheric content changed in pace with the ever accelerating industrialization of the world? How much will the content change if we manage to clean our emissions in the future? How much will it change if we do not? These questions are important for the future DNI resource. Since we do not have all the data needed to answer the first of these questions, it is also challenging for us to answer the two last questions. Additionally, it is a challenge that we do not know exactly to which extend variations in anthropogenic aerosols have contributed to solar irradiance trends. In the derivation of TMY data sets solar irradiance trends are not accounted for. This also applies to more comprehensive statistical analyses of long-term solar resources such as the recent study by Fernández-Peruchena et al. (2016). TMY data sets derived from solar irradiance data at the end of either a long-term negative or positive trend will have either too high or too low irradiance values as compared with the current conditions.

Without long-term measurements of aerosol variability, it is necessary to infer this indirectly from solar irradiance measurements. Long-term time series of GHI are available from sites around the world. Stanhill and Moreshet (1992) found significant decreases of 9 W/m^2 in average over global land areas between 1958 and 1985. Many local studies have confirmed that GHI has been decreasing (dimming) during this period (Gilgen et al. 1998 *and references therein*; Liepert 2002; Liepert and Tegen 2002). Later, Wild et al. (2005) found that this dimming trend had reversed and brightening had been observed since the late 1980'ies in many places around the world. They found the trend reversal both in clear sky GHI and cloudy sky GHI, which lead them to suggest that this was due to both direct aerosols effects and indirect aerosol effects on clouds. The decreased aerosol effect they attributed partly to the air-quality regulations that were implemented in many countries from the 1980s and 1990s, and partly to the diminishing effect of stratospheric volcanic aerosols as the effects of the Pinatubo eruption gradually faded during the 1990s. Lohmann et al. (2006) also found brightening occurring from 1985 to 2005 in radiative transfer modelled irradiances based on observational data of clouds and aerosols. Combining a radiative transfer model with physical data enabled them also to estimate the trends and variability of DNI globally. Wild (2012) found support for the hypothesis that the observed global dimming was caused by an increased anthropogenic aerosol load until the mid-1980s and that the following decrease in the aerosol load caused the brightening period. Comparisons of climate modelled and measured 2-meter temperatures in the Northern Hemisphere, showed that models fail to reproduce an observed stagnation in global warming from 1960 to 1985, while they underestimated the warming trend from 1985 to 2000. Since the climate models investigated did not account for changes in anthropogenic aerosols, these were a likely cause of this discrepancy. Wild further supports the hypothesis by the fact this pattern is not observed in the temporal development of the 2-meter temperatures of the Southern Hemisphere, where anthropogenic aerosols effects are much smaller than in the more populated Northern Hemisphere. Here it should be noted that there are major regional exceptions in which brightening has not occurred. In India and China dimming trends of -10 W/m^2 and -4 W/m^2 per decade were still observed from 2000 to 2010, respectively (Wild 2012).

4.6 Sources of solar irradiance variability – global warming

The climate model simulations in the latest IPCC report suggest that global warming due to greenhouse gases does not cause significant cloud feedback effects that could again affect the solar irradiance resource (Boucher et al. 2013). Since the cloud physics in climate models is still being improved, this should not be taken as the final answer, but it is the best answer we have so far. Regional changes in clouds, due to overall shifts in weather patterns, are likely to occur in many regions. The current knowledge of regional climate changes is reviewed and summarized in the IPPC AR5 report chapter on regional climate change (Christensen et al. 2013).

4.7 References

Benedetti, A., J.-J. Morcrette, O. Boucher, A. Dethof, R. J. Engelen, M. Fisher, H. Flentje, N. Huneeus, L. Jones, J. W. Kaiser, S. Kinne, A. Mangold, M. Razinger, A. J. Simmons, M. Suttie, 2009: Aerosol analysis and forecast in the European Centre for Medium-Range Weather Forecasts Integrated Forecast System: 2. Data assimilation. J. Geophys. Res., 114, D13205.

Bjerkness, J., 1969. Atmospheric teleconnections from the Equatorial Pacific, Mon. Weather Rev., 97 (3), 163-172.

Blanc, P., B. Espinar, N. Geuder, C. Gueymard, R. Meyer, R. Pitz-Paal, B. Reinhardt, D. Renné, M. Sengupta, L. Wald, S. Wilbert, 2014. Direct normal irradiance related definitions and applications: The circumsolar issue, Sol. Energy, 110, 561-577.

Blanco-Muriel, M., D. C. Alarcón-Padilla, T. López-Moratalla, M. Lara-Coira, 2001. Computing the solar vector, Sol. Energy, 70 (5), 431-441.

Boucher, O., D. Randall, P. Artaxo, C. Bretherton, G. Feingold, P. Forster, V.-M. Kerminen, Y. Kondo, H. Liao, U. Lohmann, P. Rasch, S. K. Satheesh, S. Sherwood, B. Stevens, X. Y. Zhang, 2013. Clouds and Aerosols. *In* Climate Change 2013: The Physical Science Basis. Contribution of Working Group I to the Fifth Assessment Report of the Intergovernmental Panel on Climate Change. Cambridge University Press, Cambridge, United Kingdom and New York, NY, USA.

Bösenberg, J., H. Linné, V. Matthias *et al.*, 2003. EARLINET: A European Aerosol Research Lidar Network to Establish an Aerosol Climatology. Report No. 348, Max-Planck-Institut für Meteorologie, Hamburg, Germay.

Brassuer, G., S. Solomon, 1986. Aeronomy of the Middle Atmosphere. D Reidel Publishing Company, 3300 AA Dordrecth, Holland.

Chiacchio, M., M. Wild, 2010. Influence of NAO and clouds on long-term seasonal variations of surface solar radiation in Europe, J. Geophys. Res., 115, D00D22.

Christensen, J. H., K. Krishna Kumar, E. Aldrian, S.-I. An, I. F. A. Cavalcanti, M. de Castro, W. Dong,

P. Goswami, A. Hall, J. K. Kanyanga, A. Kitoh, J. Kossin, N.-C. Lau, J. Renwick, D. B. Stephenson, S.-P. Xie, T. Zhou, 2013. Climate Phenomena and their Relevance for Future Regional Climate Change. In: Climate Change 2013: The Physical Science Basis. Contribution of Working Group I to the Fifth Assessment Report of the Intergovernmental Panel on Climate Change. Cambridge University Press, Cambridge, United Kingdom and New York, NY, USA.

Crowley, T., M. Unterman, 2012. Technical details concerning development of a 1200-year proxy index for global volcanism, Earth Syst. Sci. Data Discuss., 5, 1-28.

De la Cruz-Reyna, S., 1991. Poisson-distributed patterns of explosive eruptive activity, Bull. of Volcanol., 54 (1), 57-67.

Dubovik, O., B. N. Holben, T. F. Eck, A. Smirnov, Y. J. Kaufman, M. D. King, D. Tanré, I. Slutsker, 2002. Variability of absorption and optical properties of key aerosol types observed in worldwide locations, J. Atmos. Sci., 59 (3), 590-608.

Eissa, Y., P. Blanc, A. Oumbe, H. Ghedira, L. Wald, 2014. Estimation of the circumsolar ratio in a turbid atmosphere, Energy Proc., 57, 1169 – 1178.

Fernández-Peruchena, C. M., L. Ramírez, M. A. Silva-Pérez, V. Lara, D. Bermejo, M. Gaston, S. Moreno-Tejera, J. Pulgar, J. Liria, S. Macías, R. Gonzalez, A. Bernardos, N. Castillo, B. Bolinaga, R. X. Valenzuela, L. F. Zarzalejo, 2016. A statistical characterization of the long-term solar resource: Towards risk assessment for solar power projects, Sol. Energy, 123, 29-39.

Gray, L. J., J. Beer, M. Geller, J. D. Haigh, M. Lockwood, K. Matthes, U. Cubasch, D. Fleitmann, G. Harrison, L. Hood, J. Luterbacher, G. A. Meehl, D. Shindell, B. van Geel, W. White, 2010. Solar influences on climate, Rev. Geophys., 48, RG4001.

Grena, R.: An algorithm for the computation of the solar position, 2008. Sol. Energy, 82 (5), 462-470.

Haigh, J. D., A. R. Winning, R. Toumi, J. W. Harder, 2010. An influence of solar spectral variations on radiative forcing of climate, Nature, 467, 696-699.

Hansen, J., A. Lacis, R. Ruedy, M. Sato, 1992. Potential climate impact of Mount Pinatubo eruption, Geophys. Res. Lett., 19 (2), 215-218.

Hoff, T. E., R. Perez, 2012. Modeling PV fleet output variability, Sol. Energy, 86 (8), 2177-2189.

Holben, B. N., T.F. Eck, I. Slutsker, D. Tanré, J.P. Buis, A. Setzer, E. Vermote, J.A. Reagan, Y.J. Kaufman, T. Nakajima, F. Lavenu, I. Jankowiak, A. Smirnov, 1998. AERONET – A federated instrument network and data archive for aerosol characterization, Remote Sens. Environ., 66 (1), 1-16.

Holzer-Popp, T., M. Schroedter-Homscheidt, H. Breitkreuz, D. Martynenko, L. Klüser, 2008. Improvements of synergetic aerosol retrieval for ENVISAT, Atmos. Chem. Phys., 8, 7651-7682.

Jackson, L. S., J. A. Crook, A. Jarvis, D. Leedal, A. Ridgwell, N. Vaughan, P. M. Forster, 2015. Assessing the controllability of Arctic sea ice extent by sulfate aerosol geoengineering, Geophys. Res. Lett., 42, 1223–1231.

Kandler, K., K. Lieke, N. Benker, C. Emmel, M. Küpper, D. Müller-Ebert, M. Ebert, D. Scheuvens, A. Schladitz, L. Schütz, S. Weinbruch, 2011. Electron microscopy of particles collected at Praia, Cape Verde, during the Saharan Mineral Dust Experiment: particle chemistry, shape, mixing state and complex refractive index, Tellus B, 63 (4), 475-496.

Köpke, P., M. Hess, I. Schult, E. P. Shettle, 1997. Global aerosol data set. Report No. 243, Max-Planck-Institut für Meteorologie, D-20146 Hamburg, Germany.

Kopp, G., J. L. Lean, 2011. A new, lower value of total solar irradiance: Evidence and climate significance, Geophys. Res. Lett., 38 (1), L01706.

Lave, M., J. Kleissl, 2013. Cloud speed impact on solar variability scaling – Application to the wavelet model, Sol. Energy, 91, 11-21.

Levy, R. C., L. A. Remer, S. Mattoo, E. F. Vermote, Y. J. Kaufman, 2007. Second-generation operational algorithm: Retrieval of aerosol properties over land from inversion of Moderate Resolution Imaging Spectroradiometer spectral reflectance, J. Geophys. Res., 112, D13211.

Liepert, B. G., 2002. Observed reductions of surface solar radiation at sites in the United States and worldwide from 1961 to 1990, Geophys. Res. Lett., 29 (10), 61-1.

Liepert, B. G., I. Tegen, 2002. Multidecadal solar radiation trends in the United States and Germany and direct tropospheric aerosol forcing,J. Geophys. Res., 107, D12, 4153.

Lohmann, S., C. Schillings, B. Mayer, R. Meyer, 2006. Long-term variability of solar direct and global radiation derived from ISCCP data and comparison with reanalysis data, Sol. Energy, 80, 1390–1401.

Madden, R. A., P. R. Julian, 1971. Detection of a 40-50 day oscillation in the zonal wind in the Tropical Pacific, J. Atmos. Sci., 28, 702-708.

Madden, R. A., P. R. Julian, 1972. Description of global-scale circulation cells in the Tropics with a 40-50 day period, J. Atmos. Sci., 29, 1109-1123.

McCormick, M. P., 1992. Initial assessment of the stratospheric and climatic impact of the 1991 Mount Pinatubo eruption: Prologue, Geophys. Res. Lett., 19 (2), 149.

Meyer, R., S. Lohmann, C. Schilling, C. Hoyer, 2006. Climate statistics for planning and siting of solar energy systems: Long-term variability of solar radiation derived from satellite data, in: Solar Energy Resource Management for Electricity Generation from Local Level to Global Scale. Nova Science Publishers, Hauppauge NY 11788, USA.

Michalsky, J. J., 1988. The astronomical Almanac's algorithm for approximate solar position (1950-

2050), Sol. Energy, 40, 227-235.

Michalsky, J. J., R. Perez, R. Seals, P. Ineichen, 1994. Degradation of solar concentrator performance in the aftermath of Mount Pinatubo, Sol. Energy, 52 (2), 205-213.

Molineaux, B., P. Ineichen, 1996. Impact of Pinatubo Aerosols on the seasonal trends of global, direct and diffuse irradiance in two northern mid-latitude sites, Sol. Energy, 58 (1-3), 91-101.

Morcrette, J.-J., O. Boucher, L. Jones, D. Salmond, P. Bechtold, A. Beljaars, A. Benedetti, A. Bonet, J. W. Kaiser, M. Razinger, M. Schulz, S. Serrar, A. J. Simmons, M. Sofiev, M. Suttie, A. M. Tompkins, A. Untch, 2009. Aerosol analysis and forecast in the European Centre for Medium-Range Weather Forecasts Integrated Forecast System: Forward modeling, J. Geophys. Res., 114, D6206.

NASA GSFC, 2015. AERONET Aerosol Robotic Network, Data Access and Dissemination Tools. http://aeronet.gsfc.nasa.gov/, accessed December 2015, National Aeronautics and Space Administration, Goddard Space Flight Center, Greenbelt, MD 20771, USA.

NASA GISS, 2015. Forcings in GISS climate model: Stratospheric aerosol optical thickness. http://data.giss.nasa.gov/modelforce/strataer/, accessed November 2015, National Aeronautics and Space Administration, Goddard Institute for Space Studies, New York, NY 10025, USA.

Newhall, C., S. Self, 1982. The Volcanic Explosivity Index (VEI): an estimate of explosive magnitude for historical volcanism, J. Geophys. Res., 87, 1231-1238.

NOAA, 2015a. Earth System Research Laboratory: Multivariate ENSO Index (MEI). http://www.aoml.noaa.gov/phod/regsatprod/enso/enso34/index.php, accessed December 2015, National Oceanic and Atmospheric Administration, Washington, DC 20230, USA.

NOAA, 2015b. Physical Oceanography Division (PHOD) of AOML: El-Niño Southern Oscillation ENSO 3.4. http://www.esrl.noaa.gov/psd/enso/mei/, accessed November 2015, National Oceanic and Atmospheric Administration, Washington, DC 20230, USA.

Perez, R., S. Kivalov, J. Schlemmer, K. Hemker Jr., T. E. Hoff, 2012. Short-term irradiance variability: Preliminary estimation of station pair correlation as a function of distance, Sol. Energy, 86, 2170-2176.

Pozo-Vázquez, D., J. Tovar-Pescador, S. R. Gámiz-Fortis, M. J. Esteban-Parra, Y. Castro-Díez, 2004. NAO and solar radiation variability in the European North Atlantic region, Geophys. Res. Lett., 31, L05201.

Reda, I., A. Andreas, 2004. Solar position algorithm for solar radiation applications, Sol. Energy, 76 (5), 577-589.

Reda, I., A. Andreas, 2007. Corrigendum to “Solar position algorithm for solar radiation applications” [Solar Energy 76 (2004) 577–589], Sol. Energy, 81 (6), 838.

Reinhardt, B., 2013. On the Retrieval of Circumsolar Radiation from Satellite Observations and Weather Model Output. Ph.D. Thesis, der Fakultät für Physik, der Ludwig-Maximilians-Universität, D-80539 München, Germany.

Sato, M., J. E. Hansen, M. P. McCormick, J. B. Pollack, 1993. Stratospheric aerosol optical depths, 1850–1990, J. Geophys. Res., 98 (D12), 22987–22994.

Sheridan, P. J., R. C. Schnell, D. J. Hofmann, T. Deshler, 1992. Electron microscope studies of Mt. Pinatubo aerosol layers over Laramie, Wyoming during Summer 1991, Geophys. Res. Lett., 19 (2), 203-206.

Sigl, M., M. Winstrup, J. R. McConnell, K. C. Welten, G. Plunkett, F. Ludlow, U. Büntgen, M. Caffee, N. Chellman, D. Dahl-Jensen, H. Fischer, S. Kipfstuhl, C. Kostick, O. J. Maselli, F. Mekhaldi, R. lvaney, R. Muscheler, D. R. Pasteris, J. R. Pilcher, M. Salzer, S. Schüpbach, J. P. Steffensen, B. M. Vinther and T. E. Woodruff, 2015. Timing and climate forcing of volcanic eruptions for the past 2,500 years, Nature **523** (7562), 543-549.

Solomon, S., J. S. Daniel, R. R. Neely III, J.-P. Vernier, E. G. Dutton, L. W. Thomason, 2011. The persistently variable background stratospheric aerosol layer and global climate change, Science, 333, 866-870.

Stanhill, G., S. Moreshet, 1992. Global radiation climate changes: The world network, Clim. Change, 21 (1), 57-75.

Stephenson, D. B., H. Wanner, S. Brönnimann, J. Luterbacher, 2003. The history of scientific research on the North Atlantic Oscillation, Geophysical monograph-American Geophysical Union, 134, 37-50.

Stowe, L. L., R. M. Carey, P. P. Pellegrino, 1992. Monitoring the Mt. Pinatubo aerosol layer with NOAA/11 AVHRR data, Geophys. Res. Lett., 19 (2), 159-162.

Takamura, T., T. Nakajima, 2004. Overview of SKYNET and its Activities. Óptica Pura y Aplicada, 37 (3): 3303.

Valero, F. P. J., P. Pilewskie, 1992. Latitudinal survey of spectral optical depths of the Pinatubo volcanic cloud – derived particle sizes, columnar mass loadings, and effects on planetary albedo, Geophys. Res. Lett., 19 (2), 163-166.

Vignola, F., J. Michalsky, T. Stoffel, 2012. Solar and Infrared Radiation Measurements. Appendix D: Solar Position Algorithms, CRC Press, Boca Raton, FL 33487, USA.

Vignola, F., A. McMahan, C. Grover, 2013. Statistical analysis of a solar-radiation data set: Characteristics and requirements for P50, P90, and P99 evaluation, in: Solar Energy Forecasting and Resource Assessment. Elsevier, Amsterdam 1043 NX, Netherlands.

Wagner, T., S. Beirle, M. Grzegorski, S. Sanghavi, U. Platt, 2005. El Niño induced anomalies in global data sets of total column precipitable water and cloud cover derived from GOME on ERS-2,

J. Geophys. Res., 110 (D15).

Walker, G. T., 1923. Correlation in seasonal variations of weather, VIII: A preliminary study of world weather, Memoirs of the Indian Meteorological Department. Calcutta, India. 24 (4), 75-131.

Walker, G. T., 1924. Correlation in seasonal variations of weather, IX: A further study of world weather, Memoirs of the India Meteorological Department. Calcutta, India. 24 (9), 275-332.

Wilcox, S., 2007. National Solar Radiation Database 1991-2005 Update: User's Manual. http://www.nrel.gov/docs/fy07osti/41364.pdf (accessed May 2016). NREL/TP/581-41364, National Renewable Energy Laboratory, Golden, CO 80401, USA.

Wild, M., H. Gilgen, A. Roesch, A. Ohmura, C. N. Long, E. G. Dutton, B. Forgan, A. Kallis, V. Russak, A. Tsvetkov, 2005. From Dimming to Brightening: Decadal Changes in Solar Radiation at Earth's Surface, Science, 308: 847-850.

Wild, M., 2012. Enlightening global dimming and brightening, Bull. Amer. Meteorol. Soc., 93 (1), 27-36.

Zhang, C, 2005. Madden-Julian Oscillation, Rev. Geophys., 43 (2), 1-36.

5. Statistical characterization of the solar resource long-term variability

The objective of this chapter is to describe the current methods used for the statistical characterization of the solar resource long-term inter-annual variability.

5.1 Introduction

The objective of this chapter is to describe the current methods used for the statistical characterization of long-term inter-annual variability of DNI, since it is the solar radiation component that is converted by concentrating solar power (CSP). Output of both CSP technologies Solar Thermal Electricity (STE) and Concentrating Photo-Voltaics (CPV) primarily depend on DNI input.

The characterization of the long-term inter-annual variability of the yearly DNI is a complementary analysis to the estimation of the typical yearly DNI: it consists of estimating the minimal yearly DNI value corresponding to a given ***probability of exceedance (PoE)***, *as* explained in the previous chapter. For example, the ***P90*** corresponds to the yearly DNI value that will be exceeded by at least 90% of the years, during the lifetime of the project (Cebecauer and Šúri, 2014). It corresponds to the complementary of the percentile the P90 value of the yearly DNI, which corresponds to its 10th percentile.

More generally, in this document, we will consider the estimation of the PoE values for the average of n consecutive yearly DNI. Having n greater than 1 enables filtering out isolated "accidental" years and enable to analyze the PoE value of the DNI for the whole life time of the project (e.g. $n = 20$), or every 5 five years ($n = 5$), for example.

Determining the n-year average of yearly DNI and corresponding scenarios for the probabilities of exceedance of P50, P75, P90 or even P99 are now commonly requested by the banks for the financial feasibility studies of solar energy projects.

In this document, we only consider approaches determining the PoE values with a historical data set of DNI for the site of interest. This historical data set may come from *in-situ* measurements, satellite or numerical weather based-estimations or from a merging process from these different sources (e.g. site adaptation). The uncertainty of this historical data set may have an influence on the computation of the PoE values: this aspect is discussed in section 2.5. In this chapter, only the observed long-term variability of the DNI is considered.

5.2 Notations

Let $B(y)$ be the yearly DNI for the year y, expressed in kWh/m^2.
The n-year average of $B(y)$ is noted B_n:

$$B_n(y) = \frac{1}{n}\sum_{k=0}^{n-1} B(y-k) \tag{5.1}$$

For the statistical analysis, we have at our disposal a DNI data set for nd years. Typically, nd is ranging from 10 to 20 years.

If B corresponds to the underlying stochastic process of the annual DNI, we note $P(v)[B]$ the value of B corresponding to a PoE of v %. If $CDF[B]$ is the cumulative distribution function of B then, by definition,

$$CDF[B](b) = \boldsymbol{P}(B \leq b) \tag{5.2}$$

We have the following relationship between $P(v)[B]$ and $CDF[B]$:

$$CDF[B](P(v)[B]) = 1 - \frac{v}{100} \tag{5.3}$$

or

$$P(v)[B] = CDF[B]^{-1}\left(1 - \frac{v}{100}\right) \tag{5.4}$$

Where $CDF[B]^{-1}$(p) is the inverse function of $CDF[B]$(x).

5.3 Data set used for the illustrations

For illustration purpose, we have selected a very long-term (36 years) and high quality *in-situ* measurements of DNI from the pyranometric station in Eugene (USA). This station belongs to the radiometric network UO SRML (University of Oregon Solar Radiation Monitoring Laboratory). The station is located at (44.05°N, 123.07°W, 150 **m.a.s.l.**) and the DNI data set spans from 1978 to 2013 (36 years). These yearly DNI values can be seen in Table 5.1 and Figure 5.1.

Year	DNI (kWh/m^2)	Year	DNI (kWh/m^2)
1978	949	1996	1431
1979	1336	1997	1391
1980	1270	1998	1274
1981	1241	1999	1365
1982	1292	2000	1387
1983	971	2001	1445
1984	1303	2002	1573
1985	1500	2003	1453
1986	1281	2004	1369
1987	1478	2005	1438
1988	1402	2006	1537
1989	1365	2007	1456
1990	1332	2008	1369
1991	1329	2009	1478
1992	1299	2010	1292
1993	1212	2011	1237
1994	1460	2012	1354
1995	1354	2013	1402

Table 5.1. Yearly direct normal irradiation (kWh/m^2) measured from 1976 to 2013 at the solar monitoring station in EUGENE (USA) belonging to the radiometric network UO SRML.

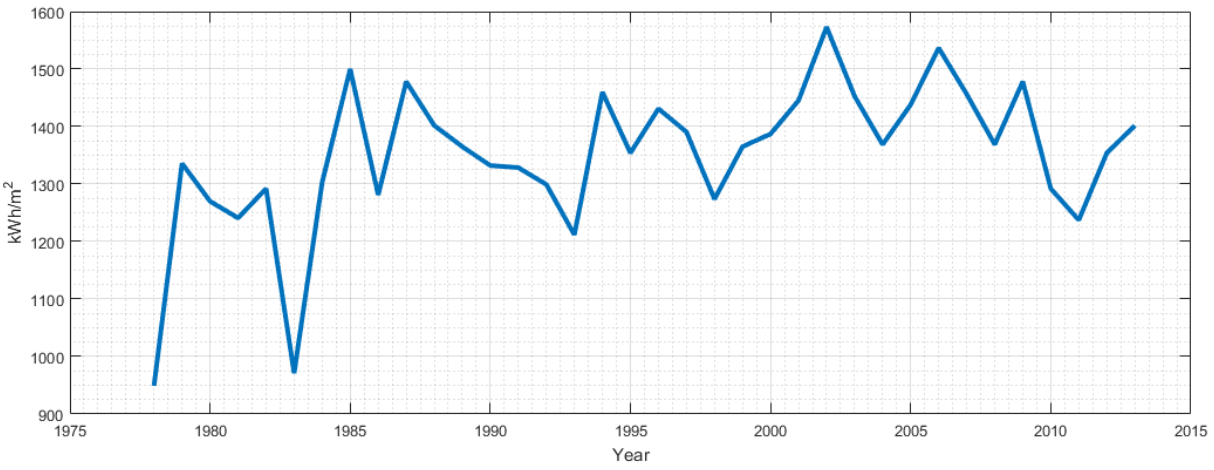

Figure 5.1. Time series of yearly direct normal irradiation measured from 1976 to 2013 at the solar monitoring station in EUGENE (USA) belonging to the radiometric network UO SRML

5.4 The current approaches for the statistical analysis

The objective is to have an estimation of $P(v)[B_n]$ from the historical data set $\{B(y_k)\}_{k\in[1,nd]}$ of nd years. The set $\{y_k\}_{k\in[1,nd]}$ corresponds to the list of the nd years in the historical data set (see Table 5.1).

We have listed three approaches to estimate the PoE $P(v)[B_n]$:

- The estimation based on the empirical cumulative distribution function (CDF);
- The estimation based on fitted parametric CDF;
- The estimation based on non-parametric CDF using the technique of the kernel density estimator (KDE).
-
- The different methods will be exposed in the document, with illustrations and discussions based on experiments with the data set described in the previous section.

5.4.1 The estimation based on the empirical CDF

The first and simple approach makes uses of empirical CDF ($eCDF$) without any probability density function (PDF) modeling or assumption.

$$eCDF[X](x) = \frac{\#\{X \leq x\}}{\#X} \tag{5.5}$$

Where $\#X$ represent the number of elements of the data set X.

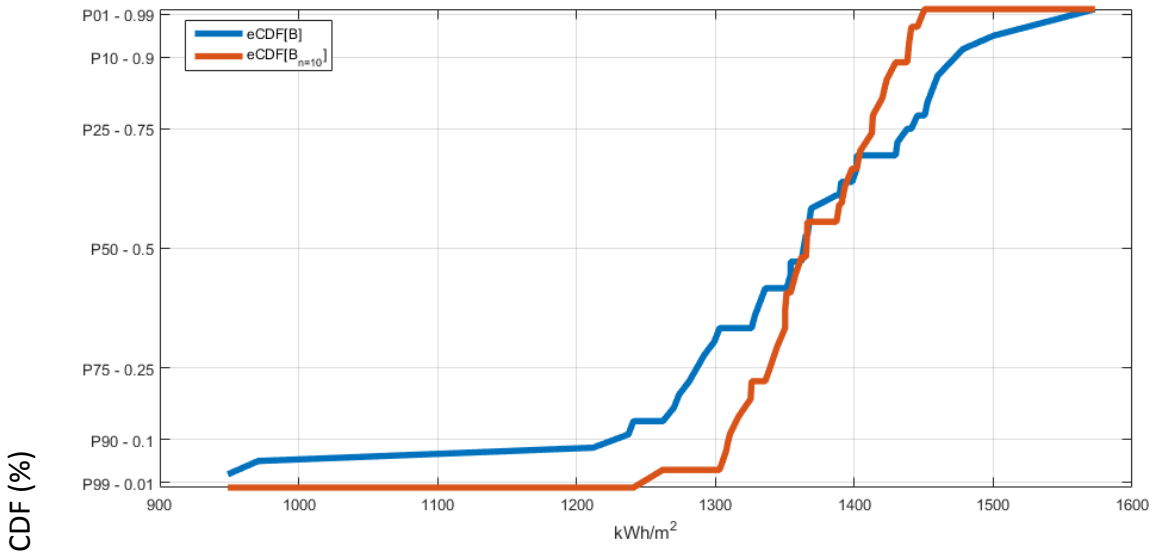

Figure 5.2. Examples of empirical CDFs estimated from the historical data set of yearly direct normal irradiations $\{B(y_k)\}_{k\in[1,nd]}$ (in blue) and the historical data set of 10-years average direct normal irradiations $\{B_{n=10}(y_k)\}_{k\in[n+1,nd]}$.

This method is very straightforward, very simple to implement and to use. Nevertheless, for small number of years nd (typically 10 and less), many –and complex– solutions exist to get optimal –to a certain sense– estimations of percentiles (Zieli, 2004).

Figure 5.2 presents, as an example, the empirical CDFs estimated from the historical data set of yearly DNI $\{B(y_k)\}_{k\in[1,nd]}$ and from the 10-year average DNI data set $\{B_{n=10}(y_k)\}_{k\in[n+1,nd]}$.

The estimations of $P90[B]$ and $P90[B_{n=10}]$ are respectively 1238 kWh/m^2 and 1312 kWh/m^2.

As noticed by Fernández Peruchena et al. (2016), the approach based on the empirical CDF is strongly limited by the historical data set: no PoE value can be lower –or higher– than the minimum –or maximum– value observed DNI values in the historical data set.

5.4.2 The estimation based on fitted parametric CDF

To circumvent this limitation, another approach consists of modeling the distribution of B_n from the historical data set with a parametric probability distribution function (PDF). The difficulty is to find the suitable parametric PDF that is able to model the observed PDF of the historical data set of yearly DNI $\{B(y_k)\}_{k\in[1,nd]}$.

In Figure 5.3 (a-c) a comparison of the empirical histogram of $\{B(y_k)\}_{k\in[1,nd]}$ with the corresponding fitted PDF for three parametric PDF are shown:

- The normal PDF (Figure 5.3a);
- The Weibull PDF (Figure 5.3b);
- The Gumbel PDF (Figure 5.3c);

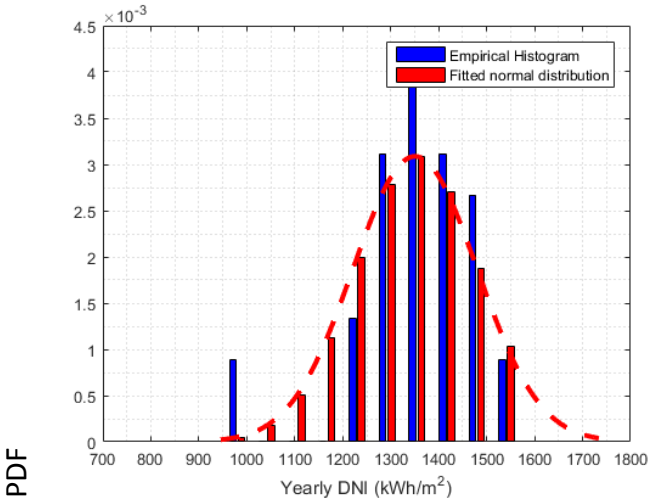

(a)

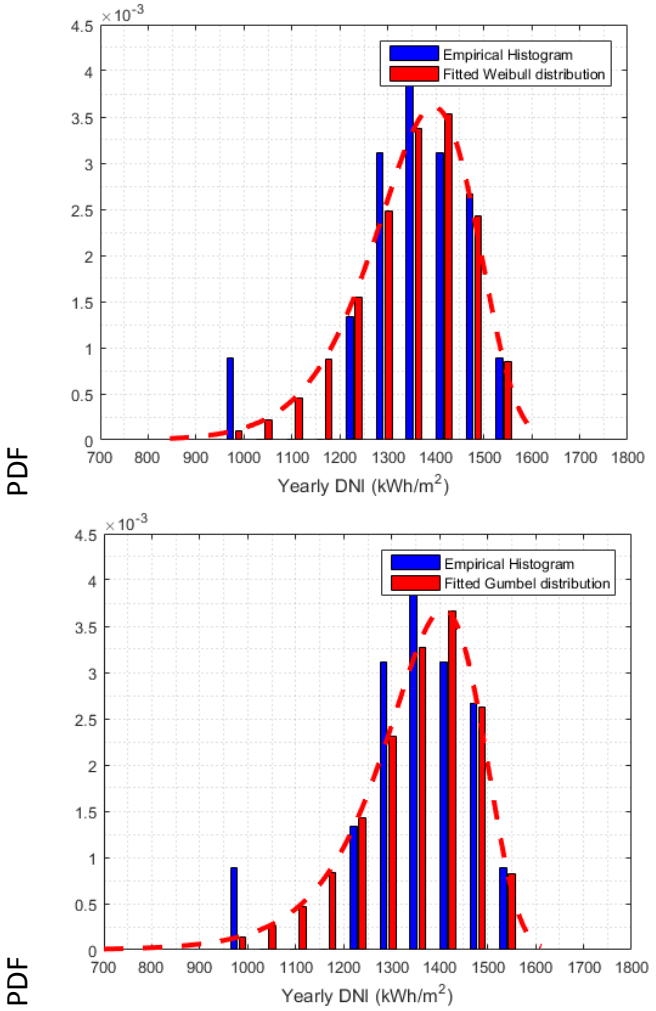

Figure 5.3. Comparison of the empirical histogram of the of historical data set of yearly DNI from Eugene $\{B(y_k)\}_{k\in[1,nd]}$ with three standard parametric PDFs: Normal (a), Weibull (b) and Gumbel (c).

Statistical tests exist that can be used to assess the goodness of fit for these parametric PDF. The "standard" test is the ***Kolmogorov-Smirnov (KS) test*** (Massey, 1951). Of course many other statistical tests exist, as reported by Fernández Peruchena et al. (2016). This test aims at accepting or rejecting the null hypothesis stating that the observed and fitted CDF have been generating by the same underlying distribution (the fitted one). A high value of the associated asymptotic p-value indicates low evidence to reject the null hypothesis.

The results of KS test applied to the fitted PDFs (Figure 5.3) are presented in the following (Table 5.2):

1.	Rejecting the null-hypothesis	Asymptotic p-value
Normal PDF	No	0.5608
Weibull PDF	No	0.9322
Gumbel PDF	No	0.9129

Table 5.2. Results of the KS tests for the parametric PDFs (Normal, Weibull, Gumbel) fitted to the historical data set of DNI $\{B(y_k)\}_{k\in[1,nd]}$ (see Figure 5.2)

Once the parametric PDFs have been fitted to the data set, the Pxx values can be easily computed, using the corresponding modeled CDFs. In addition, by using a Monte Carlo technique, it is possible to assess the confidence interval for each estimation of $P(v)[\mathrm{B}]$. Indeed, considering the fitted CDF, it is possible to randomly draw, with its inverse and a uniform random generator, a large number (e.g. 1000) of synthetic data sets of the same size as the original historical data set. The fitting procedure is then applied to these synthetic data sets, leading to new estimatedPoE values from which the corresponding 95% confident intervals can be assessed.

Despite the statistical "impossibility" to reject any of the parametric PDFs, the corresponding estimations of $P(v)[B]$ may be different, notably for P99. The Figure 5.4 presents the estimation of P99, P90, P75 and P50 estimated with the different fitted PDFs (Normal, Weibull, Gumbel) and their respective 95% confident interval.

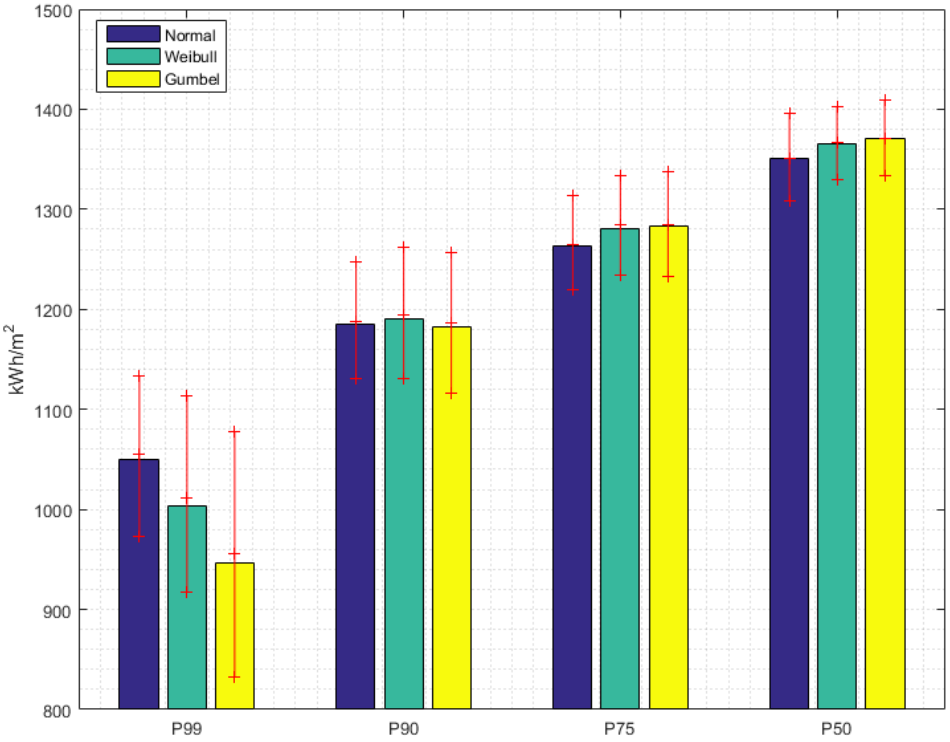

Figure 5.4. **Estimations of P99, P90, P75 and P50 of B and the corresponding 95% confident interval, with the three fitted PDFs (Normal, Weibull, and Gumbel PDFs) (note: the y-axis is not zero-intercept).**

Considering n –the number of years for the multi-year average of DNI– being greater than one could be of interest: the corresponding aggregation has a smoothing effect on the distribution of B_n that should ease the fitting procedure. Theoretically speaking, if we assume that B is an independent and identically distributed (IID) stochastic process, then, owing to the central limit theorem (CLT), the underlying distribution of B_n converges to the normal distribution $\aleph\left(E[B], \frac{\sigma[B]^2}{n}\right)$ where $E[B]$ and $\sigma[B]$ are respectively the expectation and the standard deviation of B.

Under the assumption of the CLT and if n is "large enough", a straightforward estimation method, generalized from (Cebecauer and Suri, 2015) is to rely on the CLT: in that case, one can use the following equation for the $P(v)[B_n]$ estimation:

$$P(v)[B_n] \approx m_{nd}[B] - \frac{\sqrt{2}\,\mathrm{erf}^{-1}\left(\frac{v}{50}-1\right)\sigma_{nd}[B]}{\sqrt{n}} \tag{5.6}$$

Where

- erf^{-1} is the inverse of the error function erf:

$$erf(x) = \frac{2}{\sqrt{\pi}} \int_0^x \mathrm{e}^{-t^2}\, dt \tag{5.7}$$

- $m_{nd}[\mathrm{B}]$ is the estimation of the mean value of $\{B(y_k)\}_{k\in[\mathbf{1},nd]}$:

$$m_{nd}[B] = \frac{1}{nd}\sum_{k=1}^{nd} B(y_k) \approx E[B] \tag{5.8}$$

- $\sigma_{nd}[\mathrm{B}]$ is the estimation of the mean value of $\{B(y_k)\}_{k\in[\mathbf{1},nd]}$

$$\sigma_{nd}[B] = \frac{1}{nd-1}\sum_{k=1}^{nd}\left(B(y_k) - m_{nd}(B)\right) \approx V[B]^{0.5} \tag{5.9}$$

In Table 5.3 the results of the KS tests are presented for the fitted parametric PDFs (Normal, Weibull, Gumbel) to the 10-year average data set $\{B_{n=10}(y_k)\}_{k\in[n+1,nd]}$. None of the parametric PDFs are rejected. One can note nevertheless that the p-value for the Normal PDF has increased from 0.6 to 0.9 whereas the p-values for the Weibull and Gumbel PDFs have decreased from 0.9 to 0.4: this can be interpreted as a "gaussianization" of B_n for large value of n.

	Rejecting the null-hypothesis	Asymptotic p-value
Normal PDF	No	0.8870
Weibull PDF	No	0.4418
Gumbel PDF	No	0.4091

Table 5.3. **Results of the KS tests for the parametric PDFs (Normal, Weibull, Gumbel) fitted to historical data set of 10-year average DNI $\{B_{n=10}(y_k)\}_{k\in[n+1,nd]}$.**

The Figure 5.6 presents the estimations of P99, P90, P75 and P50 of $B_{n=10}$ and the corresponding 95% confidence interval, with the three fitted PDFs (Normal, Weibull, and Gumbel PDFs). The red circles correspond to the CLT based analytical expressions of the PoE with the estimated mean and standard deviation of B.

As expected, the P99, P90, P75 values for $n = 10$ have increased compared to the case for which $n = 1$: due to the aggregation effect, the range of B_n is compacter than the range of B. The P99 estimated from the different fitted PDFs are notably different but their 95 % confident intervals overlap.

The CLT based analytical expressions of the PoE do not exactly correspond to the estimation with the fitted Normal PDF. The main reason of these differences is due to differences between the mean and standard deviation estimated during the fitting procedure of the historical data set of yearly DNI $\{B_{\boldsymbol{n}}(y_k)\}_{k\in[\boldsymbol{n+1},nd]}$ and the one directly computed from the mean and standard deviation of $\{B(y_k)\}_{k\in[\mathbf{1},nd]}$, assuming the conditions for the CLT. In other words, B seems to be not perfectly an independent and identically distributed (IID) stochastic process.

The Figure 5.5 represents the autocorrelations of $\{B(y_k)\}_{k\in[\mathbf{1},nd]}$ with respect different yearly lags (in blue) and their corresponding p-values. Except for the lags of 3 and 13 years, the levels of autocorrelation seem to be not really significant. For the lags 3 and 13 years, the p-values are only slightly higher than 0.05. Even if it is not definitive, we can have doubt about the independence of B.

In addition, considering the historical data set of yearly DNI $\{B(y_k)\}_{k\in[\mathbf{1},nd]}$ (see Figure 5.1), one can notice an increasing trend. With a Kendall's tau of 0.29, the Mann-Kendal non parametric test indicates a trend with a low p-value of 0.014 (Mann, 1945 ; Kendall, 1955), Besides, the KS test on the first half and the second half of the time series clearly rejects the null-hypothesis with a very low p-value (4×10^{-3}). These two facts clearly indicate that the time series $\{B(y_k)\}_{k\in[\mathbf{1},nd]}$ is not identically distributed.

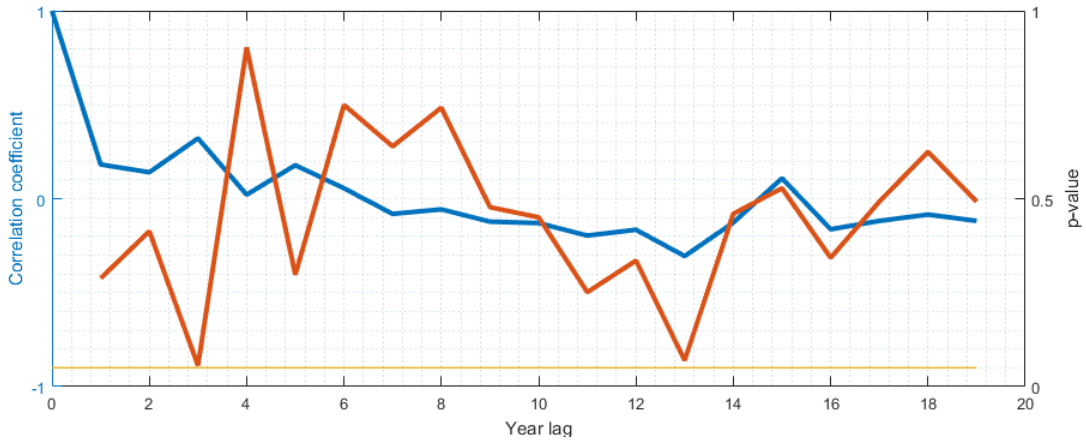

Figure 5.5. Autocorrelation of $\{B(y_k)\}_{k\in[\mathbf{1},nd]}$ (in blue) and the corresponding p-value (in red).

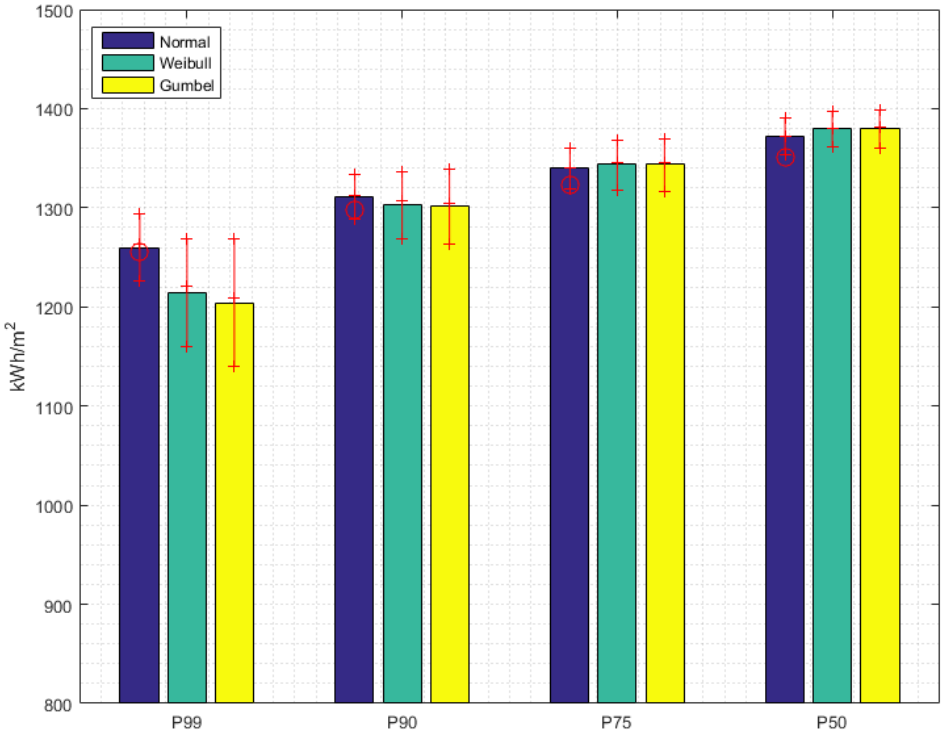

Figure 5.6. **Estimations of P99, P90, P75 and P50 of $B_{n=10}$ and the corresponding 95% confident interval, with the three fitted PDFs (Normal, Weibull, and Gumbel PDFs). The red circles correspond to the CLT based analytical expression of the Pxx with the estimated mean and standard deviation of B.**

5.4.3 The estimation based on non-parametric CDF using the technique of the kernel density estimation (KDE)

The method of kernel density estimation (KDE) is a non-parametric method to estimate the PDF – and therefore the CDF – from a data set (Parzen, 1962). This technique may be used to estimate the PDF of the underlying stochastic (Vignola, 2013).

The KDE technique consists of estimating the PDF of a data set $\{x_k\}_{k\in[1,n]}$ with the following KDE non-parametric function:

$$KDE(x) = \frac{1}{hn}\sum_{k=1}^{n} K\left(\frac{x-x_k}{h}\right) \quad (5.10)$$

Where:

- K is the a kernel function: a non-negative symmetric function such that $\int K(u)\,du$=1
- h is a smoothing parameter defining the bandwidth;

If the kernel function is simply the uniform function ($K(x) = \frac{1}{2}\mathbf{1}(|x| \leq 1)$, the KDE estimation corresponds to the empirical histogram estimation.

If the support of the kernel is finite, then the support of the corresponding CDF will be limited to the range $[min(\{x_k\}_{k\in[1,n]}) - h/2, max(\{x_k\}_{k\in[1,n]}) + h/2]$. For a normal kernel, the range is in practice limited to $[min(\{x_k\}_{k\in[1,n]}) - 3h, max(\{x_k\}_{k\in[1,n]}) + 3h]$ (at 99.7 %).

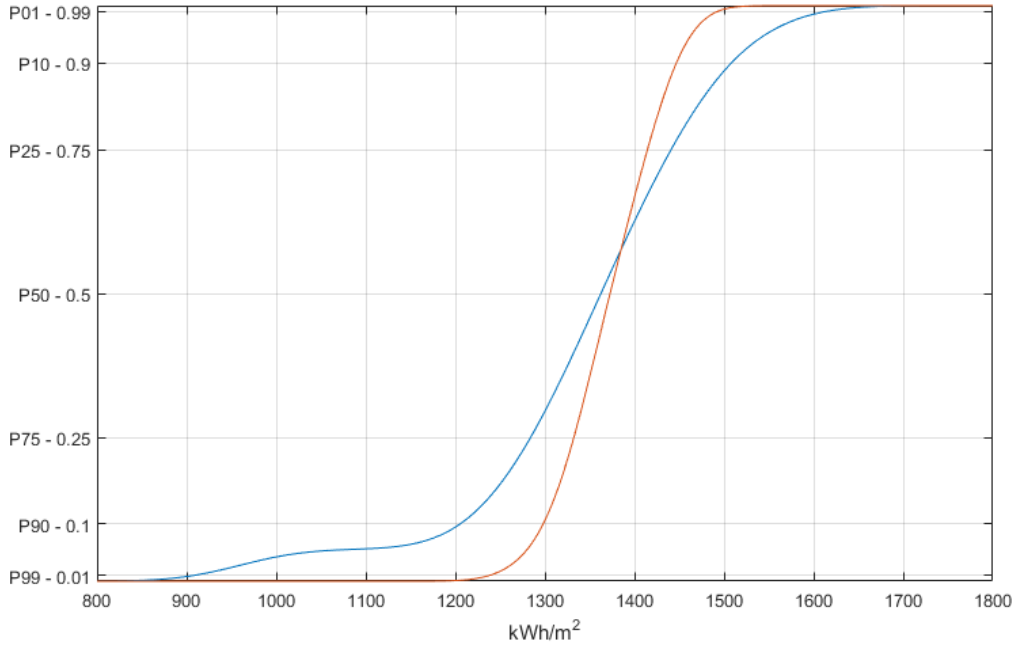

Figure 5.7. **Examples of KDE CDFs estimated from the historical data sets of yearly DNI $\{B(y_k)\}_{k\in[1,nd]}$ (in blue) and 10-year average DNI $\{B_{n=10}(y_k)\}_{k\in[n+1,nd]}$ (in red) from Eugene (to be compared to Figure 5.2).**

The Figure 5.7 presents, as an example, the CDFs estimated by the KDE technique from the historical data set $\{B(y_k)\}_{k\in[1,nd]}$ and the corresponding 10-year average DNI data set $\{B_{n=10}(y_k)\}_{k\in[n+1,nd]}$. The estimations of $P90[B]$ and $P90[B_{n=10}]$ are 1206 kWh/m^2 and 1298 kWh/m^2, respectively.

5.5 Inter-comparisons of the different approachs

We have presented six different approaches to estimate $P(v)[B_n]$:

- NORMFIT: estimation from the fitted Normal PDF;
- WBLFIT: estimation from the fitted Weibull PDF;
- GBLFIT: estimation from the fitted Gumbel PDF;
- ECDF: estimation from the empirical PDF;
- KDE: estimation from the KDE-based PDF (normal kernel);
- CLT: estimation from the assumption of the CLT and the equation (5.6);

Using a Monte-Carlo technique, we have assessed the uncertainty of $P(v)[B]$ estimations with the 6 different methods (NORMFIT, WBLFIT, GBLFIT, ECDF, KDE, CLT), for different lengths nd of the historical data set, ranging from 10 years to 50 years with a time step of 2 years.

To randomly generate this large number (1000) of synthetic data sets, we have used three different random generators of independent and identically distributed stochastic process, which parameters have been fitted with respect to the historical data set of yearly DNI $\{B(y_k)\}_{k\in[1,nd]}$:

- The Normal random generator;
- The Weibull random generator;
- The Gumbel random generator;

In order to have a fair comparison of the six methods, we have mixed all the estimations resulting from the three random generators, having, as a whole, 3000 synthetic randomly drawn data sets of yearly DNI.

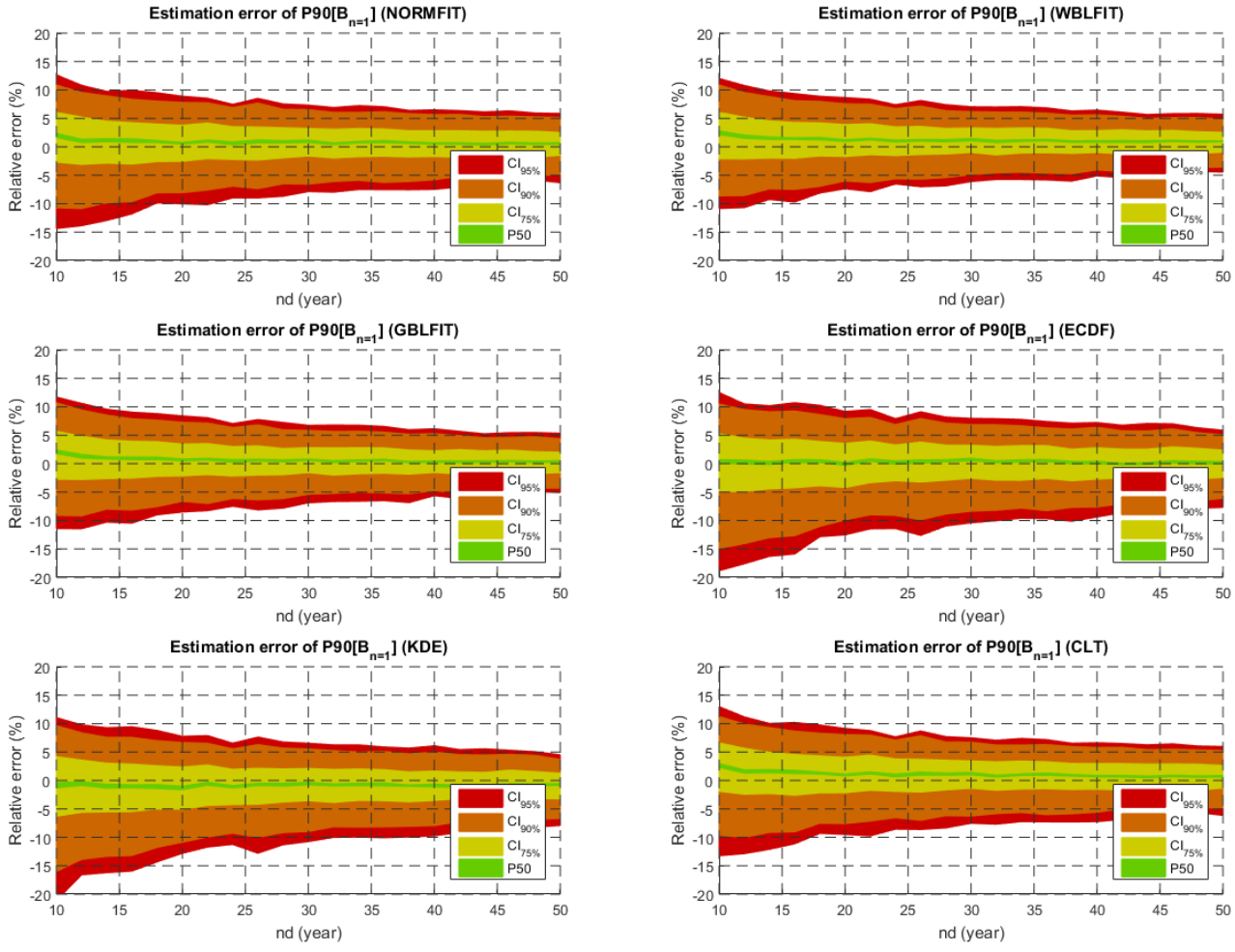

Figure 5.8. **Median errors (P50) and confidence intervals (CI) for different level (75%, 90% and 95%) of the estimation of $P90[B]$ with the six tested methods (NORMFIT, WBLFIT, GBLFIT, ECDF, KDE, CLT).**

In Figure 5.8 the results of the Monte Carlo analysis are presented: the median errors (P50) and *confidence intervals (CI)* for different level (75%, 90% and 95%) of the estimation of $P90[B_{n=1}]$ with the six tested methods (NORMFIT, WBLFIT, GBLFIT, ECDF, KDE, CLT).

One can first observe that the six methods enable CI at 75% of the estimation error below approximately 5 % with 10 years of historical data set, and more. The ECDF and KDE methods enable estimations of the P90 values with a median error close to 0. The other four approaches have a tendency to overestimate the P90 value, notably for the shorter historical periods from 10 to 15 years.

Globally, for all the methods, the confidence intervals at the level 95% are large and go below +/- 10% only after 20 years. One can notice for the methods ECDF and KDE, lower minimum values of confident intervals at the levels 90% and 95%, notably for the shorter historical periods. These "accidental" underestimations of the P90 values can be explained by the limitation of tail extrapolation of these two methods.

Despite the slight overestimations –positive P50 errors– of some methods, all of them are more or less equivalent for historical data set larger than 20 years. Globally, for shorter historical data sets, the WBLFIT method appears to be the slightly more accurate than the other methods.

As expected, the methods are significantly more accurate for the estimation of the P75 values (see Figure 5.9) and are more or less of comparable accuracy each other. The median errors of the ECDF method are close to 0, while the other methods present slight median underestimations, notably for the NORMFIT method.

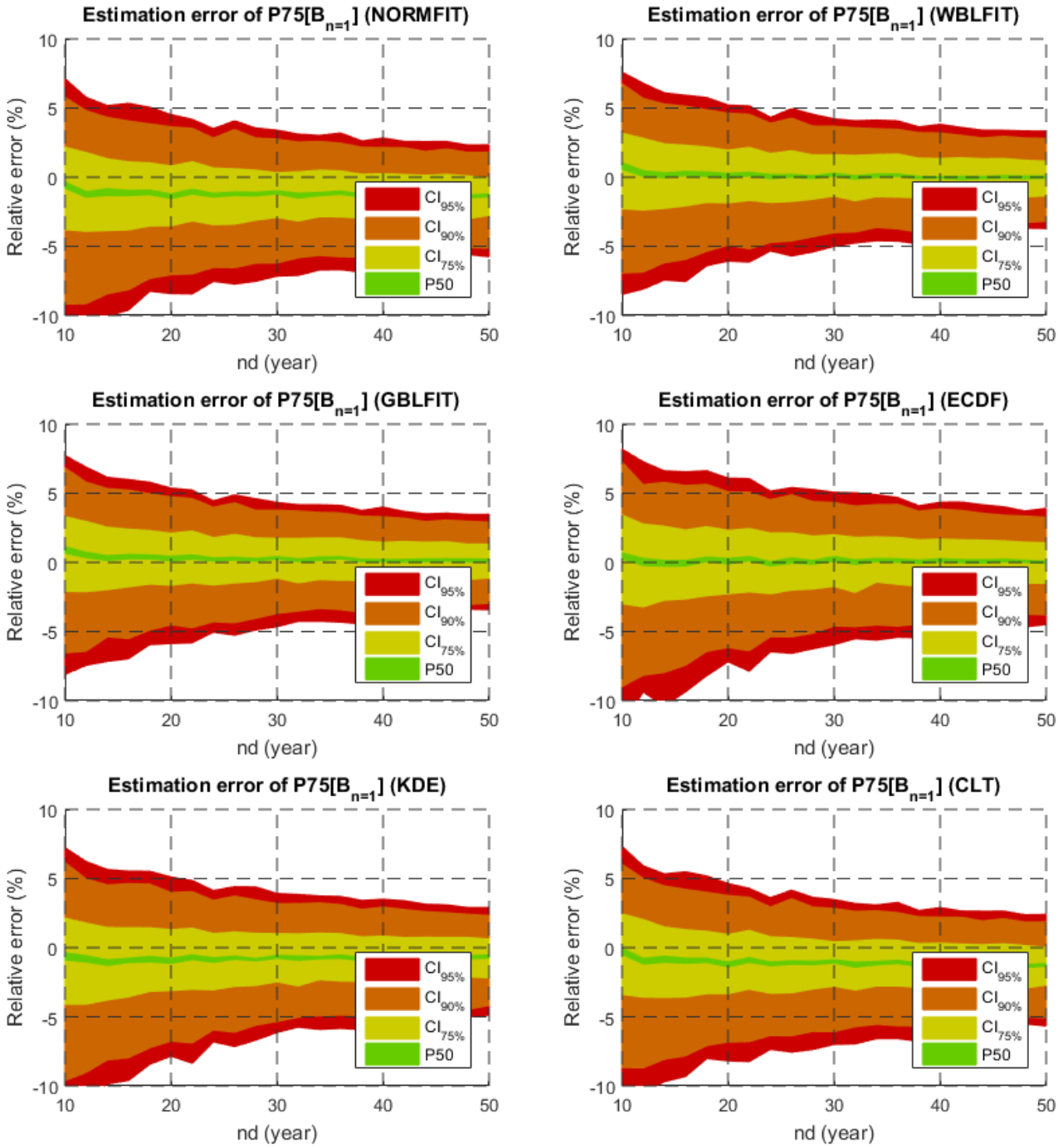

Figure 5.9. **Median errors (P50) and confident intervals (CI) for different level (75%, 90% and 95%) of the estimation of $P75[B]$ with the six tested methods (NORMFIT, WBLFIT, GBLFIT, ECDF, KDE, CLT).**

5.6 Conclusion

Six statistical methods to assess PoE values of yearly DNI from historical data sets have been described and illustrated for a specific case (36 years of yearly DNI at Eugene, USA). Except for the methods using empirical cumulative distribution function (ECDF) and kernel density estimator (EFDE), the four other approaches explicitly assume that the yearly DNI is an independent identically distributed process.

Under this assumption, a Monte Carlo analysis has been conducted to assess the uncertainty on the PoE estimations with the six methods, for different lengths of the historical data set, from 10 to 50 years. Since this Monte Carlo analysis has been done using the Eugene DNI data set as a reference for the random generations of synthetic data set, the presented uncertainty results can't be safely used for other situations. This study should be understood only as an example of a methodology that can be applied with a long-term DNI data set of interest, to get specific conclusions about the method to use and its related uncertainty.

Nevertheless, it is important to note that this uncertainty is only "theoretical". Indeed, this Monte-Carlo methodology is based on the very important assumption that the yearly DNI is an independent identically distributed process. In the example of the yearly DNI data set from Eugene, Oregon (USA), this assumption is clearly questionable, and we can suspect that it is not an exception as opposed to the rule.

Using statistical tools based on assumptions that are not clearly verified for their applications could be risky. There is a need of advanced statistical methodology to be able to detect and to handle non-identically distributed and/or non-independent process.

As a perspective, one can consider Monte-Carlo Markov Chain and fractional Gaussian noise random generators to be able to account for observed long-range correlation in time series (Mandelbrot, 1971 ; Hurst 1956 ; Handschy et al. 2015). These techniques of "realistic" or plausible time series generation meant to reproduce observed inter-annual correlation, trends, long-range memory (Hurst exponent) may be efficient to generate large numbers of representative synthetic very long term historical DNI data set to be used to assess the PoE values and their related uncertainties.

5.7 References

Cebecauer, T., M. Šúri, 2014. Improved Method for Generating Typical Meteorological Year Data for Solar Energy Simulations. *In* Solar Paces 2014, 39 pages.

Fernández Peruchena, C. M., L. Ramírez, M. A. Silva-Pérez, V. Lara, D. Bermejo, M. Gastón, S. Moreno-Tejera, J. Pulgar, J. Liria, S. Macias, R. Gonzalez, A. Bernados, N. Castillo, B. Bolinaga,

R. X. Valenzuela, L. F. Zarzalejo, 2016. A Statistical Characterization of the Long-Term Solar Resource: Towards Risk Assessment for Solar Power Projects. Solar Energy 123: 29–39. doi:10.1016/j.solener.2015.10.051.

Handschy, M., C. St. Martin, J. K. Lundquist, 2015. Reducing Wind Power Variability by Quantifying Geographic Diversity Length Scales, ICEM conference, poster 27, Boulder (CO).

Hurst, H. E. 1956. The Problem of Long-Term Storage in Reservoirs. International Association of Scientific Hydrology. Bulletin 1 (3): 13–27. doi:10.1080/02626665609493644.

Kendall, M.G., 1955. Rank Correlation Methods. Griffin, London. Kendall, M.G., Stuart, A., 1976. The Advanced Theory of Statis- tics, Vol. I: Distribution Theory. Griffin, London.

Mandelbrot, B. 1971. A Fast Fractional Gaussian Noise Generator. Water Resources Research 7 (3): 543–553. doi:10.1029/WR007i003p00543.

Mann, H.B., 1945. Nonparametric tests against trend, Econometrica, 13, 245-259.

Massey, F J., 1951. The Komolgorov-Smirnov Test for Goodness of Fit. Journal of American Statistical Association 46 (523): 68–78.

Parzen, E., 1962. On Estimation of a Probability Density Function and Mode. The Annals of Mathematical Statistics 33 (3), 1065(76), doi:10.1214/aoms/1177704472.

Vignola, F., 2013. Chapter 5 - Bankable Solar-Radiation Data sets, Solar Energy Forecasting and Resource Assessment, Editor Kleissl J., Elsevier, ISBN: 9780123971777.

Zieli, R., 2004. Optimal Quantile Estimators Small Sample Approach. IMPAN, preprint 653, 105 pages. (access: https://www.impan.pl/wydawnictwa/preprints_impan/p653.pdf*).*

6. Current methods for assessing the quality of a TMY data set

Once the typical meteorological year (TMY) data set has been generated with a given method, some statistical assessment procedures can be applied to assess –and report– its quality.

Three types of assessments can be considered:

- The standard meteorological quality check procedures (QCP);
- The statistical comparison of the TMY data set with respect the long-term (LT) data set;
- The representativeness of the short term variability of the TMY data set.

6.1 The meteorological quality check procedures (QCP)

A LT data set was used to generate the TMY data set. This LT data set should have passed standard quality check procedures to avoid invalid or suspicious data. But, possibly, gap filling methods, fusion processes between satellite estimations and ground measurements or the TMY generation procedure itself may have introduced artifacts on the final TMY data set. In addition, namely for the irradiance components in the TMY data set, the corresponding QCP should be reapplied on the TMY data set: indeed, the timestamp of these data sets in the TMY is "virtual" –because associated to a hypothetical year– and therefore may induce slight incoherency between the horizontal and direct normal time series of irradiance.

For all these reason, it is useful to reapply the standard QCPs on the TMY data set such as the one described by Espinar et al. (2012) and notably inspired by the QCPs recommended by BSRN (Ohmura et al., 1998). These QCPs are summarized in Table 6.1, depending on the time resolution:

	Hourly	Sub-hourly (1-minute average except for WS which is 2-minute)
GHI (Wm^{-2})	QCP based on extrema $0.03\ GHItoa < GHI < \min(1.2\ I_0, 1.5\ I_0 \cos(SZA)^{1.2} + 100$ QCP based on rare observations $0.03\ GHItoa < GHI < 1.2\ I_0 \cos(SZA)^{1.2} + 50$	QCP based on extrema $0.03\ GHItoa < GHI < \min(1.2\ I_0, 1.5\ I_0 \cos(SZA)^{1.2} + 100)$ QCP based on rare observations $0.03\ GHItoa < GHI < 1.2\ I_0 \cos(SZA)^{1.2} + 50$ Step QCP Maximum step for two following measures: 1000 W m^{-2}
BNI (Wm^{-2})	QCP based on extrema $0 < BNI < I_0$ QCP based on rare observations $0 < BNI < 0.95\ I_0 \cos(SZA)^{0.2} + 10$	QCP based on extrema $0 < BNI < I_0$ QCP based on rare observations $0 < BNI < 0.95\ I_0 \cos(SZA)^{0.2} + 10$
DHI (Wm^{-2})	QCP based on extrema $0.03\ GHItoa < DHI < \min(0.8\ I_0, 0.95\ I_0 \cos(SZA)^{1.2} + 50)$ QCP based on rare observations $0.03\ GHItoa < DHI < 0.75\ I_0 \cos(SZA)^{1.2} + 30$	QCP based on extrema $0.03\ GHItoa < DHI < \min(0.8\ I_0, 0.95\ I_0 \cos(SZA)^{1.2} + 50)$ QCP based on rare observations $0.03\ GHItoa < DHI < 0.75\ I_0 \cos(SZA)^{1.2} + 30$
Temp (°C)	QCP based on extrema $-90 < Temp < +60$ QCP based on rare observations $-80 < Temp < +50$ Step QCP Maximum step for two following measures: 8 °C	QCP based on extrema $-90 < Temp < +60$ QCP based on rare observations $-80 < Temp < +50$ Step QCP Maximum step for two following measures: 3 °C Minimum step over the past 60 minutes: 0.1 °C
Hum (%)	QCP based on extrema $0 < Hum < 100$ Step QCP Maximum step for two following values: 30 %	QCP based on extrema $0 < Hum < 100$ Step QCP Maximum step for two following values: 10 % Minimum step over the past 120 minutes: 0.1 %
WS ($m\ s^{-1}$)	Step QCP maximum step for two following values: 15 m s^{-1}	QCP based on extrema (2-min average) $0 < WS < 150$ QCP based on rare observations (2-min average) $0 < WS < 80$ Step QCP maximum step for two following values (2-min average): 20 m s^{-1} Minimum step over the past 60 minutes except for no wind periods (1-minute average): 0.5 m s^{-1}
Cosistency checks	For GHI > 20 W m^{-2} (if not, test not possible) $GHI / (BHI + DHI) = 0.15$ $DHI \leq 1.1\ GHI$	For GHI > 50 (if not, test not possible): DHI/GHI < 1.05, for SZA < 75° DHI/GHI < 1.10, for 93° > SZA > 75° For DHI+BHI > 50 (if not, test not possible) $GHI / (BHI+DHI) \leq 0.08$, for SZA < 75° $GHI / (BHI+DHI) \leq 0.15$, for 75°< SZA <93°

Table 6.1: **QCPs for the main meteorological parameters extracted from Espinar et al. (2012) and notably inspired by QCPs proposed for BSRN (Ohmura et al., 1998).**

6.2 The statistical comparison of the TMY data set with respect the LT data set

Once the TMY data set has been generated, it is worth assessing –and checking– *a posteriori* if the TMY data set is indeed representative of the corresponding LT meteorological data set. This as-

sessment is based on statistical comparisons, in the TMY and LT data sets, of some specific individual meteorological parameters or some specific combinations of them.
One possible combination of meteorological parameters is the combination of relevant meteorological parameters leading to a representative estimation of the electric production, or at least those on which it depends most. This type of electric-production related combination has been introduced in the framework of the FP7 project ENDORSE by Espinar et al. (2012) as the *driver* component of the TMY.

TMY data sets can be generated using this specific driver component or using weighting coefficients or the different meteorological parameters as proposed in TMY2 or TMY3 (Wilcox and Marion, 2008). Cebecauer and Suri (2015) have proposed in addition other weighting coefficients depending on the solar energy application (e.g. PV or CSP/CPV).

Whatever the method used for the TMY generation, it is worth assessing the representativeness of the TMY data set by comparing the representativeness of the driver component computed from the TMY data set and the one computed with the original LT meteorological data set.

For example, let us consider a TMY data set generated for a CSP project with parabolic troughs. The driver component of interest could be for example the thresholded effective DNI as discussed by Rheinländer (2008) and Meyer et al. (2009), to take into account:

- the solar angle of incidence for the parabolic trough to assess the effective DNI;
- the shut down and the dumping effects respectively for too low and too high effective DNI;
- the effect of wind speed above a certain speed threshold for which the sun tracking system is in a secure mode.

For a North-South parabolic system, the following driver D could be considered:

$$D = Min(D_m, D_{max})T(D_m \geq D_{min})T(WS < WS_{max}) \quad (6.1)$$

$$D_m = DNI\sqrt{1 - \cos(\gamma_s)^2 \cos(\phi_s)} \quad (6.2)$$

Where:

- γ_s is the sun elevation angle (rad);
- ϕ_s is the sun azimuth angle (rad);
- DNI is the direct normal irradiance component of the meteorological data set (W/m^2);
- D_m is the effective DNI (W/m^2);
- D_{min} is the minimum effective DNI for the shut-down effect;
- D_{max} is the maximum effective DNI for the dumping effect;
- WS_{max} is the maximum wind speed for the secure mode;
- $T(C)$ is the threshold function equal to one if the condition C is true, zero otherwise.

It is to be noted that the minimum and maximum effective DNI correspond to a very simplified model to take into account the shut-down and dumping effects.
The representativeness assessment of the TMY data set for each individual meteorological parameter could be also of interest to answer the following "side" question: does the TMY data set have normal or "unusual" time series of temperature, relative humidity, etc.?

Mathematically, these statistical comparisons are in fact applied between $F(TMY)$ and $F(LT)$, where F can be the exact extraction of one particular parameter among the meteorological parameters or a combination of them. Since $F(TMY)$ and $F(LT)$ have of course unequal samples, it is technically impossible to use the standard comparison criteria such as the root mean square error, the standard deviation of the errors, the mean absolute error or the correlation coefficient. Indeed, these criteria require comparisons on a sample-by-sample basis.

The statistical comparisons are based on the experimental histograms or the experimental cumulative distribution functions (CDF) that can be estimated separately from the time series of $F(TMY)$ and $F(LT)$. These experimental histograms and CDFs can be assessed and compared for the whole year or for smaller time periods such as season per season, month per month, etc.
Hereinafter, the symbol $E[x]$ designates the expectation of x and the symbol $V[x]$ designates the variance of x:

$$V[x] = E[(x - E[x])^2] \tag{6.3}$$

The most obvious and natural comparison criterion is the bias or the mean error (ME):

$$ME = E[F(TMY)] - E[F(LT)] \tag{6.4}$$

The relative mean error, rME, is defined as the ratio of ME to the mean value of $F(LT)$:

$$rME = ME/E[F(LT)] \tag{6.5}$$

Comparisons of higher moments can be also made, with the order-n central moment error (M_nE):

$$M_nE = E[(F(TMY) - E[F(TMY)])^n] - [(F(LT) - E[F(LT)])^n] \tag{6.6}$$

M_2E corresponds to the comparisons of the variances of $F(TMY)$ and $F(LT)$;

For $n = 3\ or\ 4$, when these order-n central moments are normalized by the corresponding variance, we have:

- The comparisons of the skewness of $F(TMY)$ and $F(LT)$:

$$SE = E\left[\left(-\frac{F(TMY)-E[F(TMY)]}{\sqrt{V[F(TMY)]}}\right)^3\right] - \left[\left(\frac{F(LT)-E[F(LT)]}{\sqrt{V[F(LT)]}}\right)^3\right] \tag{6.7}$$

- The comparisons of the kurtosis of $F(TMY)$ and $F(LT)$:

$$KE = E\left[\left(-\frac{F(TMY)-E[F(TMY)]}{\sqrt{V[F(TMY)]}}\right)^4\right] - \left[\left(\frac{F(LT)-E[F(LT)]}{\sqrt{V[F(LT)]}}\right)^4\right] \quad (6.8)$$

Since the central moments can be used as a description of the Fourier transform of the corresponding probability density function, their comparisons aim at describing the discrepancy between the histograms of $F(TMY)$ and $F(LT)$.

There are more straightforward approaches to compare the two histograms, making use of distances between their two corresponding CDFs.

One can use the Kolmogorov-Smirnov distance defined as:

$$d_{KS} = \max\left(\left|CDF_{F(TMY)}(x) - CDF_{F(LT)}(x)\right|\right) \quad (6.9)$$

A distribution-free statistical test of goodness of fit between the two CDFs can be setup (Massey, 1951) from this distance. For large data set with more 35 samples, the null hypothesis stating that the two CDF are coming from the same distribution is rejected if d_{KS} is greater than a critical value CV_{KS}^{α} depending on the significance level α and on the effective number of samples n_e.

$$CV_{KS}^{\alpha=0.01} \approx \frac{1.63}{\sqrt{n_e}} \quad (6.10)$$

This effective number of samples n_e is defined by:

$$n_e = \frac{n_{LT}n_{TMY}}{n_{LT}+n_{TMY}} = \frac{n_{LT}^{y}}{n_{LT}^{y}+1}n_{TMY} \quad (6.11)$$

Where n_{TMY} and n_{LT} are respectively the number of samples of TMY and LT and n_{LT}^{y} is the number of years of the LT data set.

The KS can be expressed in % as the ratio of d_{KS} to its corresponding critical value:

$$KS = \frac{d_{KS}}{CV_{KS}^{\alpha=0.01}} \quad (6.12)$$

Espinar et al. (2009) have proposed the Kolmogorov-Smirnov integral test (KSI) which aims at quantifying the difference of the two CDFs over the whole range of value, not just for the maximum absolute value. This KSI consist in computing the Kolmogorov-Smirnov distances $d_{KS}(x,m)$ for M regular intervals between the minimum and maximum values x_{min} and x_{max}:

$$d_{KS}(x,m) = \begin{cases} \max_{x \in I_m}\left(\left|CDF_{F(TMY)}(x) - CDF_{F(LT)}(x)\right|\right) \; if \; x \in I_m \\ 0 \; otherwise \end{cases} \quad (6.13)$$

With:

$$I_m = [x_{min} + (m-1)\Delta x, x_{min} + m\Delta x] \text{ and } \Delta x = \frac{(x_{max} - x_{min})}{M} \quad (6.14)$$

The trapezoidal numerical integration is then used to assess the KSI that can be expressed in %:

$$KSI = \frac{\int_{x_{min}}^{x_{max}} d_{KS,m}(x)dx}{CV_{KS}^{\alpha=0.01}(x_{max} - x_{min})} \quad (6.15)$$

If the result of the KSI is greater than 100%, then the null-hypothesis stating that the two CDFs are coming from the same underlying stochastic process is rejected.

Example:

Let consider a TMY generated from a LT data set (13 years between 1997 and 2009), following the TMY3 algorithm (Wilcox and Marion, 2008), but solely considering the DNI component (the other weighting coefficients are set to 0). The temporal resolution is, in this case 15 min.

The F function used for the statistical comparison is the driver D with $D_{min} = 150\ \mathrm{W/m^2}$ and $D_{max} = 850\ \mathrm{W/m^2}$.

Figure 6.1 presents the correlogram of the driver D versus the corresponding DNI and highlights the non-linear effect of the driver function.

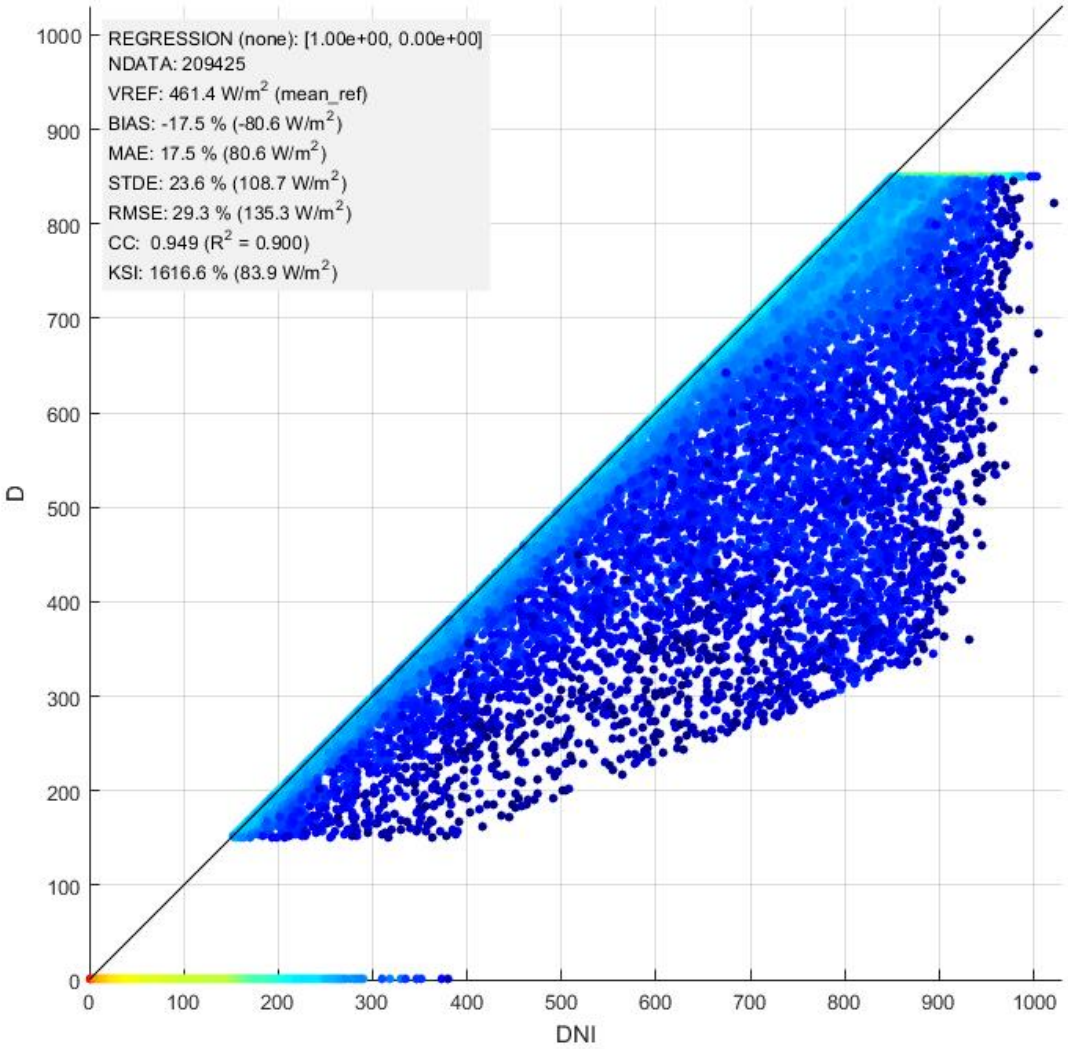

Figure 6.1. **Correlogram of the driver $D(LT)$ versus the corresponding DNI for the LT data set. The color represent the density in log-scale of the scatterplot (red: highest density, blue: lowest density).**

The relative mean errors at the monthly and yearly basis are presented in Figure 6.2:

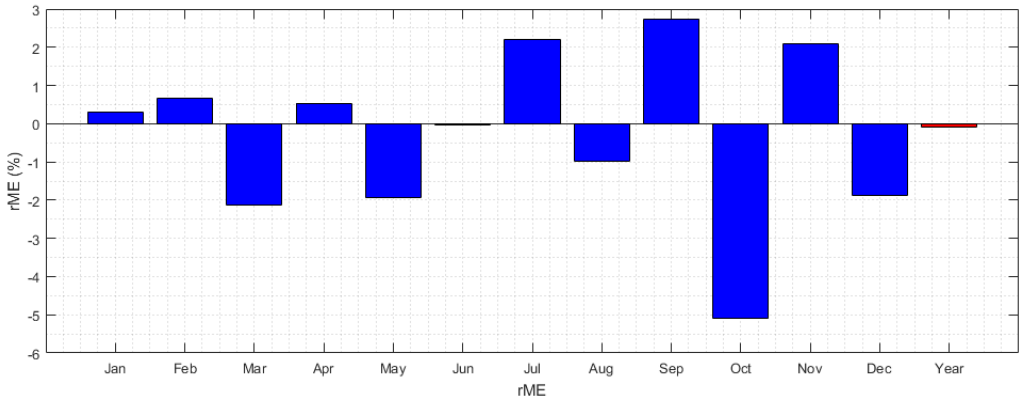

Figure 6.2. **Relative mean errors between $D(TMY)$ and $D(LT)$ at the monthly basis and for the whole year.**

For the whole year, $D(TMY)$ presents a very small underestimation of less than 0.01% with respect to the mean value of the original LT data set. Nevertheless, this yearly rME "hides" some compensating effects at the monthly basis with overestimation of approximately 2% for the months July, September and November and underestimations larger than 2% (up to 6%) for the months March, May and October.

Figure 6.3 presents the comparison between the two CDFs for the computation of KS for the whole year.

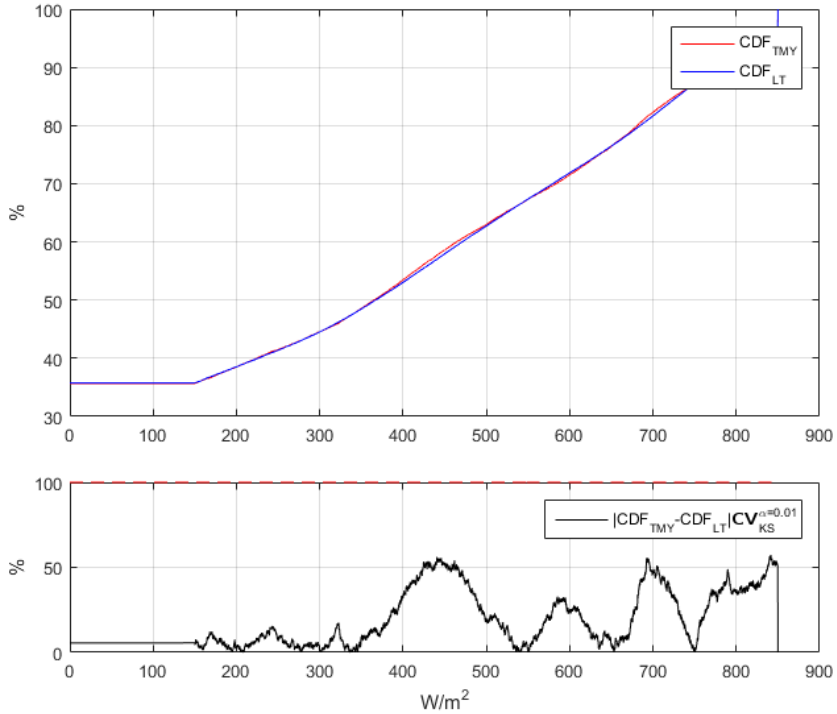

(a)

(b)

Figure 6.3. **(a) Comparison of the CDFs of $D(TMY)$ and $D(LT)$ for the whole year. (b) Ratio of the absolute difference between the two CDFs to the corresponding critical value (%).**

This comparison shows that KS is slightly greater than 57%: in this case, the null-hypothesis of the KS test is accepted, meaning that the difference between the two CDFs is not significant.
The same analysis can be done at the monthly basis, as presented by Figure 6.4:

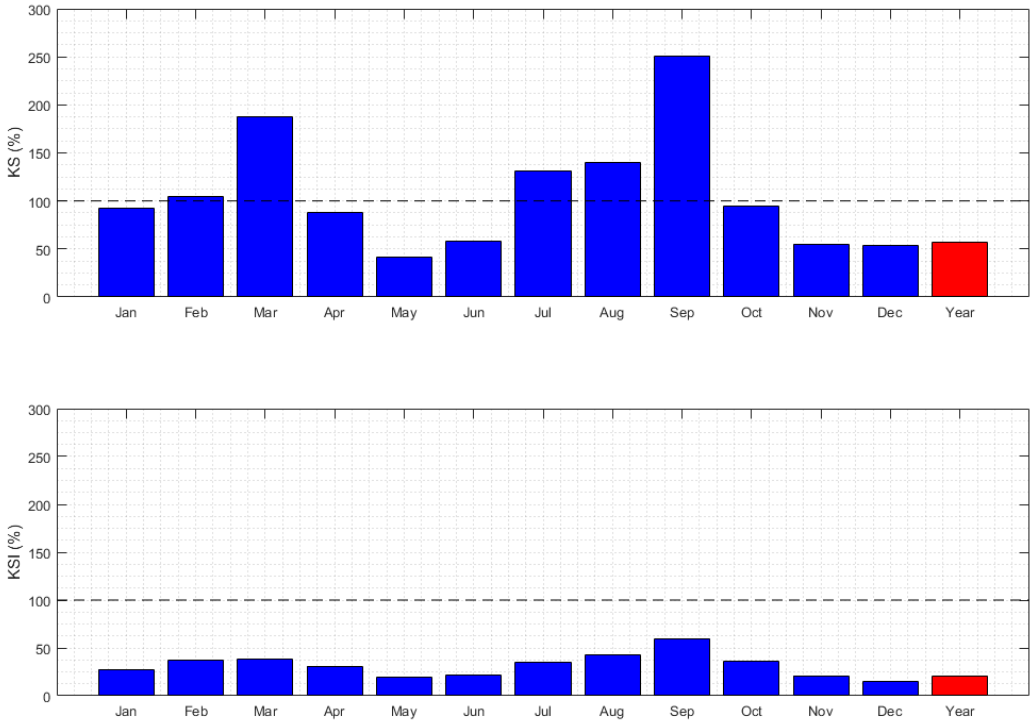

Figure 6.4. KS and KSI criteria for the comparison of the two CDFs, at the monthly and yearly basis.

The null-hypothesis of the KS test should be rejected for the months February, March, July, August and September. However, the KSI shows that the differences between the two CDFs are not so significant, when considering the whole range of values.

6.3 The representativeness of the short term variability of the TMY data set (future work)

The different comparisons described in the previous section aims at assessing the representativeness of the TMY data set with respect to the LT meteorological data set at the monthly, seasonally or yearly basis. Another important aspect for the statistical analysis of the quality of the TMY data set is the representativeness of the TMY data set with respect to the short term variability, typically at the hourly and even the intra-hourly basis. Indeed, short term variability of the DNI may have some important –and non-linear– impacts on the electric production of a CSP plant and on the management of its thermal storage: at least the DNI of the TMY data set should be also typical for this aspect.

To compare the short term variability of the DNI time series of TMY data set, it is important to consider as a reference a time series provided by an in-situ sensor with the adequate temporal resolution. The LT data set composed of satellite-based estimation of DNI cannot be used as a reference, since the satellite images used for the estimation generally suffer from a deficit of both spatial and temporal resolutions.

The following approach could be tested in future works to assess the representativeness of the short variability of the DNI time series in the TMY data set (TMY-DNI) with respect to oa DNI time series of reference (REF-DNI).

This approach is based on the comparison of the scatter diagrams "*Arrow Head*" proposed by Stein et al. (2012). This scatter diagram is composed of:

- the daily Sandia variability index VI on the x-axis, defined as:

$$VI = \frac{\sum \sqrt{\left(DNI(k) - DNI(k-1)\right)^2 + \Delta t^2}}{\sum \sqrt{\left(DNI_{cls}(k) - DNI_{cls}(k-1)\right)^2 + \Delta t^2}} \tag{6.16}$$

- the daily direct clearness index KC_b on the y-axis, defined as:

$$KC_b = \frac{\sum DNI(k)}{\sum DNI_{cls}(k)} \tag{6.17}$$

The index k is the time index within the day and Δt corresponds to the corresponding time sampling period. DNI_{cls} has been computed from clear-sky model of the direct normal irradiance. This clear-sky model should be in this case "neutral" and only based on climatology in order not to account for ozone, water-vapor or aerosol induced short term variability. The ESRA model (Rigollier et al., 2004) that makes use of the worldwide climatological monthly averages of Linke turbidity (Remund et al., 2003) may be used for this analysis.

Again the Kolmogorov-Smirnov test can be used to accept or reject the null hypothesis stating that the 2-dimensionnal samples of (KC_b, VI) from the TMY-DNI and the REF-DNI time series have the same underlying probability distributions.

Figure 6.5 presents examples of "Arrow Head" diagrams of:

- REF-DNI (a) that corresponds to the 15-min DNI of the LT data set used as an example in the previous section;
- TMY-DNI (b) that corresponds to the 15-min DNI from the TMY data set;
- TMY-DNI-h (c) that corresponds to the hourly aggregated version of TMY-DNI that has been resampled to the 15-min temporal resolution.

The Kolmogorov-Smirnov 2D test accepts the null-hypothesis for TMY-DNI (p-value: 0.2) and rejects it for TMY-DNI-h (p-value: 6×10^{-21}). Indeed, owing to (a) and (b), many "intermediate" situations of clearness index correspond to high variability index, larger than 3. For these situations, TMY-DNI-h has a variability index limited to 3.

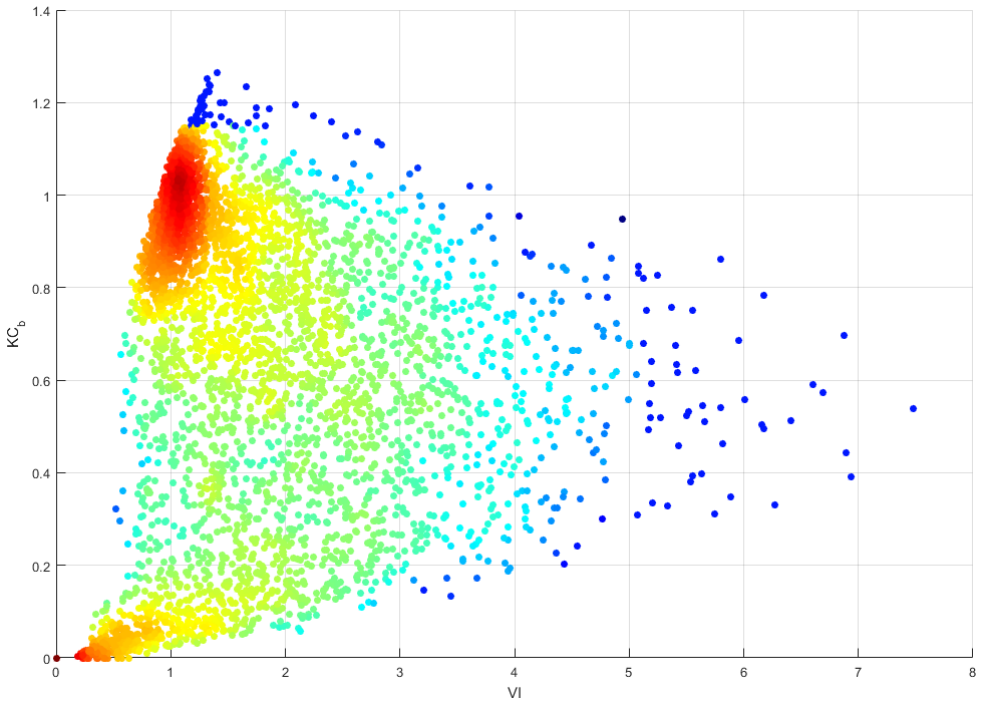

(a)

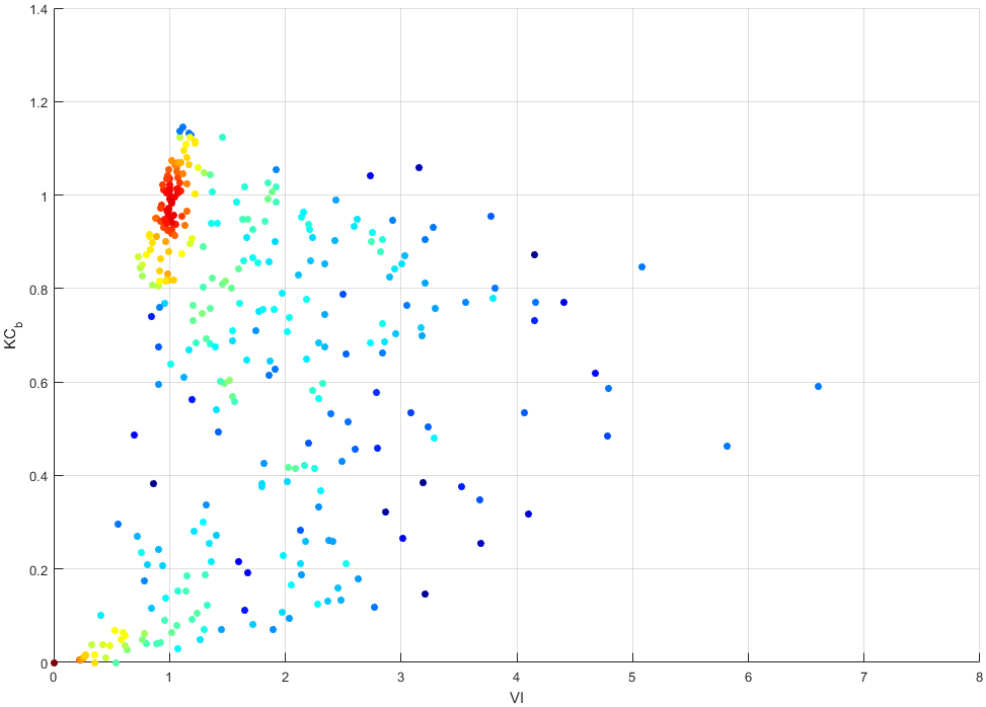

(b)

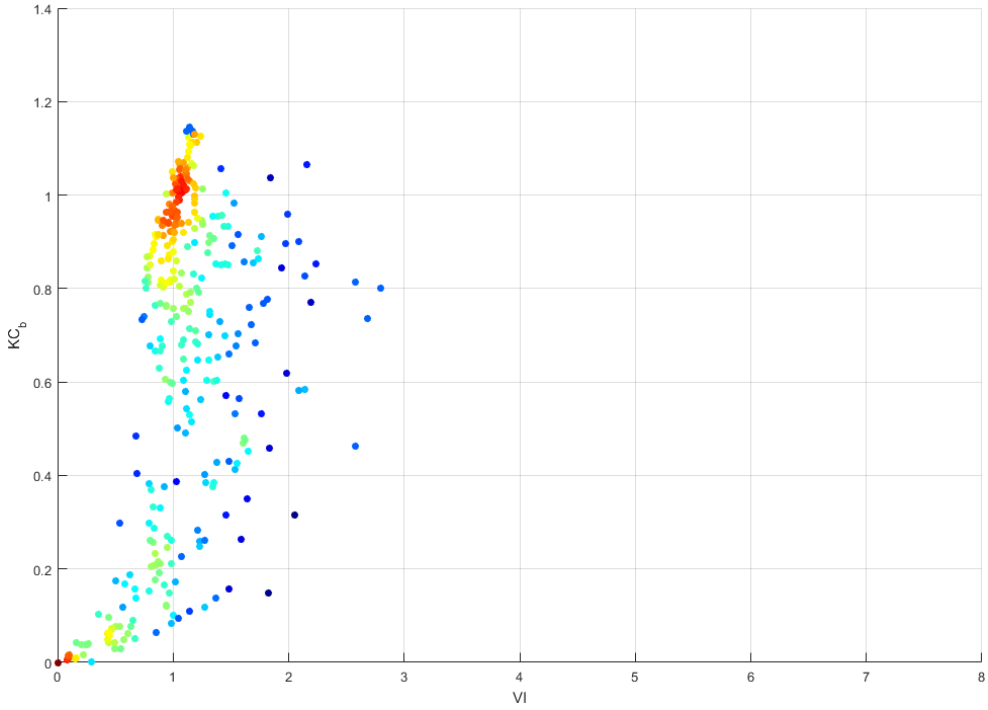

(c)

Figure 6.5. **Examples of "Arrow Head" diagrams of the REF-DNI (a), the TMY-DNI (b) and the TMY-DNI aggregated at the hourly basis (c). The color corresponds to the density of the scatterplots, in log-scale (red: highest density, blue: lowest density).**

Another possible approach for the short term variability assessment would be to compare the intra-daily power spectral density (PSD) of the TMY-DNI and REF-DNI.

The two PSDs can be estimated using the Welch's method (Welch, 1967) and could be used for a graphical comparison, as presented by the following figure (6.6):

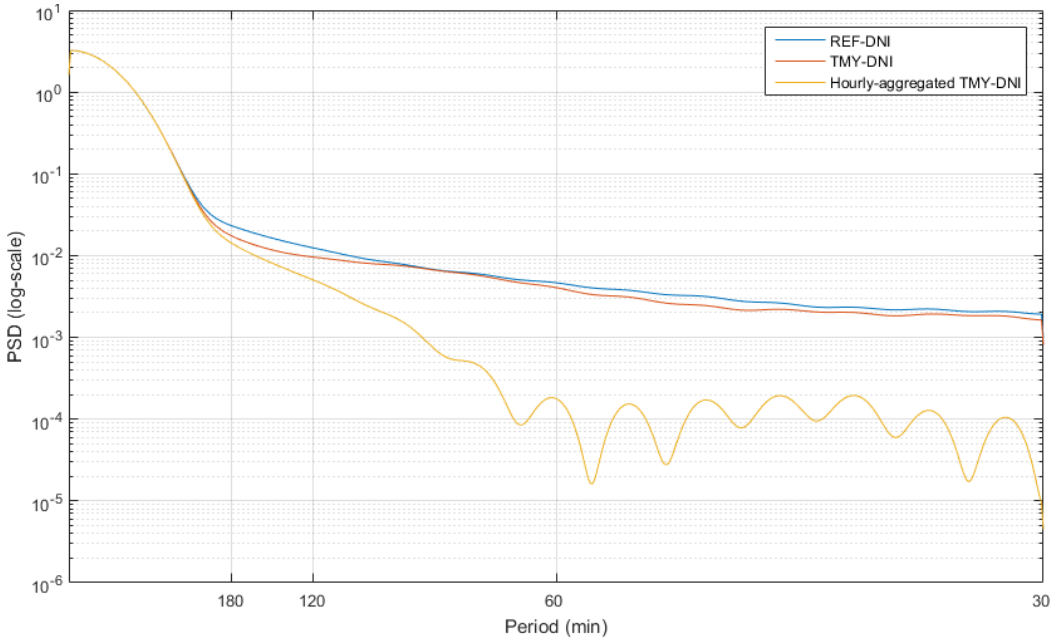

Figure 6.6: PSD comparison of REF-DNI, TMY-DNI and TMY-DNI-h.

The PSD of REF-DNI and TMY-DNI present small discrepancy: TMY-DNI presents slightly less energy for short term variability with temporal periods less than 180 min. As expected, TMY-DNI-h presents obvious and large deficit of its short term variability, for temporal periods less than 180 min that is even more important for temporal periods less than 60 min.

Statistical tests for spectral density comparisons with unequal samples exist (Preuß and Hildebrandt, 2013 ; Jentsch and Pauly, 2010 ; Caiado et al., 2007 ; Diggle and Fisher, 1991). Diggle and Fisher (1991) notably proposed to set up a statistical test based on the Kolmogorov-Smirnov distance on the cumulative power spectral densities.

Nevertheless, these different tests are quite complex to implement and to use: bootstrap techniques in the frequential domain (Dahlhaus and Janas, 1996) should be used to determine the critical values and the power of the tests are difficult to assess. Using these complex comparison techniques is out of the scope of this study.

6.4 References

Caiado, J., N. Crato, D. Pena, 2007. Comparison of Time Series with Unequal Length. MPRA Paper n° 6605, 19 pages.

Cebecauer, T., and M. Suri. 2015. “Typical Meteorological Year Data: SolarGIS Approach.” Energy Procedia 69. Elsevier B.V.: 1958–69. doi:10.1016/j.egypro.2015.03.195.

Dahlhaus, R., D. Janas, 1996. A Frequency Domain Bootstrap for Ratio Statistics in Time Series Analysis. The Annals of Statistics 24 (5): 1934–1963.

Diggle, P.J., N. I. Fisher, 1991. Nonparametric Comparison of Cumulative Periodograms. Applied Statistics 40 (3): 423–434.

Espinar, B., L. Ramirez, A. Drews, H. G. Beyer, L. F. Zarzalejo, J. Polo, L. Martin, 2009. Analysis of Different Comparison Parameters Applied to Solar Radiation Data from Satellite and German Radiometric Stations. Solar Energy, 83, 1, 118–125. doi:10.1016/j.solener.2008.07.009.

Espinar, B., P. Blanc, L. Wald, C. Hoyer-Klick, M. Schroedter Homscheidt, and T. Wanderer. 2012. "On Quality Control Procedures for Solar Radiation and Meteorological Measures, from Sub-hourly to Montly Average Time Periods." In EGU General Assembly 2012. Vienne, Austria.

Espinar, B., P. Blanc, L. Wald, 2012. Report on the product S4 "TMY for production". FP7 project ENDORSE (Grant Agreement no 262892), D404.1, 12 pages (access: http://www.endorse-fp7.eu/sites/www.endorse-fp7.eu/files/docs/ENDORSE_D404_S4_Ed1.2.pdf).

Jentsch, C., M. Pauly, 2010. Testing Equality of Spectral Densities Using Randomization Techniques (2008).

Massey, F J. 1951. The Komolgorov-Smirnov Test for Goodness of Fit. Journal of American Statistical Association 46 (523): 68–78.

Meyer, R., H.G. Beyer, J. Fanslau, N. Geuder, A. Hammer, T. Hirsch, C. Hoyer-klick, N. Schmidt, M. Schwandt, 2009. Towards Standardization of CSP Yield Assessments. SolarPACES, Germany, 8 pages.

Ohmura, A., E. G. Dutton, B. Forgan, C. Fröhlich, H. Gilgen, H. Hegner, A. Heimo, G. König-Langlo, B. McArthur, G. Müller, R. Philipona, R. Pinker, C. H. Whitlock, K. Denne and M. Wild, 1998. Baseline Surface Radiation Network (BSRN/WCRP): New Precision Radiometry for Climate Research. Bulletin of the American Meteorological Society 79 (10): 2115–36. doi:10.1175/1520-0477(1998)079<2115:BSRNBW>2.0.CO;2.

Preuß, P., T. Hildebrandt, 2013. Comparing Spectral Densities of Stationary Time Series with Unequal Sample Sizes. Statistics & Probability Letters 83 (4) (April): 1174–1183. doi:10.1016/j.spl.2013.01.015.

Remund, J., L. Wald, M. Lefèvre, T. Ranchin, J. Page, 2003. Worldwide Linke Turbidity Information. In ISES Solar World Congress, 13 pages.

Rheinländer, J., 2008. Technical and economic performance of parabolic trough solar power plants – a computational tool for plant feasibility studies. *In* 14th SolarPACES, USA.

Stein, J. S, M. J. Reno, C. W. Hansen, 2012. The variability index: a new and novel metric for quantifying irradiance and pv output variability. *In* WREF, 7 pages (access: http://energy.sandia.gov/wp-content/gallery/uploads/Stein_ASES_2012_VI_paper_SAND2012-2088C.pdf)

Welch, P. D., 1967. The Use of Fast Fourier Transform for the Estimation of Power Spectra: A

Method Based on Time Averaging Over Short, Modified Periodograms. IEEE Transactions on Audio Electroacoustics, AU-15, 70–73.

Wilcox, S., W. Marion, 2008. Users Manual for TMY3 Data sets. Renewable Energy. doi:NREL/TP-581-43156.

7. Modeling the variability of DNI in advanced stochastic CSP/STE plant feasibility analysis

7.1 Introduction

Like most renewable energy technologies, Concentrating Solar Power (CSP) Solar Thermal Electric (STE) power plants are capital intensive (Hirth and Steckel, 2016). While in all investment decisions it is important to have an accurate appraisal of the risks involved, in capital-intensive projects this is essential. As (Westney, 2011) indicates , to assess the attractiveness of capital-intensive energy projects one has, among other things, to estimate:

1. The investment cost or Capital Expenditure (CAPEX) of the energy production facility.
2. The time required for construction, commissioning and starting-up of the energy production facility.
3. The maximum cash impairment one is likely to experience before positive cash-flow.
4. The time require for achieving full production.
5. The Operating Expenditures (OPEX) during the lifetime of the energy production facility.
6. The likelihood of achieving sufficient operating margin to service the debt obligations.

Based upon these estimations, one should strive to obtain a sound estimate of the likelihood of achieving the desired economic return.

7.1.1 Traditional economic feasibility analysis

To obtain all of these estimates and to assess the economic return on the investment and the associated risk, the traditional approach is a deterministic one. It combines an energy performance model and an economic model to estimate costs and revenues through the whole stages of the project's lifetime (design, construction, commissioning, years of operation and final decommissioning). Its deterministic character derives from the fact that:

1. The input values fed to the models are point values, i.e., they are not ranges, but singular values.
2. The output values generated by the models are also point values.

3. A particular set of inputs values fed to the models always yield the same set of output values.

Within the framework of the deterministic approach, the feasibility study of a CSP/STE power plant is carried as indicated in Figure . Cost input data is supplied as input to the Financial Model best estimates for each relevant CAPEX and OPEX cost item, while the Annual Electricity Generation is obtained using an energy model that takes as input data a Typical Meteorological Year (National Climatic Data Center/NESDIS/NOAA/U.S. Department of Commerce et al., 1981), which represents the average long-term estimates of the meteorological variables along the year, typically with an hourly frequency. With this input and the input needed to establish basic financial assumptions, such as the Inflation Rate, the weighted average cost of capital (WACC), etc., the Financial Model generates estimates of key financial performance parameters of the investment project, such as the Net Present Value (NPV), the Internal Rate of Return (IRR), the Debt Coverage Ratio (DCR), or the Levelized Cost of the Electricity (LEC) that will assist the investors in deciding if the project should be pursued.

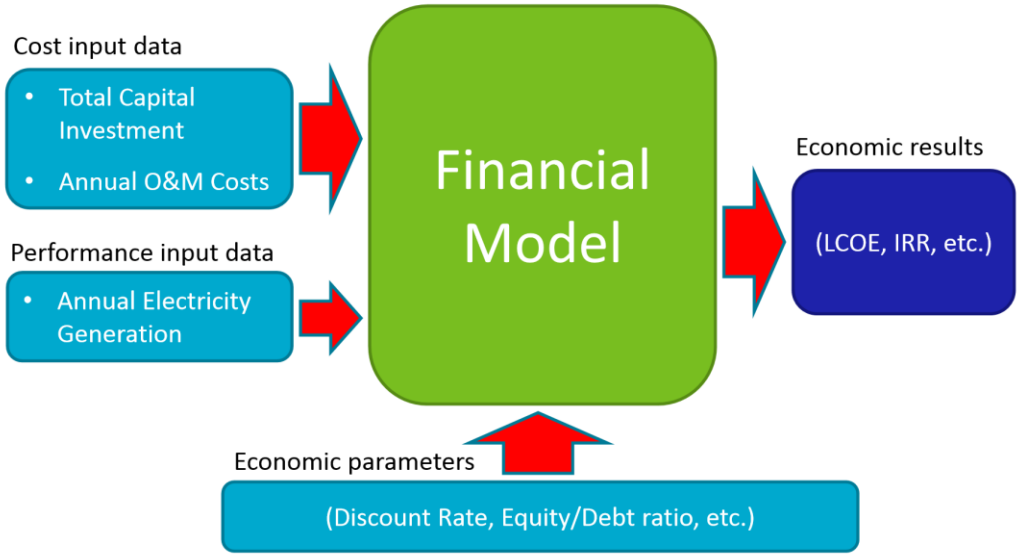

Figure 7.1. Traditional deterministic economic analysis of a CSP/STE power plant. The Annual Electricity Generation is obtained using an energy model that takes as input data a Typical Meteorological Year, which represents the average long-term estimates of the meteorological variables along the year, typically with an hourly frequency.

Within this deterministic framework, the assessment of the project risk related to the uncertainty and/or the variability of many of the assumptions that determine the inputs to energy performance and financial models, is addressed by carrying out a series of sensitivity analyses, where the most relevant parameters are varied within some range and the effect of this variation on the outputs of the financial model is analyzed. However, as pointed out by Marshall (Marshall, 1999):

"the major disadvantage of sensitivity analysis is that there is not explicit probabilistic measure of risk exposure. That is, although one might be sure that one of several outcomes might happen, the analysis contains no explicit measure of their respective likelihoods." In other words, the traditional sensitivity analysis is ill-prepared to assess risk.

7.1.2 Stochastic economic feasibility analysis

To overcome the limitations of the traditional approach, many have proposed stochastic approaches. As pointed out by (Crudden, 2012):

> *"Stochastic analysis, based on the Monte Carlo simulation technique, introduces an additional dimension to risk analysis by bringing objectivity and dynamism to project evaluation making it a logical extension to sensitivity and scenario analyses. Monte Carlo utilises a project's key risk variables to build up a large number of random scenarios in order to provide a comprehensive probability distribution of the expected risk and return profile for a given project. Monte Carlo augments traditional investment appraisal by providing a full array of investment outcomes and expands the probability of those outcomes eventuating over the single value number that is provided by deterministic appraisal. Importantly, the simulation must be managed so that model does not infringe any known or suspected correlations between variables. For example, it is likely that a protracted construction period will also result in additional construction costs and this positive correlation should be factored into the model."*

The application of the stochastic approach to obtain the estimates of all the relevant techno-economic parameters associated with the design, construction, and operation of a CSP/STE power plant and to assess the economic return on the investment and its associated risk is done as explained in Figure .

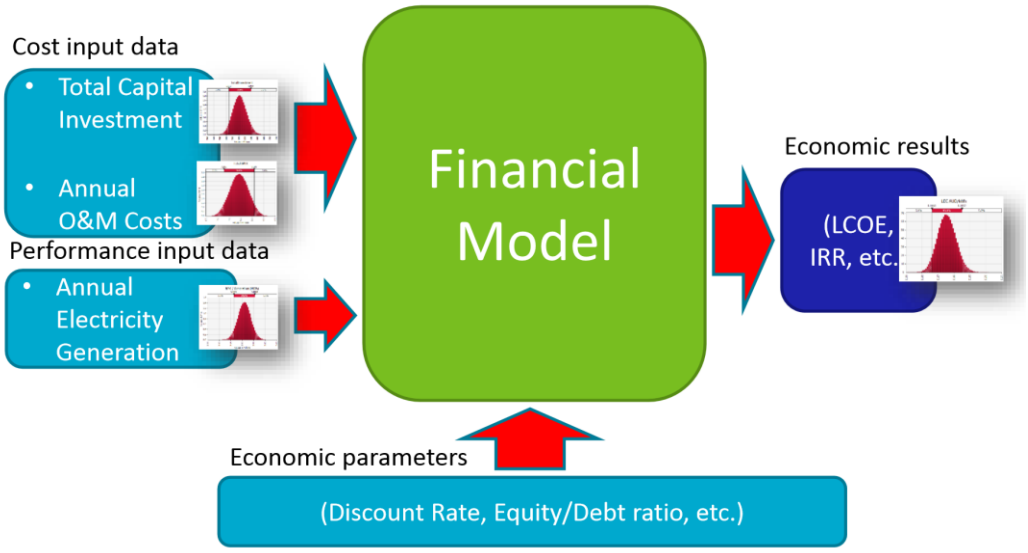

Figure 7.2. Stochastic economic analysis of a CSP/STE power plant. All inputs to the model are represented by probability distributions. The variability of the annual electricity generation is obtained using an energy model and running it for a long series of "plausible" meteorological years that are compatible with the Typical Meteorological Year at the plan location. For each plausible meteorological year annual energy yield for the plant is obtained, based on many of those values an appropriate probability distribution is derived.

For every cost item a probabilistic distribution is assigned to represent either its uncertainty, its variability or the combination of both. Uncertainty is associated with the lack of knowledge regarding the exact price of the cost item and it is expected to decrease as the project progresses towards implementation, as more knowledge about the different cost items and their prices are obtained. Variability, however, is associated with the inherent variation of the price of the cost of the item due to market price fluctuations. Thus, it is not expected to decrease as the project progresses, since the progress of the project is not likely to affect in any substantial way the market price of the cost item or its fluctuations. While all cost items have uncertainty, only those cost items which are commodities are expected to have a relevant variability. In addition to assigning probability distributions to the cost items to model their uncertainty and variability, the stochastic approach also assigns uncertainty and variability to the annual electricity generation of the CSP/STE power plant.

The uncertainty in the production of the CSP/STE power plant is associated with the uncertainty of the performance parameters of the plant and with the uncertainty regarding how well the energy model of the plan reflects its behavior. The variability in the annual energy generation of the plan is associated with the intrinsic variability of the solar Direct Normal Irradiance (DNI) and of the rest of the other relevant meteorological variables. How the variability of the DNI and the rest of the meteorological variables translate into the variability of the production of the CSP/STE power plant depends on the specific CSP/STE technology and configuration of the plant.

The variability of the annual electricity generation is obtained using an energy model and running it for a long series of "plausible" meteorological years that are compatible with the Typical Meteorological Year at the planning location. For each plausible meteorological year annual energy yield for the plant is obtained, based on many of those values an appropriate probability distribution is derived. This chapter discusses several methods for how this can be achieved.

7.2 Modelling the DNI variability to derive the annual electricity generation variability of a CSP/STE power plant

As stated in the previous section, the stochastic feasibility analysis of CSP/STE power plants requires assigning probability distributions to all relevant input parameters of the financial model of the CSP/STE power plant investment project. These probability distributions should represent both the uncertainty and variability of those input variables.

Of particular importance is to model the variability of the annual energy production of the CSP/STE power plant, since this input variable plays an essential role in determining the economic performance of the CSP/STE power plant investment project.

The variability of the annual energy production of the plant is essentially determined by the variability of the DNI and, to a much lesser degree, by the variability of the rest of the meteorological variables at the plant location. However, the relationship between the variability of the DNI and the rest of meteorological variables and the variability of the annual energy production of the plan is complex as shown in Figure . It depends on the specific technology of the CSP/STE power plant (tower, trough, or Linear Fresnel) but also, and heavily, on the specificities of the configuration of plan (nominal power, capacity factor, solar multiple, storage type, configuration and capacity, etc.).

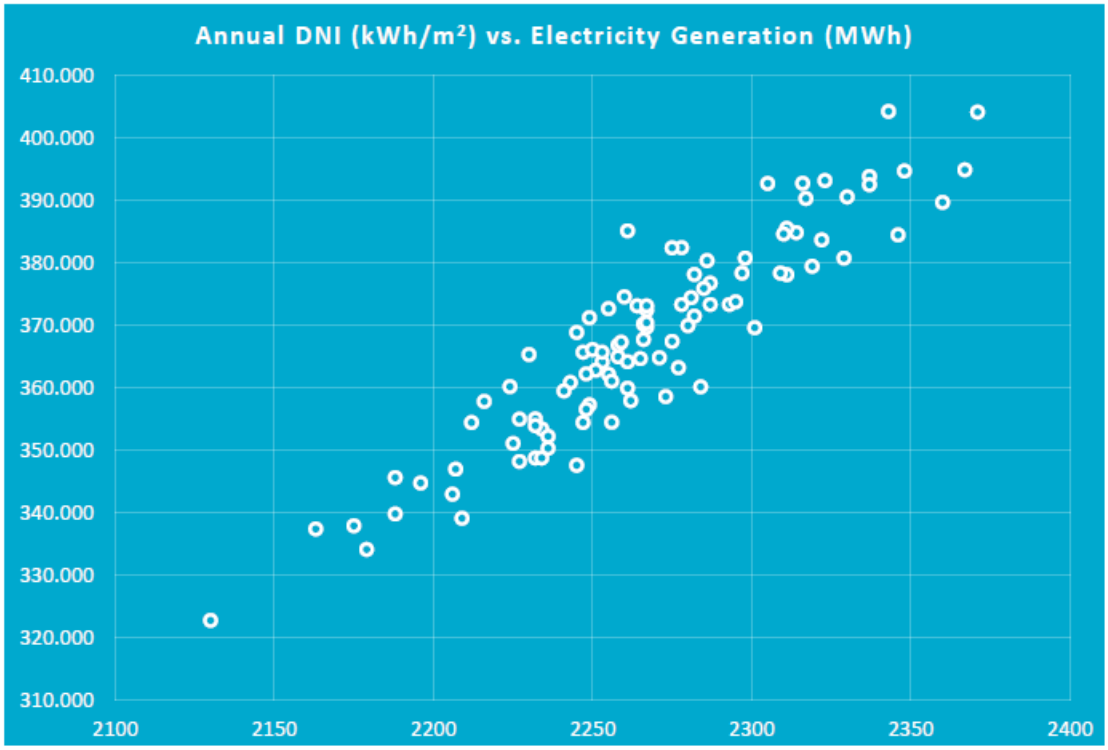

Figure 7.3. Typical relationship between the variability of the annual solar DNI and the variability of the annual solar electricity generation for a parabolic trough solar power plant. Although the electricity generation clearly is proportional to the annual DNI, the range of annual electricity output can be seen also to depend on other variables.

Because of this, the most straightforward approach to derive the variability of the annual production of the CSP/STE power plant induced by the variability of the DNI and other meteorological variables is to:

1. Generate many meteorological years that are “plausible” for the plant´s location, i.e., that can be consider as samples of a population of meteorological years whose long-term values at different time scales are those of the Typical Meteorological Year for the plant´s location.

2. Run the energy model of the CSP/STE power plant for each one of the “plausible” years generated to obtain the corresponding “plausible” values of the plant´s annual energy production.

3. Analyze the set of the CSP/STE power plant´s annual energy production values to derive from them a probability distribution, representing the variability of the plant´s annual energy production.

In this approach, two main issues have to be addressed to achieve and appropriate estimate of the probability distribution associate to the CSP/STE power plant annual energy output.

1. What should be the time resolution of the plausible meteorological years?
2. How to generate large series of plausible meteorological years with the required time resolution?

7.2.1 High frequency series

During recent years there have been two different lines of research focused on improving new solar radiation data sets. Due to the lack of measurements with high spatial resolution and the lack of continuous measurements during more than ten years, most of the data sets used are estimations from satellite images or numerical weather prediction (NWP) models.

One line of research strives to develop models to generate good datasets, which are able to cover the Earth surface with high spatial resolution. In the recent literature, these data sets are referred to as gridded data sets (Habte et al., 2014). In general, they are either based upon solar radiation data derived from satellite images, or upon solar radiation data derived from NWP models. Typically, the data derived from satellite images compare better with ground measurement data (Pagola et al., 2014) than the data derived from NWP models (Boilley and Wald, 2015).

The other line of research strives to increase the temporal resolution of the solar radiation and other meteorological data because of the importance of using meteorological years of 1-minute resolution in the simulation of CSP/STE power plants (Meyer et al., 2009). This choice is supported by numerous recent 1- minute forecasting studies (e.g. Chow et al., 2011; Yang et al., 2014; Alonso-Montesinos et al., 2015). If 1 minute temporal resolution meteorological data are not available for a given site, the minimum temporal resolution in the stochastic approach should be 1 hour (Billinton and Bagen, 2006).

These two lines of research are not converging yet. High-temporal resolution data sets are yet only available form ground measurements and not from gridded data sets. The time resolution of data sets derived from satellite images are typically hourly, although depending on the place of the world and the period of time under analysis their temporal resolution can go down to a minimum of 15-minutes. The time resolution of data sets derived from numerical weather prediction models is typically from 3 up to 1 hours, but recently fifteen-minute datasets start to be generated.
In order to combine both lines of research, new models are emerging trying to improve the time resolution of modeled gridded datasets. These models improve the time frequency either using autoregressive models as Markov chains (Bright et al., 2015), or combining stochastic and deterministic methods (Larrañeta et al., 2015).

A complementary approach, to improve the time-resolution of solar radiation data sets derived by combining estimated data with real solar radiation measurements, consists in improving the versatility of measured high-temporal resolution daily solar DNI curves (Fernández-Peruchena et al., 2014).

By non-dimensionalizing the two axis of the daily solar DNI curve, any solar DNI curve can be transformed into a curve which is contained within a non-dimensional 1-unit side square, as shown in Figure 7.4 (Fernández-Peruchena et al., 2014).

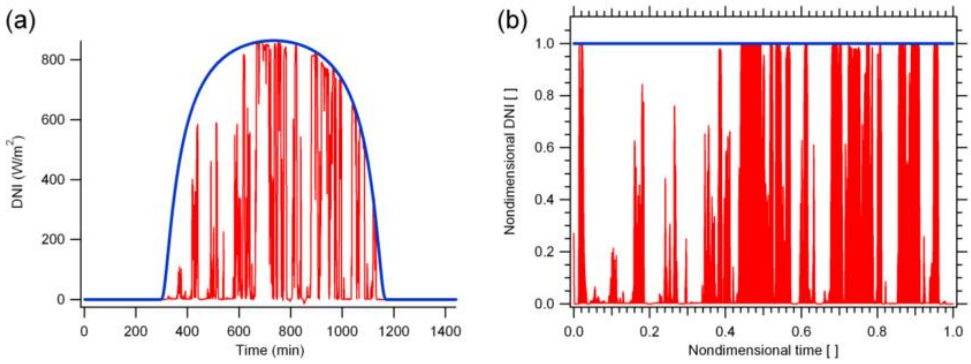

Figure 7.4. (a) Instantaneous DNI daily curve and its clear-sky envelope; (b) nondimensionalized DNI curve.

To non-dimensionalize the temporal x-axis, the time from sunrise is divided by the total day span, i.e., the time between sunrise and sunset. To non-dimensionalize de DNI y-axis, the measured DNI values are divided for the corresponding DNI values of the clear-day envelope. This transformation can be undone, however, by multiplying the x-dimension by a different day span and the y-direction by a different clear day envelope. This trick makes it possible to elegantly fill gaps in measured solar DNI years but can also be used for other purposes, such as part of an strategy to generate large numbers of high temporal resolution plausible days, which in turn, properly arranged, can be used to generate large series of high-temporal resolution plausible years as shown in the article by Fernández-Peruchena et al. previously indicated.

7.2.2 Multi-annual series generation

The generation of hundreds of meteorological years with, at least, 1-hour temporal resolution can be achieved using many different approaches.

One approach is synthetic generation (Fernández-Peruchena et al., 2015). This approach starts with the estimation of the long-term expected values of the annual global horizontal irradiation (GHI and its variability. It is assumed that the variability of the annual GHI values can be represented by a normal distribution. Each annual GHI is obtained by randomly sampling its normal distribution. Annual DNI values are then estimated from the sampled GHI values using (Rabl, 1981) model. This model assumes a linear dependence among annual values of GHI and DNI. After this, GHI monthly values consistent with the previously obtained GHI annual values are derived from

historical data of the monthly clearness index frequency distribution, assuming this to be normally distributed. Once this is done, monthly DNI values are then estimated from the monthly GHI values in the same manner as the annual values were estimated. Finally, daily, hourly and 1-min synthetic generation procedures are proposed to generate high frequency series of meteorological years consistent with the estimated variability of the monthly GHI and DNI values. A variation of the synthetic generation approach has been described by Röttinger et al. (2015). They assume the annual DNI values to be normally distributed.

For all of these types of stochastic approaches, one needs to know the shape of the probability density function of the annual and monthly GHI and DNI. Even though many authors assume normally distributed annual and monthly GHI and DNI values, some authors claim the Weibull distribution to provide a better representation of the variability of the annual and monthly DNI values (e.g. Fernández Peruchena et al., 2016). See also Chapter 5 of this report. The variation around the mean differs whether GHI or DNI is considered. For GHI Ineichen (2011) found up to more than 10% annual deviation from the mean. For DNI Lohmann et al. (2006) found up to more than 20% annual deviation from the mean.

An additional approach to obtaining hundreds of plausible solar radiation years is sampling from a data bank of measured data. In (Usaola, 2014) a method based on Bootstrap Sampling is proposed, which can be used if one has a data bank with enough representative data. The bootstrap methodology has been also tested in (Ramírez et al., 2015) using 4 years of data, but without satisfactory results. Figure 7.5 shows the results of applying the bootstrap methodology to daily DNI values. The red line is the same for all graphs in the figure. It shows the Cumulative Density Function (CDF) for all April data relative to the long term behavior. The blue line differs from graph to graph in the figure. For each graph in the second line, it shows the CDF corresponding to the year of the graph obtained applying the bootstrap methodology, using as input data each single month from year 2009 to 2011. A chain length of 3 days and 100 tries were defined as boundary conditions. It is clear from Figure 7.5 that the CDF obtained applying the bootstrap methodology does not change depending on the tested years and does not match the long term behavior well if the month is far from it. Due to the fact that the autoregressive correlation is not always relevant (Tiba and Fraidenraich, 2004), bootstrap sampling methodologies may not have an added value compared to simple sampling.

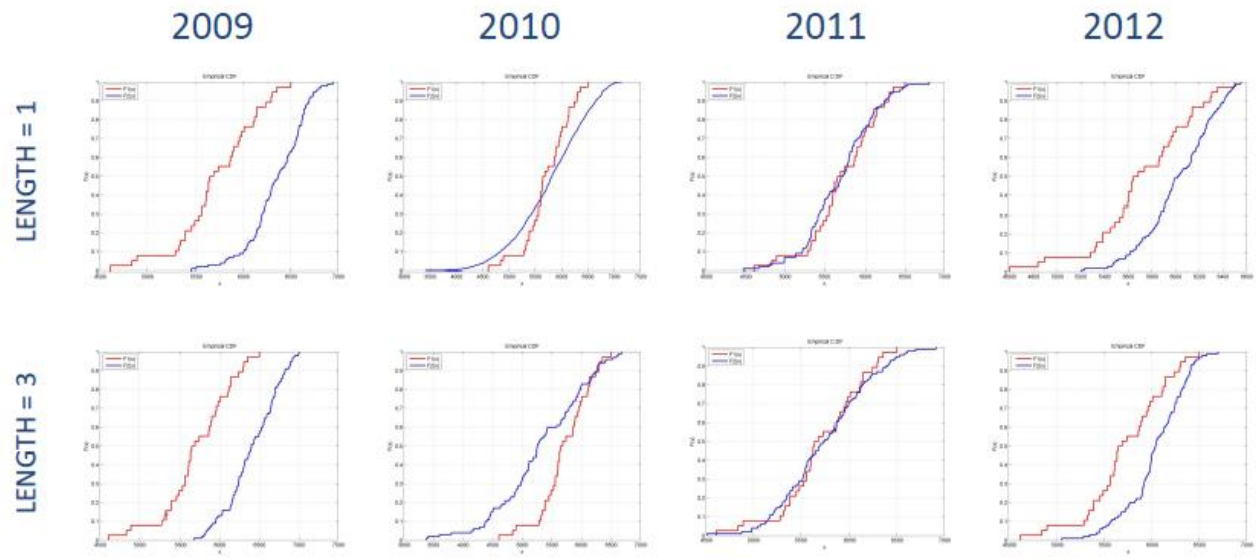

Figure 7.5. Results of April for different years and daily chain lengths. The tested series are shown with blue curves, while the reference series are shown with red curves.

Finally, combining some of the mentioned approaches is also an interesting option to be explored.

7.3 Conclusions

The traditional approach of using reference or typical meteorological yearly data sets, which is still extensively used nowadays to carry out techno-economic feasibility studies of CSP/STE power plant investment projects, is not well-suited to assess the associated risks involved in the design, construction, and operation of the CSP/STE power plant during its lifetime.

This approach falls short of properly modeling and taking into account the effects of the uncertainty and variability associated with the different cost items that compose the CAPEX and OPEX of the plant investment project and are associated with the technical design and operating parameters of the plant, which determine the variability of its performance and of the annual electricity generated by the plant.

A properly implemented stochastic multi-year data approach will do a better job in assessing risks and in providing a clearer picture of the uncertainty and variability associated with all the relevant economic and technical parameters of the CSP/STE power plant. This will necessarily results in useful uncertainty and variability assessments of the main economic indicators of the CSP/STE plant investment project.

Stochastic approaches, because of their advantages, are increasingly being adopted in many fields that require high capital intensive investments – for instance large infrastructure projects or projects related to other renewable energy technologies.

A technology specific and very critical step in adapting the stochastic approach to the techno-economic feasibility analysis of CSP/STE power plants is the modeling of the variability associated with the production of the plant due to the variability of the solar DNI and, to a lesser degree, other meteorological variables.

The research community is addressing this issue and is making substantial progress, to the point that several approaches have already being tested and presented in the literature, as outlined here.

7.4 References

Alonso-Montesinos, J., Batlles, F.J., Portillo, C., 2015. Solar irradiance forecasting at one-minute intervals for different sky conditions using sky camera images. Energy Convers. Manag. 105, 1166–1177. doi:10.1016/j.enconman.2015.09.001

Billinton, R., Bagen, 2006. Reliability Considerations in the Utilization of Wind Energy, Solar Energy and Energy Storage in Electric Power Systems, in: 2006 International Conference on Probabilistic Methods Applied to Power Systems. IEEE, pp. 1–6. doi:10.1109/PMAPS.2006.360204

Boilley, A., Wald, L., 2015. Comparison between meteorological re-analyses from ERA-Interim and MERRA and measurements of daily solar irradiation at surface. Renew. Energy 75, 135–143. doi:10.1016/j.renene.2014.09.042

Bright, J.M., Smith, C.J., Taylor, P.G., Crook, R., 2015. Stochastic generation of synthetic minutely irradiance time series derived from mean hourly weather observation data. Sol. Energy 115, 229–242. doi:10.1016/j.solener.2015.02.032

Chow, C.W., Urquhart, B., Lave, M., Dominguez, A., Kleissl, J., Shields, J., Washom, B., 2011. Intra-hour forecasting with a total sky imager at the UC San Diego solar energy testbed. Sol. Energy 85, 2881–2893. doi:10.1016/j.solener.2011.08.025

Crudden, M., 2012. A discussion of the Monte Carlo technique applied to commercial property. Examining risk in perspective. Public Infrastruct. Bull. 1.

Fernández-Peruchena, C. M., M. Blanco, A. Bernardos, 2014. Generation of series of high frequency DNI years consistent with annual and monthly long-term averages using measured DNI data, Energy Procedia 49, 2321-2329. doi:10.1016/j.egypro.2014.03.246.

Fernández-Peruchena, C.M., Gastón, M., Sánchez, M., García-Barberena, J., Blanco, M., Bernardos, A., 2015. MUS: A multiscale stochastic model for generating plausible meteorological years

designed for multiyear solar energy yield simulations. Sol. Energy 120, 244–256. doi:10.1016/j.solener.2015.07.037

Fernández Peruchena, C.M., Ramírez, L., Silva-Pérez, M.A., Lara, V., Bermejo, D., Gastón, M., Moreno-Tejera, S., Pulgar, J., Liria, J., Macías, S., Gonzalez, R., Bernardos, A., Castillo, N., Bolinaga, B., Valenzuela, R.X., Zarzalejo, L.F., Ramı, L., Silva-pe, M.A., Ferna, C.M., Moreno-Tejera, S., Lara, V., Bermejo, D., Liria, J., Macı, S., Bolinaga, B., Valenzuela, R.X., Zarzalejo, L.F., 2016. A statistical characterization of the long-term solar resource: Towards risk assessment for solar power projects. Sol. Energy 123, 29–39. doi:http://dx.doi.org/10.1016/j.solener.2015.10.051

Habte, A., Lopez, A., Sengupta, M., Wilcox, S., 2014. Temporal and Spatial Comparison of Gridded TMY, TDY, and TGY Data Sets, NREL/TP-5D00-60886. National Renewable Energy Laboratory.

Hirth, L., Steckel, J.C., 2016. The role of capital costs in decarbonizing the electricity sector. Environ. Res. Lett. 11. doi:10.1088/1748-9326/11/11/114010

Ineichen, P., 2011. Global irradiation: average and typical year, and year to year annual variability. University of Geneva, Institute for Environmental Science, Geneva (Switzerland).

Larrañeta, M., Moreno-Tejera, S., Silva-Pérez, M.A., Lillo-Bravo, I., 2015. An improved model for the synthetic generation of high temporal resolution direct normal irradiation time series. Sol. Energy 122, 517–528. doi:10.1016/j.solener.2015.09.030

Lohmann, S., Schillings, C., Mayer, B., Meyer, R., 2006. Long-term variability of solar direct and global radiation derived from ISCCP data and comparison with reanalysis data. Sol. Energy 80, 1390–1401. doi:10.1016/j.solener.2006.03.004

Marshall, H.E. (National I. of S. and T., 1999. Sensitivity Analysis, in: Dorf, R. (Ed.), Technology Management Handbook. CRC Press LLC, Boca Raton, Fl., p. 8/59-63.

Meyer, R., Beyer, H.G., Fanslau, J., Geuder, N., Hammer, A., Hirsch, T., Hoyer-klick, C., Schmidt, N., Schwandt, M., 2009. Towards Standardization Of CSP Yield Assessments, in: Proceedings of the SolarPACES Conference. Munich, pp. 1–8.

Moreno-Tejera, S., Ramírez-Santigosa, L., Silva-Pérez, M.A., 2015. A proposed methodology for quick assessment of timestamp and quality control results of solar radiation data. Renew. Energy 78, 531–537. doi:10.1016/j.renene.2015.01.031

Morf, H., 2013. A stochastic solar irradiance model adjusted on the Ångström–Prescott regression. Sol. Energy 87, 1–21. doi:10.1016/j.solener.2012.10.005

National Climatic Data Center/NESDIS/NOAA/U.S. Department of Commerce, Air Resources Laboratory/OAR/NOAA/U.S. Department of Commerce, U.S. Department of Energy, 1981. NCDC TD9734 Typical Meteorological Year, Solar and Surface.

Pagola, I., Gastón, M., Bernardos, A., Fernández-Peruchena, C., 2014. A Combination of Heliosat-1

and Heliosat-2 Methods for Deriving Solar Radiation from Satellite Images. Energy Procedia 57, 1037–1043. doi:10.1016/j.egypro.2014.10.088

Pernigotto, G., Prada, A., Cóstola, D., Gasparella, A., Hensen, J.L.M., 2014. Multi-year and reference year weather data for building energy labelling in north Italy climates. Energy Build. 72, 62–72. doi:10.1016/j.enbuild.2013.12.012

Rabl, A., 1981. Yearly average performance of the principal solar collector types. Sol. Energy 27, 215–233. doi:10.1016/0038-092X(81)90123-7

Ramírez, L., González, M., Usaola, J., Blanco, M., Vindel, J.M., 2015. Applying Moving Blocks Bootstrap for the Creation of Multi-Year Time Series for STE Simulation, in: Proceedings of the SolarPACES Conference. Cape Town, South Africa, p. 2.

Röttinger, N., Remann, F., Meyer, R., Telsnig, T., 2015. Calculation of CSP Yields with Probabilistic Meteorological Data Sets: A Case Study in Brazil. Energy Procedia 69, 2009–2018. doi:10.1016/j.egypro.2015.03.210

Tiba, C., Fraidenraich, N., 2004. Analysis of monthly time series of solar radiation and sunshine hours in tropical climates. Renew. Energy 29, 1147–1160. doi:10.1016/j.renene.2003.11.016

Usaola, J., 2014. Synthesis of hourly wind power series using the Moving Block Bootstrap method, in: 2014 International Conference on Probabilistic Methods Applied to Power Systems (PMAPS). IEEE, pp. 1–6. doi:10.1109/PMAPS.2014.6960602

Westney, R., 2011. Assessing the risk in capital-intensive opportunities. Oil Gas Financ. J.

WRDC, 2014. Solar radiation and radiation balance data (The World Network), WRDC Issue October - November 2014. World Radiation Data Centre.

Yang, H., Kurtz, B., Nguyen, D., Urquhart, B., Chow, C.W., Ghonima, M., Kleissl, J., 2014. Solar irradiance forecasting using a ground-based sky imager developed at UC San Diego. Sol. Energy 103, 502–524. doi:10.1016/j.solener.2014.02.044